POLITECNICO DI MILANO

School of Industrial and Information Engineering

Master of Science in Automation and Control Engineering

POLITECNICO
MILANO 1863

Operational space impedance shaping using optimization- based non-linear controllers for dexterous manipulation of robots

Supervisor: Prof. Paolo Rocco

Co-supervisor: Dr. Davide Nicolis

Master Thesis dissertation of:

Shobhit Yadav

ID 877404

Academic Year 2017-2018

ACKNOWLEDGEMENTS

Having reached the conclusion of this academic track, I would like to summarize my gratitude to all the people without their support and encouragement this would not have been the same.

First of all, I would like to thank my advisor(s), Professor Paolo Rocco and Professor Andrea Zanchettin for providing me the opportunity to be a part of MeRLIn Lab. I have profound gratitude for Davide Nicolis who played an instrumental role in information sharing, helping me deepening the concepts and for the constant support in this engagement.

A heartfelt thanks to all my friends from the University and the Polimi Residences with whom I shared these years. A special thanks to my friends Miguel, Ivan, Federico, Carolina, Dany, JP, Aitor, Fabio, Paolo and Marcelo with whom I shared bountiful timeless experiences. Thank you for the valuable peer-to-peer coaching over these years. Your support and love made this journey more joyful.

Finally, I would like to dedicate this work to my family: my father, mother and twin brother. Without your unconditional support and love it would not have been possible to make through this process or any of the tough times in my life. Thank you.

Shobhit Yadav

CONTENTS

LIST OF FIGURES

LIST OF TABLES

ACRONYMS

CARE Continuous Algebraic Ricatti Equation.

HOSMC Higher Order Sliding Mode Control.

HRC Human-robot Collaboration.

ISMC Integral Sliding Mode Control.

MPC Model Predictive Control.

QP Quadratic Programming.

SMC Sliding Mode Control.

SMPC Sliding-mode Model Predictive Control.

STA Super Twisting Algorithm.

VSCS Variable Structure Control Systems.

ABSTRACT

With the latest trends in robotics and industrial automation, the terms like collaborative robotics, compliant robotics and teleoperation are widespread due to their evident advantages of better adaptability and productivity over traditional fully autonomous variants. Thanks to the recent technological developments, the computational capabilities of the machines disposed to data processing have enormously increased. While the advantages of operational space control are well-understood from an analytical point of view, it can be inordinately hard to accurately control complex robots in the face of modelling errors or other sources of instability. For these reasons, constraint optimal control problem is considered in this thesis to develop robust control strategy that enables dexterous manipulation in the task space. The proposed controller is able to guarantee desired impedance robustly in task space. The crucial components addressed include uncertainties of the system, joint friction and communication delay in the network that notably affect the stability of the operation. To address them, a model predictive sliding mode control has been developed for a generic multi-degree of freedom system. It is an optimization based controller that solves a quadratic objective function satisfying constraints as desired by the operation or imposed by the environment. The experiments validate the effectiveness of the approach and its capability to achieve robust operation in the presence of extrinsic and intrinsic uncertainties and the communication delay on the torque channel.

SOMMARIO

Con le ultime tendenze della robotica e dell'automazione industriale, i termini come la robotica collaborativa, la robotica compliant e la teleoperazione sono diffusi a causa dei loro evidenti vantaggi di una migliore adattabilità e produttività rispetto alle varianti tradizionali completamente autonome. Grazie ai recenti sviluppi tecnologici, le capacità computazionali delle macchine disposte all'elaborazione dei dati sono enormemente aumentate. I vantaggi del controllo dello spazio operativo sono ben compresi, può essere estremamente difficile controllare accuratamente robot complessi di fronte a errori di modellazione o altre fonti di instabilità. Per queste ragioni, in questa tesi viene considerato un problema di controllo ottimale dei vincoli per sviluppare una solida strategia di controllo che consenta una corretta manipolazione nello spazio delle attività. Il controller proposto è in grado di garantire l'impedenza desiderata in modo robusto nello spazio delle attività. Le componenti cruciali affrontate includono incertezze del sistema, attrito congiunto e ritardo di comunicazione nella rete che influiscono notevolmente sulla stabilità dell'operazione. Per affrontarli, è stato sviluppato un controllo predittivo della modalità di scorrimento per un sistema generico di grado multiplo di libertà. È un controller basato sull'ottimizzazione che risolve una funzione obiettivo quadratica che soddisfa i vincoli desiderati dall'operazione o imposti dall'ambiente. Gli esperimenti convalidano l'efficacia dell'approccio e la sua capacità di ottenere un funzionamento robusto in presenza di incertezze estrinseche e intrinseche e il ritardo di comunicazione sul canale di coppia.

Chapter 1

Introduction

Dexterous manipulation is one of the most impressive characteristic features of human motor skills. It has the ability to perform highly accomplished movements with quite an ease. In the robotic community it is widely accepted that dexterity is desirable and robots with this capability should be developed. Humans employ a highly compliant operational space control where the prime focus is the task variables while keeping the redundant degrees-of-freedom compliant to disturbances or the constraints due to the environment.

Robotics is widely employed to extend these capabilities through interactive and collaborative robotics. For instance *Human-robot Collaboration (HRC)*, where a human can control and monitor production while the robot performs strenuous work. A decisive strategy for the omnipresent Industry 4.0 where both contribute their specific capabilities. This compliant robot motion is a result of dexterous manipulation capabilities where the control focus on some selective task variables while the redundant degrees-of-freedom are kept as compliant as possible. Or, *Teleoperation* systems that enable to control remotely located manipulators. A smooth information exchange is instrumental to realize this so that the operator is provided with similar conditions as will be felt by being in the remote location. In short, operational-space control serves as one of the most elegant approaches to task control due to the potential for dynamically consistent control, compliant

control, force control, hierarchical control, and many other favorable properties. The operational space impedance controller can be effectively used for dexterous manipulation while overcoming the main problems faced i.e. joint friction, unmodeled dynamics and occurrences of singularity conditions [46].

The *mechanical impedance* of the system represents the relationship between force and velocity during the interaction with the environment. It is possible to control the value of this impedance to enforce the desired behaviour as required by the system. A completely assignable end-effector impedance is often desirable for reliable operation in aforementioned applications. As reported, several factors like uncertainty in robot dynamic model, joint friction, delay in torque channel etc. can adversely affect the system performance. The following sections of this work will provide various strategies explored to deal with the above mentioned problems and evaluate their relative performance over previously employed strategies. The primary focus will be the impedance tracking for operational space control.

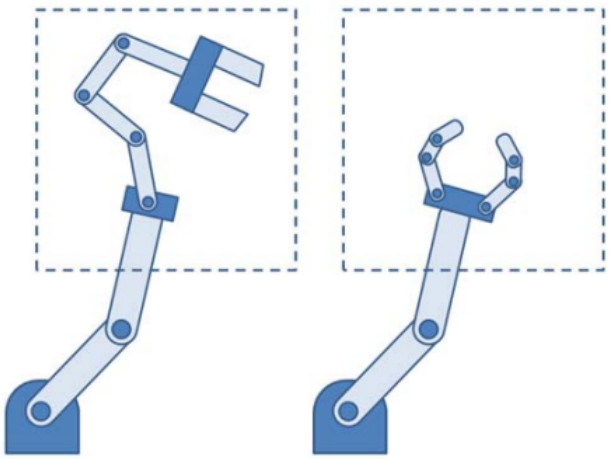

Figure 1.1: Redundancy increases system dexterity [1]

Impedance control is an approach to the control a manipulator's dynamic interaction with its environment. It does not simply regulates the position but the entire relationship between force and position as well as the velocity and acceleration. The inclusion of force information increases the adaptability of robots to

uncertain environments.

A substantial body of literature has been published focusing on the control of impedance of a manipulator. One of the pioneers of this control approach are O. Khatib, J. Burdick [36], who implemented operational space approach to obtain nearly perfect decoupling of end-effector motions and forces of the manipulators. It used a simple mass/spring model to formulate the active force control. While Neville Hogan presented a unified approach to manipulation as "impedance control" [37]. It required the controller to monitor the changes in the environment continuously to adapt it's own behaviour. A highly desirable characteristics as the changes in environmental parameters can be very rapid rendering the system identification process infeasible. It structured the controller to impress a force in relation to the motion i.e. it behaves as an impedance. Operational space formulation provides a comprehensive framework to describe end-effector dynamic behaviour and these advantages have pushed the research further continuously. An extension to operational space control to redundant manipulators is presented in [38] that highlighted the coupling between OS dynamics and NS (null-space) dynamics. In [41, 42, 43] various approaches using Sliding Mode Control (SMC) and Model Predictive Control (MPC) have demostrated their effectiveness to counter uncertainties and disturbances affecting the robot manipulation tasks. A significant study on these topics has been performed for the decentralized control of robotic manipulators. In [44] the operational space control is applied to a 7-dof space robotic manipulator *SPIDER* that demonstrated it as an effective approach to position/force control.

Thanks to the technological development of the last few years, diffusion of control techniques that require high computational capabilities is becoming common in robotic applications. This is particularly applicable to the optimization based control fameworks. This has enabled to harness the capabilities of redundant manipulators to fulfill multiple tasks at the same time. In [39] a control is developed for redundant manipulators that generalizes the task-priority framework to inequality task. In [40] a reactive path planner is developed for redundant ma-

nipulators in dynamic environments with moving obstacles has been developed. In [45] optimization based approach is used to execute dexterous manipulation of a redundant manipulator realizing a visual servoing task. The work [3] provides a comprehensive analysis of decentralized control for enforcing joint space impedance and the theoretical results are validated on 7 degrees-of-freedom manipulator, *ABB IRB14000 YuMi*. It also discusses the operational space impedance tracking. But, the obtained results are implemented on a 2-DOF planar manipulator.

1.1 Motivation and Objective

The main objective of this thesis is to develop an optimization based robust controller that can realize operational space impedance tracking. To robustly impose the required dynamics, sliding mode control technique is adopted. It is well established that it is able to reject the the unmodeled dynamics and uncertainties and disturbances affecting the system. The previous work by Fabio Allevi [3], demonstrated this specifically through an implementation on bilateral teleoperation. But, the main focus remained the decentralized control implementation while the operational space control is considered through a simplistic 2-DOF planar manipulator model. In this thesis, a comprehensive analysis of operational space impedance shaping is reported. The effect of communication delay on the control signal is also considered, as it can significantly affect the controller performance. Finally, the presence of filter on the torque channel is evaluated as this is a common internal architecture in many industrial robots. This limits the available bandwidth of the desired control action. Another value proposed in this work is the extension of stability results to each task space coordinate which is an instrumental requirement for practical applications. Another interesting variation to the previously proposed algorithm is explored where the sliding gain of SMC or gains for STA are adaptive to the measure of uncertainty of the system.

The need for the aforementioned analysis is motivated by the fact that there

exist many robotic applications interactive robotics, teleoperation among others where a desired impedance relationship is to be imposed between end-effector and the external environment. There is a lack of literature on optimization based operational space robust controls to realize dexterous manipulation. Moreover, considerations in the past have been dominated by analysis of simplified mechanisms with little practical applications. In this thesis, methodologies are developed in the view of one of the world's first collaborative robots *ABB FRIDA*.

1.2 Synopsis

This thesis dissertation is organized as follows:

- **Chapter 2, Background - Impedance & Robust Control:** It presents a background on the control techniques namely inverse dynamics control, impedance control and non-linear sliding mode control. A brief introduction to quadratic optimization formulation (*qpOASES*) is then introduced which will be later used as the logic for generating trajectories as per the desired end-effector impedance. The figure 1.2 summarizes major obstacles for our objective (in red) and the possible ways to encounter them (in green). Finally, the key features of the experimental setup that will later influence the decisions for control are mentioned.

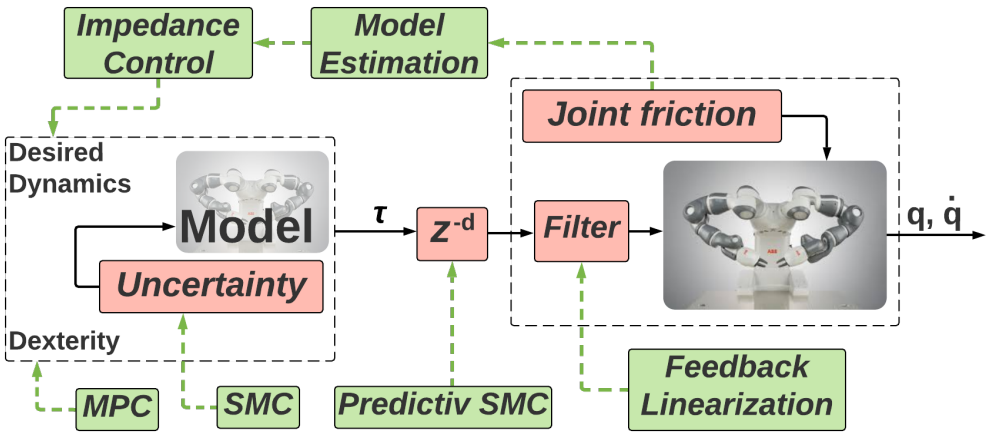

Figure 1.2: Global scheme with sources of instabilities and the proposed solution

- **Chapter 3, Decentralized Control:** the focus of this chapter is to introduce a detailed analysis of the decentralized control scheme. The stability issues due to uncertainties, joint friction and delay on torque channel acting on the manipulators have been addressed. The development of the control is performed with step-wise addition of source of instabilities to better capture their influence on system stability. In particular, non-linear sliding mode control has been developed that robustly ensures the desired impedance relationship among the kinematic quantities of the system. A comparison based on various simulations is presented to analyze the obtained results and highlight the drawbacks.

- **Chapter 4, Robust Centralized Control:** the results obtained in the previous chapter form the basis of the further development of the proposed robust control in operational space. The analysis is divided in two broad groups:

  ⋆ Centralized Control without filter on the torque channel

  ⋆ Centralized Control with the filter on torque channel

  In this chapter, the focus is on the first. It introduces the concept of operational space impedance and methods to control it. It presents a comprehensive analysis null-space robust control and optimal constraint fulfilment. It also presents a mathematical discussion of the MPC formulation. Finally, the developed theory is tested on a 7-DOF manipulator model. Various sources of instabilities like uncertain dynamic model, joint friction and delay on the control signal have been analyzed to develop a robust impedance controller.

- **Chapter 5, Impedance Control with Torque Filtering:** The chapter follows the theory developed in chapter 4 to the presence of filter on the torque channel. The primary focus is to integrate feedback linearization with Sliding Mode Control (SMC) to realize the desired operational space

impedance. Two approaches to feedback linearization have been proposed namely analytical approach and numerical approximation. The results obtained through the classical approach are tested on a 2-DOF manipulator model on MATLAB-Simulink for a decentralized SMC. A brief extension of decentralized SMC for third order dynamics is also included here. Finally, another approach to feedback linearization is presented for operational space control. The centralized control results have been derived for this new system. These results are later implemented on a 7-DOF manipulator model. A comparison of various control strategies specifically SMC, Predictive SMC is also presented.

- **Chapter 6, Experimental results:** The control techniques presented in the thesis are tested on ABB FRIDA robot. A brief summary of the experimental setup is also provided. The salient considerations of the experiment and the list of tuning parameters are reported. The results are presented for the final controller developed in chapter 5 which is a combination of feedback linearization and sliding mode control.

- **Chapter 7, Conclusions:** The notable findings, contributions and results of the thesis are summarized here followed by possible future actions.

Chapter 2

Background Impedance & Robust Control

This chapter will introduce the main theoretical concepts. First of all, non-linear mathematical model of the manipulator is introduced. Then various control techniques relevant for our objective of operational space robust impedance control are briefly introduced. Feedback linearization control technique is reported as a unified approach for the development of non-linear controllers. The theory is then extended to the widely used inverse dynamics control. This is followed by a brief review of impedance control which when combined with inverse dynamics scheme can enable us to enforce the desired dynamics on the manipulator system. Then, a robust control technique namely sliding mode control (SMC) is introduced. The major drawbacks of SMC are then reported and various strategies to counter them by transforming SMC have been considered namely continuous approximation of signum function, Super Twisting Algorithm (STA), Integral Sliding Mode Control (ISMC) and finally Sliding Mode Model Predictive Control (SMPC). A comparison among the above techniques is provided through MATLAB - Simulink simulations for a 7-DOF manipulator model of ABB Yumi shown in figure 2.1. To realize our objective of dexterous manipulation an objective function needs to be solved that will serve as an input to the SMC control. This input will be provided by a quadratic optimization (qpOASES: a QP solver) and so, an introduction to this QP formulation is also reported at the end.

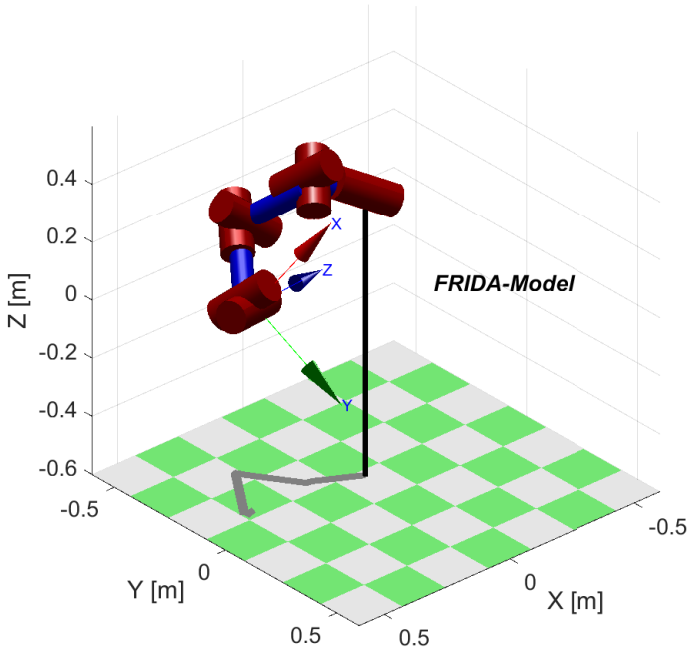

Figure 2.1: 7-DOF manipulator model

2.1 System Analysis

Let's consider the dynamic equation of a generic manipulator:

$$\boldsymbol{B}(\boldsymbol{q})\ddot{\boldsymbol{q}} + \boldsymbol{n}(\boldsymbol{q}, \dot{\boldsymbol{q}}) = \boldsymbol{\tau} + \boldsymbol{J}^{\top}(\boldsymbol{q})\boldsymbol{h} \tag{2.1}$$

where $\boldsymbol{q}, \dot{\boldsymbol{q}}, \ddot{\boldsymbol{q}}$ are joint position, velocity and acceleration vectors respectively. The term $\boldsymbol{n}(\boldsymbol{q}, \dot{\boldsymbol{q}}) = \boldsymbol{C}(\boldsymbol{q}, \dot{\boldsymbol{q}})\dot{\boldsymbol{q}} + \boldsymbol{g}(\boldsymbol{q})$ contains all Coriolis and centrifugal components while $\boldsymbol{B}(\boldsymbol{q})$ is the inertia term. $\boldsymbol{J}^{\top}(\boldsymbol{q})\boldsymbol{h}$ represents the joint-equivalent torques due to a generalized force $\boldsymbol{h}$ on the manipulator's end effector. The consideration of these forces is essential for full impedance assignment. During simulations, this can be dealt quite easily with a known force acting on the system. But in practical applications, this needs to be measured or estimated to enforce the desired dynamic behaviour. To deal with this multivariable non-linear system, non-linear control techniques are very useful to achieve global stability results.

2.2 Feedback linearization

The robot model introduced in equation 2.1 is a multivariable non-linear system. Feedback linearization provides a unified approach for the design of non-linear controllers. This in general includes the design of a static state feedback control law such that the associated feedback system is linear. It has been well studied already [16, 19, 20]. However, this technique can be used only for time-invariant systems and robustness cannot be guaranteed. So, it is often used with other control techniques [21]. A brief review for non-linear affine, time-invariant system is reported for a SISO system S:

$$\boldsymbol{S}: \begin{cases} \dot{\boldsymbol{x}} = \boldsymbol{a}(\boldsymbol{x}) + \boldsymbol{b}(\boldsymbol{x})\boldsymbol{u} \\ \boldsymbol{y} = \boldsymbol{c}(\boldsymbol{x}) \end{cases} \tag{2.2}$$

A theorem for input-output state feedback linearization exists that states if the system S has a relative degree r in x^0, then one can obtain a (locally) linear i/o map via state feedback. *Relative degree* r of a system S is given by the minimum order of the derivative of the output y that is affected directly by the input u. The control law has the following form:

$$\textit{Relative degree}: \begin{cases} \boldsymbol{L_b L_a^k c} = \boldsymbol{0}, \quad \boldsymbol{k = 0, 1, 2, ..., r-2} \\ [\boldsymbol{L_b L_a^{r-1} c}]_{\boldsymbol{x_0}} \neq \boldsymbol{0} \end{cases} \tag{2.3}$$

$$\begin{aligned} \boldsymbol{u} &= \frac{\boldsymbol{1}}{\boldsymbol{L_b L_a^{r-1} c}} (\boldsymbol{v} - \boldsymbol{L_a^r c}) \\ \boldsymbol{y^{(r)}} &= \frac{\boldsymbol{d^r y}}{\boldsymbol{dt^r}} = \boldsymbol{v} \end{aligned} \tag{2.4}$$

Figure 2.2 reports the block diagram for feedback linearization control law. Note: if $r < n$ where n is system order, there is some hidden dynamics and it needs to be analyzed using suitable canonical form.

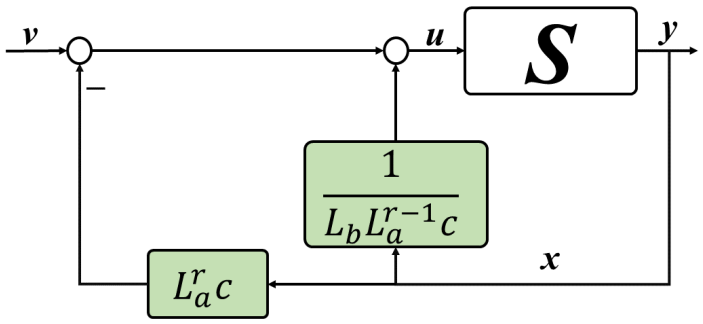

(a) Feedback linearization control law: block diagram

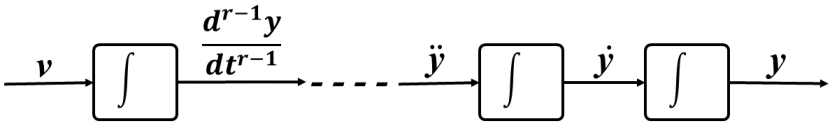

(b) Effective block diagram after feedback linearization

Figure 2.2: Feedback linearization for a generic non-linear affine system

Inverse dynamics as feedback linearization

Let's transform the robot dynamic equations into the general form of non-linear affine system. This can be obtained by replacing joint positions q as x_1 and joint velocities $\dot{q}$ as x_2. Some algebraic manipulations result in following equations:

$$\dot{\boldsymbol{x}}_1 = \boldsymbol{x}_2 \tag{2.5a}$$

$$\dot{\boldsymbol{x}}_2 = -\boldsymbol{B}^{-1}(\boldsymbol{x}_1)\Big(\boldsymbol{N}(\boldsymbol{x}_1, \boldsymbol{x}_2) + \boldsymbol{\tau}_f(\boldsymbol{x}_1, \boldsymbol{x}_2) + \boldsymbol{\tau}\Big) \tag{2.5b}$$

where the additional term τ_f represents the joint friction. The system order is 2 and it can be proved that the relative degree is also 2. Under the assumption of regularity for a(.), b(.) and c(.) we can use the results of equation 2.9 to get:

$$\begin{aligned} \boldsymbol{\tau} &= \frac{\boldsymbol{v} - \boldsymbol{L}_a^2 \boldsymbol{c}(\boldsymbol{x})}{\boldsymbol{L}_b \boldsymbol{L}_a \boldsymbol{c}(\boldsymbol{x})} \\ \boldsymbol{v} &= \boldsymbol{y}^{(2)} = \frac{\boldsymbol{d}^2 \boldsymbol{y}}{\boldsymbol{dt}^2} \end{aligned} \tag{2.6}$$

solving for the Lie Derivatives, we can obtain $\boldsymbol{L_a^2 c(x) = -B^{-1}(N + \tau_f}$ and $\boldsymbol{L_b L_a c(x) = B^{-1}}$. The final expression for the control law is:

$$\begin{aligned} \boldsymbol{\tau} &= \frac{\boldsymbol{v + B^{-1}(N + \tau_f)}}{\boldsymbol{B^{-1}}} \\ &= \boldsymbol{Bv + N + \tau_f} \end{aligned} \tag{2.7}$$

The *Inverse Dynamics* scheme basically decouples the dynamics of each robot link though cancellation of non-linear terms.When applied to equation 2.1 yields n-decoupled linear systems, e.g. $\boldsymbol{\ddot{q} = v}$ if the robot dynamic model is perfectly known, where $\boldsymbol{v}$ is the auxiliary control input that needs to be designed. However, in practical cases the dynamic model is affected by uncertainties and its non-linear, coupled nature presents the main drawback of the scheme. The general scheme for inverse dynamics architecture is shown in Figure 2.3.

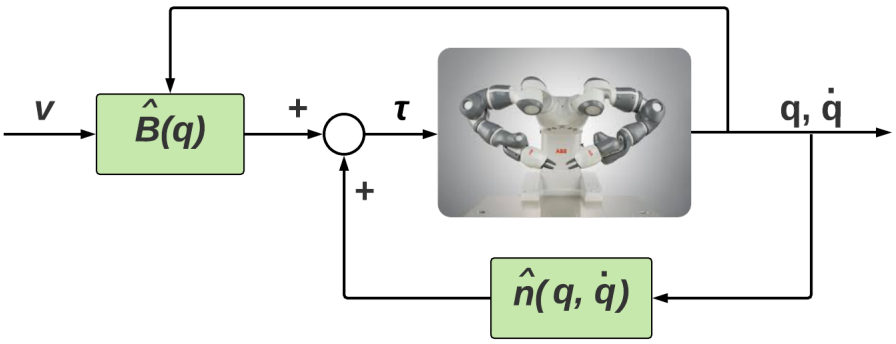

Figure 2.3: Inverse dynamics control scheme

2.3 Impedance control

The objective of this scheme is to achieve desired dynamic behaviour e.g. a second-order mechanical system characterized by a given mass, damping and stiffness parameters, known as *mechanical impedance*. This is exactly what we want to achieve. The joint space control plot reported in figure 2.4 imposes a given second-order joint space impedance using a typical choice for impedance control reported in equation 2.8 combined with inverse dynamics scheme.

$$\boldsymbol{v} = \ddot{\boldsymbol{q}}_{\boldsymbol{d}} + \boldsymbol{K_V}(\dot{\boldsymbol{q}}_{\boldsymbol{d}} - \dot{\boldsymbol{q}}) + \boldsymbol{K_P}(\boldsymbol{q}_{\boldsymbol{d}} - \boldsymbol{q}) \tag{2.8}$$

This type of control is very useful for interaction control e.g. during teleoperation to enable the operator to react to external stimuli in a predictable and safe way. An idea to pursue this goal can be to decouple and linearize the non-linear robot model. As mentioned in the introduction, this will be our main objective.

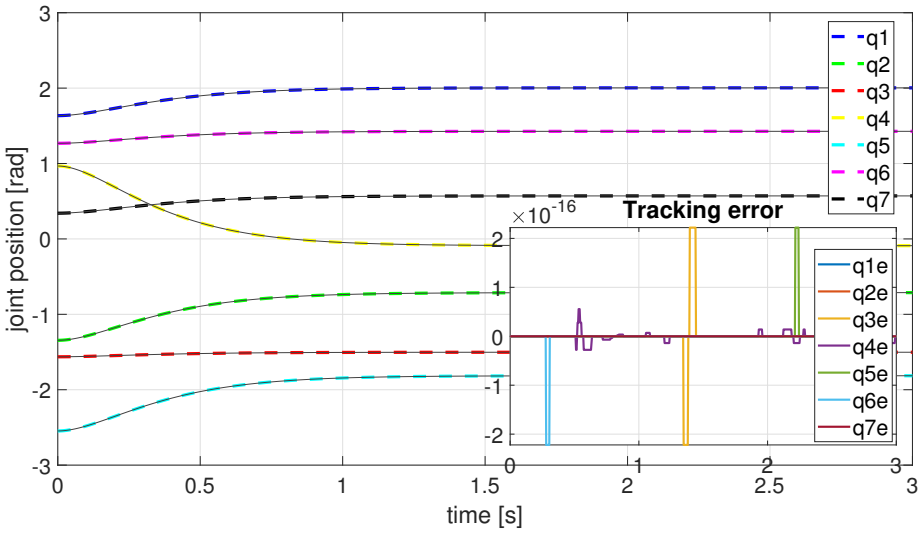

(a) Without model uncertainty

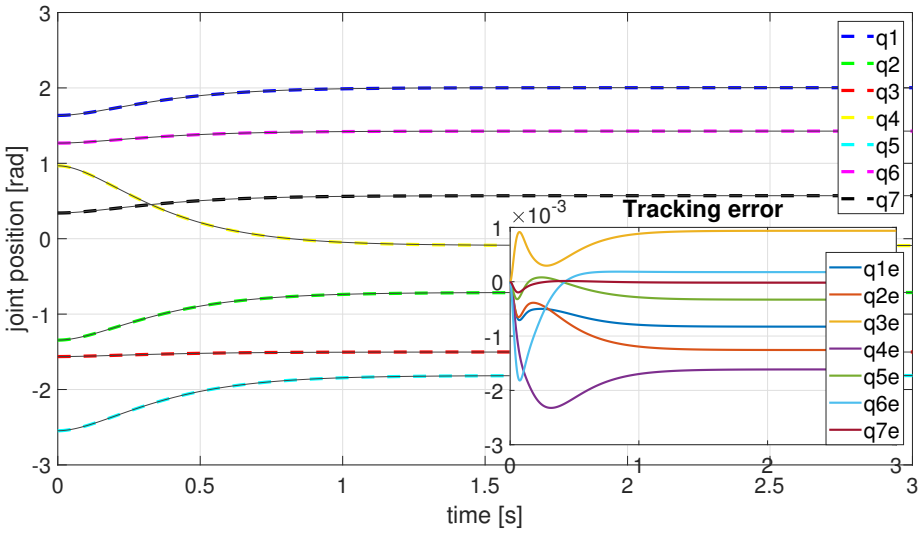

(b) With uncertain robot model

Figure 2.4: Joint space impedance control with inverse dynamics

The figure 2.4 demonstrates the impact of uncertainty on a combined impedance control and inverse dynamics scheme through a simulation on the 7-DOF manipulator model. In figure 2.4a we can see excellent tracking when the model is perfectly known while in the figure 2.4b we see the affect of the uncertainty in the robot dynamic model. As it can be observed the tracking error never goes to zero and a significant increase in the tracking error magnitude. Being strongly model dependent inverse dynamics scheme is very sensitive to uncertainties. As it will be seen later, we will use the solution of the QP formulation with sliding mode control to compute this control input. The general scheme is shown in figure 2.5.

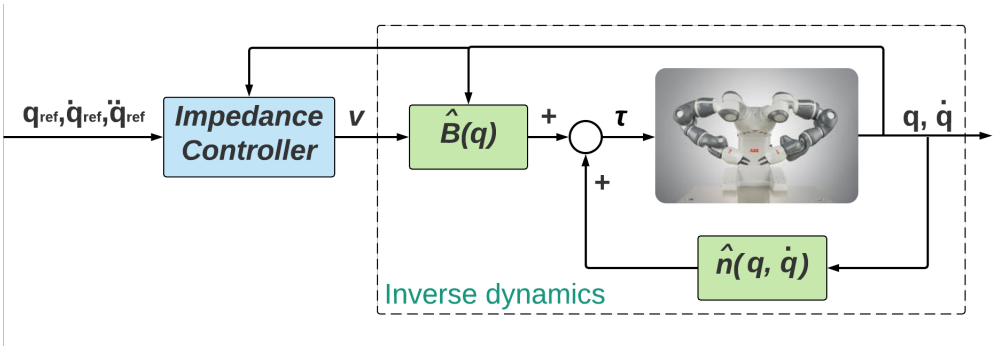

Figure 2.5: Combined Impedance control and Inverse Dynamics Scheme

2.4 Sliding mode control (SMC)

As we mentioned in the subsection 2.3, the direct implementation of impedance controller through inverse dynamics is highly susceptible to uncertainties. System variations and wrong choice of controller parameters can lead to unpredictable behaviour of the system. As discussed in 1, to robustly impose the desired dynamics the non-linear control scheme, *Sliding Mode Control*, is very effective. SMC belong to the class of controllers called Variable Structure Control Systems (VSCS). For a detailed investigation about SMC following researches by Fabio Allevi [3] and S. Spurgeon [5] can be referred. The general scheme of VSCS is shown in figure 2.6. The technique finds application in many fields like robotics, control of electrical drives among others.

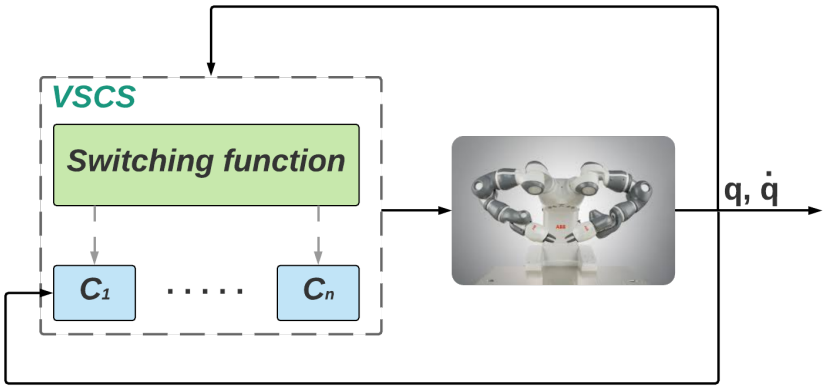

Figure 2.6: VSCS control scheme

The basic idea behind the control scheme is to have different control laws which are based on a decision rule called *switching function*. The state-feedback control law is hence a discontinuous function of time as it can switch from one continuous structure to another based on the feedback. This evolution of the system as it slides along the boundaries of different control structures is called *sliding mode* and the surface consisting these boundaries is called *sliding surface*. The main strength is its robustness and as the sliding mode can be reached in a finite time, that is even better than asymptotic behaviour. The system evolution on sliding surface is however characterized by high-frequency non-deterministic switching control which is often referred as *chattering*. Due to this discontinuous behaviour, they need to be designed with care to obtain a moderate control action.

To understand a typical decision rule, let's consider the system governed by following equations:

$$\dot{\boldsymbol{x}}(t) = \boldsymbol{f}(\boldsymbol{x}, t) + \boldsymbol{B}(\boldsymbol{x}, t)\boldsymbol{u}(t) \tag{2.9a}$$

$$\boldsymbol{x}(t) = \begin{bmatrix} \boldsymbol{x_1}(t) \\ \boldsymbol{x_2}(t) \\ \dots \\ \boldsymbol{x_n}(t) \end{bmatrix} ; \ \boldsymbol{u}(t) = \begin{bmatrix} \boldsymbol{u_1}(t) \\ \boldsymbol{u_2}(t) \\ \dots \\ \boldsymbol{u_n}(t) \end{bmatrix} \tag{2.9b}$$

$$\boldsymbol{u}(t) = \boldsymbol{v}^{eq} - \boldsymbol{v}^{SMC} \tag{2.9c}$$

The task is to design a stat-feedback control law $\boldsymbol{v}(\boldsymbol{x}(t))$ that can stabilize the

system, let say around origin. The designer needs to choose a *switching function* $\boldsymbol{\sigma}$ that in a way represents how far the system is from the sliding manifold. Then feedback gains are selected to ensure the system intersects the sliding surface and stays. It should ensure that system is capable to reach the sliding mode ($\boldsymbol{\sigma(x)} = 0$) along system trajectories and the system dynamics are approximated by $\boldsymbol{\dot{\sigma}(x) = 0}$. The control law finally has a form as equation 2.9c which has two components namely v^{eq} which is the equivalent control signal which is required to maintain the system on the sliding manifold and v^{SMC} which is the discontinuous part that overcomes the affect of uncertainties or disturbances.

Although, SMC provides advantages in terms of disturbance rejection and system robustness. But, these advantages are also accompanied by some undesired behaviours that occur mainly during the sliding mode condition. These are:

- **Excessive control signal:** The standard SMC control signal is of the form $u(t) = v^{eq} - Ksgn(\sigma)$ where the gain 'K' depends on the uncertainty affecting the system. If uncertainty is too large, this term can even dominate the equivalent control signal and the only remedy is to obtain more information about the system to reduce the uncertainty that can allow us to use lower gains.

- **Chattering:** It is the undesired stationary oscillations and in intrinsic to SMC. It affects the control signal as well as other system variables.

- **Uncontrolled reaching phase:** As the desired impedance is enforced only during the sliding phase and before that the control has no authority. Hence, it is desirable to ensure the desired dynamics right from the initial time.

2.5 SMC switching function approximations

In this section, a quick review of various switching functions for sliding mode control scheme is presented. Simulations on the 7-DOF manipulator model have

been reported for a better understanding while further theoretical details are well described in [3].

2.5.1 Signum function

A typical choice for the switching function is a signum function (equation 2.10). It is evident from the choice that we are trying to make $\boldsymbol{\sigma} = \mathbf{0}$ as an attractor for the system.

$$\textit{sliding variable} = \begin{cases} \boldsymbol{K}, & \boldsymbol{\sigma} > \mathbf{0} \\ \mathbf{0}, & \boldsymbol{\sigma} = \mathbf{0} \\ -\boldsymbol{K}, & \boldsymbol{\sigma} < \mathbf{0} \end{cases} \tag{2.10}$$

We can observe high-frequency oscillations in figure 2.7a with signum function, this is due to its discontinuous nature. Ideally an infinite switching frequency is desirable but it is practically impossible due to finite bandwidths of the actuators. To minimize chattering, the control signal should be smoothed while maintaining the robustness to disturbance and uncertainty and so we have the continuous approximations for switching functions. As reported in [7], it is the most logical and immediate way to address this problem.

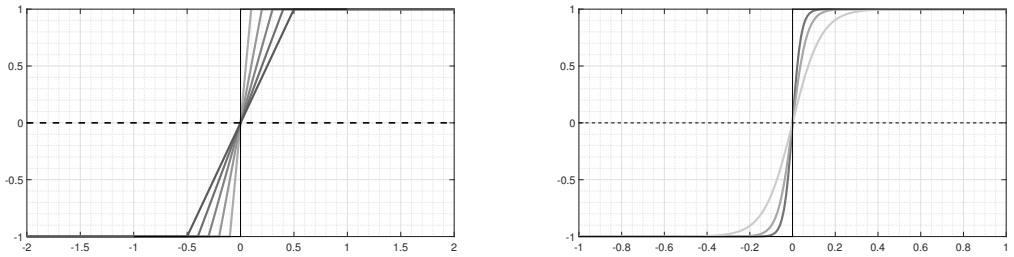

(a) Saturation (Linear) function (b) Sigmoid function

Figure 2.7: Common approximations for switching function, for various δ values

2.5.2 Saturation (Linear) function

This basically considers a linear approximation of the signum function in the neighborhood of the origin and has the following mathematical form:

$$f(\boldsymbol{\sigma}) = \begin{cases} \boldsymbol{sgn(\sigma/\delta)}, & \boldsymbol{-\delta < \sigma < \delta} \\ \boldsymbol{sgn(\sigma)}, & \boldsymbol{otherwise} \end{cases} \tag{2.11}$$

The value of δ defines the closeness to the signum function. Evidently, when $\delta \rightarrow 0$, linear approximation $\rightarrow$ sgn(σ). However, we can no longer guarantee the robustness of the standard SMC scheme. But it can be proved [8], that the system still remains close to the sliding surface although without actual convergence. These control systems are often referred to as *quasi-sliding mode controllers*. A comparison between figure 2.8a and figure 2.8b shows the apparent advantages of linear function over signum function.

2.5.3 Sigmoid function

This ensures that also the derivative of switching function is continuous and has the following mathematical form:

$$f(\boldsymbol{\sigma}) = \boldsymbol{sigmf_{\delta}\sigma} = \frac{\boldsymbol{\sigma}}{\boldsymbol{\delta + |\sigma|}} \tag{2.12}$$

The figure 2.7b shows sigmoid function for different values of δ through a graphical representation. The figure 2.8c reports the joint space tracking error and makes apparent the advantages of sigmoid approximation. The continuous approximation also gives a better control signal i.e. chattering reduction.

2.5.4 Higher-order SMC

Higher Order Sliding Mode Control (HOSMC) generalize the idea of basic SMC. Unlike the standard SMC that acts on the first derivative of the deviation they also act on the higher order time derivatives of the system deviation from the constraints. The *sliding order* defines the degree of smoothness of the system dynamics in the vicinity of the sliding mode. If desired constraint to be satisfied is given by $\sigma = 0$, then the sliding order is the number of derivatives of σ are zero. It further minimizes the chattering effect and improves the control with respect to the previous switching functions (refer figure 2.9).

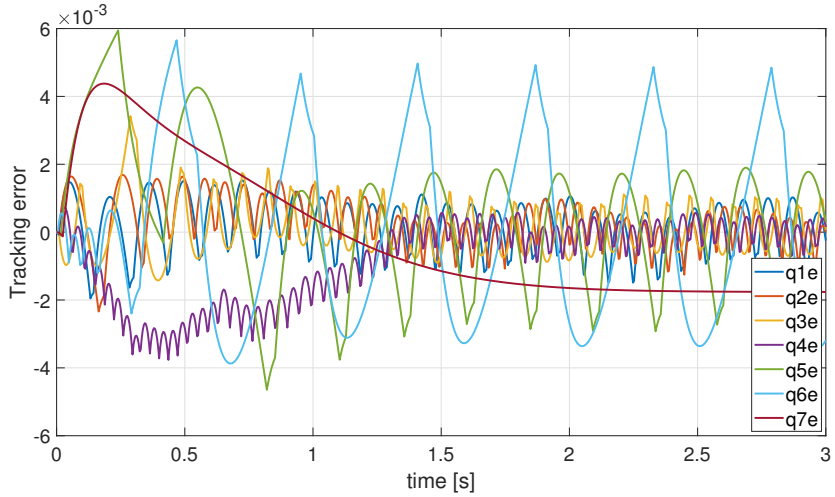

(a) With signum switching function

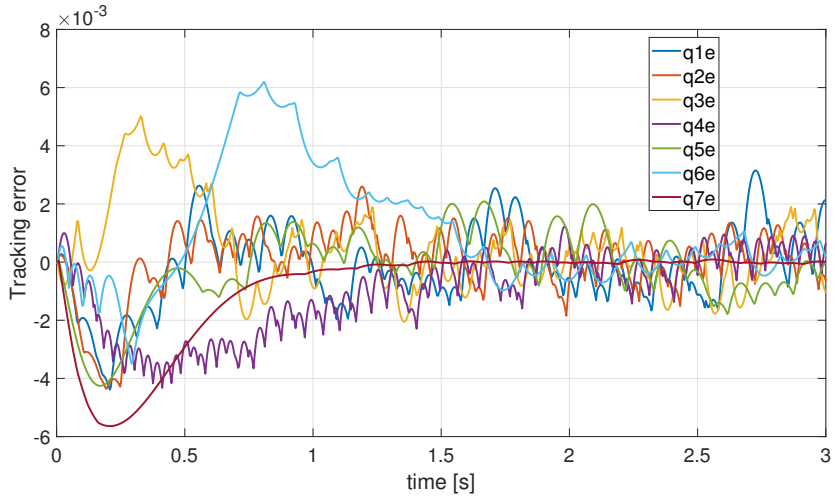

(b) With linear switching function

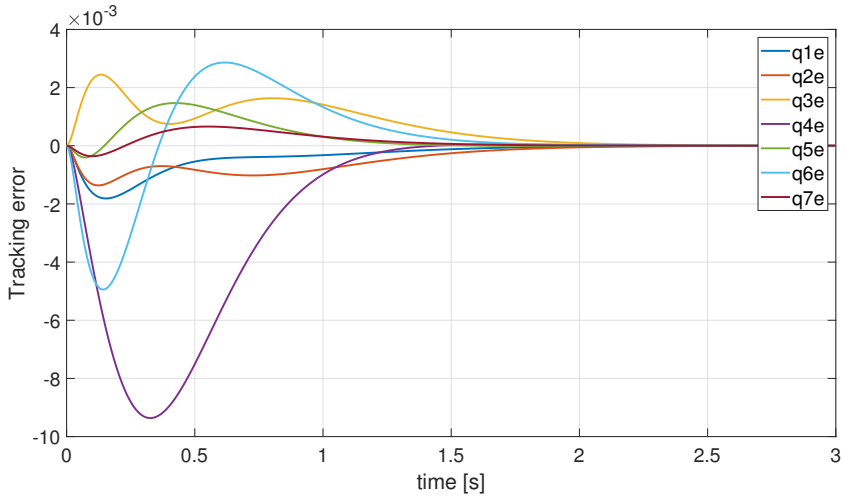

(c) With sigmoid switching function

Figure 2.8: Joint space impedance tracking error for 7-DOF manipulator model

Super twisting algorithm (STA)

Super Twisting Algorithm (STA) uses only the knowledge of σ to define a switching function (equation 2.13) that can guarantee finite time convergence. The trajectories generated are smoother owing to the presence of the term $\sqrt{|\sigma|}$ as:

$$\boldsymbol{v(t) = -k_1\sqrt{|\sigma|}sgn(\sigma) - k_2 \int sgn(\sigma)} \tag{2.13}$$

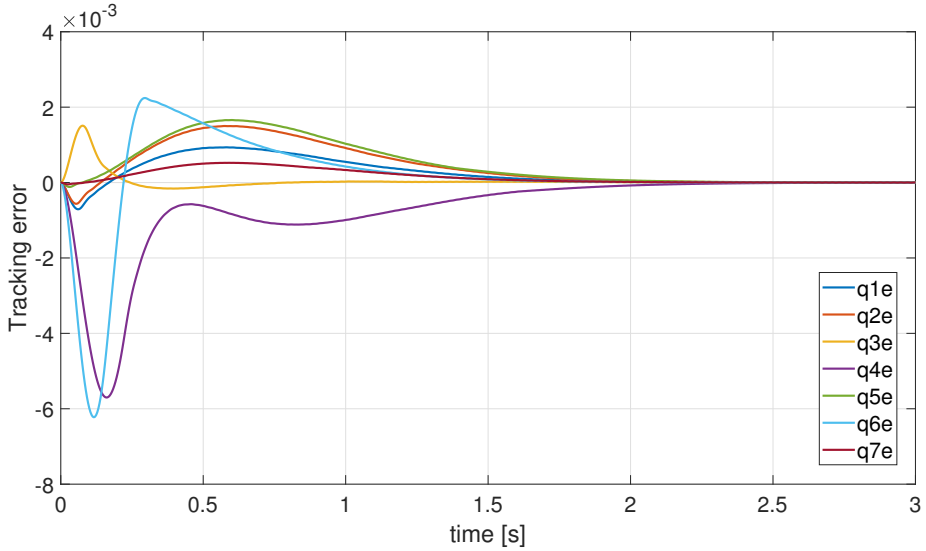

Figure 2.9: Joint space impedance tracking error for 7-DOF manipulator model with SMC with Super Twisting Algorithm

2.6 Integral sliding mode control

Now chattering can be minimized and sliding mode reachable in a finite time but we still cannot guarantee the system evolution before that. The problem is already well studied and can be referred through the literature [11], [12], [13]. The ISMC technique adjusts the SMC by certain means to ensure the sliding mode right from the initial time. A general form of the implementation has the following form:

$$\boldsymbol{\Sigma(x(t)) = \sigma(x(t)) - \lambda(t)} \tag{2.14}$$

where σ is the standard sliding surface and λ is a suitable reaching function. A comparison between figures 2.10a and 2.10b clearly reveals that with ISMC sliding mode is enforced right from the initial time i.e. condition $\sigma = 0$ is valid throughout the control period irrespective of the initial state of the system.

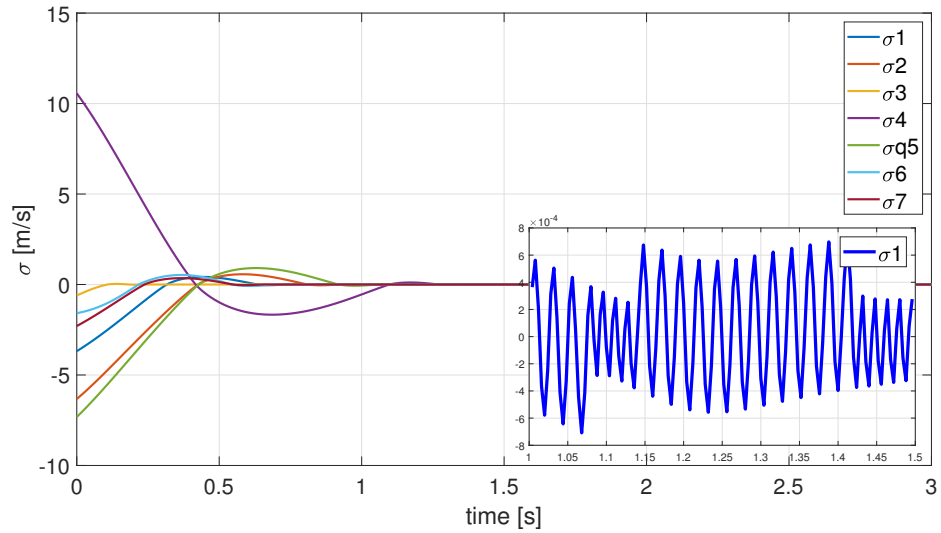

(a) SMC without correction for initial transient

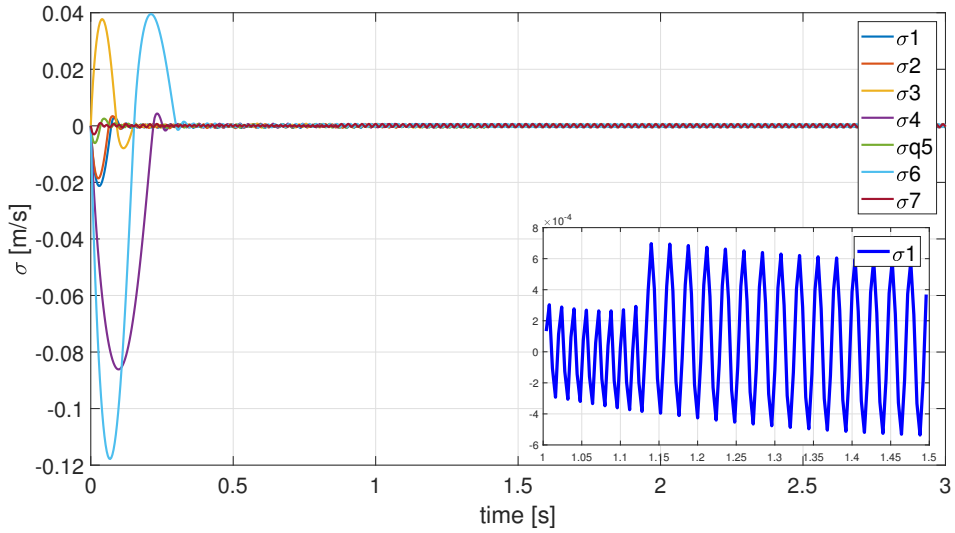

(b) Integral sliding mode control (ISMC)

Figure 2.10: Sliding variable evolution during joint space impedance tracking for 7-DOF manipulator (Standard SMC vs ISMC)

2.7 Sliding-mode Model Predictive Control

In Section 1, we talked about dexterous manipulation. In this context, we not only want to enforce a desired dynamics but we also but also to respect certain linear or non-linear constraints that may arise due to the environmental factors or some operational reasons. This basically led to the integration of robust Model Predictive Control (MPC) with SMC to what we call Sliding-mode Model Predictive Control (SMPC) [15, 17]. This approach is very powerful because it combines the compensation of uncertainties and disturbances by SMC while guaranteeing optimal evolution of the controlled system fulfilling the desired constraints. Thus, combining the versatility of MPC with robustness of SMC control. This basically translates the control task into an optimization problem [14]. A general control scheme of SMPC is shown in figure 2.11.

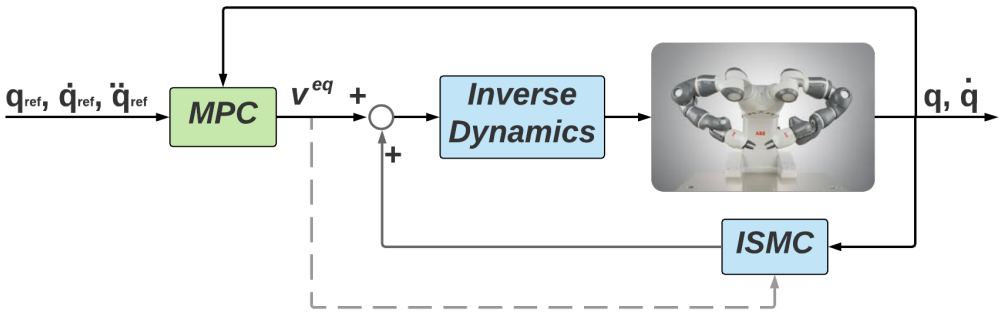

Figure 2.11: SMPC scheme: MPC + SMC to avoid constraint violation

As mentioned in the previous section, the equivalent control (v^{eq}) is calculated directly from $\dot{\sigma} = 0$ and we will see in next section how to formulate this into a Quadratic Programming (QP) problem.

2.7.1 QP Formulation

Many practical applications require a solution to optimization problem that can be either expressed as Quadratic Programming (QP) problems or require their solutions. *qpOASES* provides a reliable and efficient way which is an open source

C++ software package. The problem that the qpOASES solver is able to solve have to be expressed in the following form:

$$\boldsymbol{min_x}\left\{\frac{\mathbf{1}}{\mathbf{2}}\boldsymbol{x^T H_{qp} x} + \boldsymbol{x^T g_{qp}}\right\} \tag{2.15a}$$

$$s.t. \quad \boldsymbol{lb} \leq \boldsymbol{x} \leq \boldsymbol{ub} \tag{2.15b}$$

$$\boldsymbol{lbC} \leq \boldsymbol{Cx} \leq \boldsymbol{ubC} \tag{2.15c}$$

where equations 2.15c and 2.15c represent the constraints on the optimization. Simple algebraic manipulation can show that any task of the form $Ax = b$ can be performed by carrying out the minimization reported in equation 2.16. As we will see in the next chapter, we will solver optimization problem using this formulation. Note: multiple cost functions can be solved together while concatenating the constraints [14, 18, 22].

$$\begin{aligned} &\boldsymbol{min_x}\frac{\mathbf{1}}{\mathbf{2}}\boldsymbol{||Ax - b||_Q} \\ &\boldsymbol{H = A^T Q A} \\ &\boldsymbol{g = -A^T Q b} \end{aligned} \tag{2.16}$$

Chapter 3

Decentralized Control

In this chapter, a detailed analysis of Sliding-mode Model Predictive Control (SMPC) is conducted. The previous work by Fabio Allevi [3] has established conceptual foundations and has experimentally verified the decentralized control technique based on SMC. But, the discussion presented about SMPC was limited to the brevity of its advantages. First, a brief theory of decentralized SMC is presented. Then the effect of delayed torque is summarized. Then a detailed theory of predictive SMC is reported supported by simulation results. Here, in particular the implementation of SMC is reported in the presence of uncertainty in robot dynamic model (matrices B and n) and a delay on the torque communication channel. Generic mathematical model of the system joint variable predictors are developed. This model will be later used to compute estimators of different prediction horizon for the implementation of operational space impedance control in chapter 4 and chapter 5.

The main objective for this discussion lies in the fact that finite actuator dynamics and time delay are an additional source of chattering apart from the discontinuity in the control signal. They can result in the loss of phase margin and increased oscillations. The results have been verified through simulations on 7-DOF manipulator model of ABB YuMi introduced in section 2.1. *Peter Corke's Robotic Toolbox for MATLAB* has been used to generate this model.

3.1 Decentralized SMC

Let's consider a generic robot model introduced in section 2.1. Applying inverse dynamics control law (2.7) we will have:

$$\begin{aligned} \ddot{\boldsymbol{q}} &= \boldsymbol{v} + (\boldsymbol{B^{-1}}\hat{\boldsymbol{B}} - \boldsymbol{I})\boldsymbol{v} + \boldsymbol{B^{-1}}\widetilde{\boldsymbol{n}} \;\; = \boldsymbol{v} - \boldsymbol{\eta} \\ \boldsymbol{\eta} &= (\boldsymbol{I} - \boldsymbol{B^{-1}}\hat{\boldsymbol{B}})\boldsymbol{v} - \boldsymbol{B^{-1}}\widetilde{\boldsymbol{n}} \end{aligned} \tag{3.1}$$

where $\widetilde{n} = \hat{n} - n$. The equation 3.1 shows its strong coupling with the system uncertainties due to imperfect dynamic cancellation by inverse dynamics and if the model knowledge is sufficiently accurate, these terms η can be treated as a disturbance. As we mentioned in section 2.4, SMC is capable to reject disturbances while ensuring desired dynamics. Here, we will enforce this in the joint space independently for each joint through a decentralized scheme:

$$\bar{\boldsymbol{B}}\ddot{\boldsymbol{q}} + \bar{\boldsymbol{C}}\dot{\boldsymbol{q}} + \bar{\boldsymbol{g}}\boldsymbol{q} = -\boldsymbol{J^T}\boldsymbol{h} \tag{3.2}$$

where $\bar{\mathbf{B}} = diag(b1, b2, ...), \bar{\mathbf{C}} = diag(c1, c2, ...)\, and \bar{\mathbf{g}} = diag(g1, g2, ...)$ define the desired dynamics. Note: in further developments we will drop the term for external forces assuming that a sufficiently accurate force estimation can assist in it's successful compensation in the control signal computation. Let's derive the control signal for SMC by defining the sliding surface such that $\dot{\sigma} = 0$ is the desired dynamics.

$$\boldsymbol{\sigma} = \bar{\boldsymbol{B}}(\dot{\boldsymbol{q}} - \dot{\boldsymbol{q}}_{\boldsymbol{ref}}) + \bar{\boldsymbol{C}}(\boldsymbol{q} - \boldsymbol{q}_{\boldsymbol{ref}}) + \int_{\boldsymbol{0}}^{\boldsymbol{t}} (\bar{\boldsymbol{g}}(\boldsymbol{q} - \boldsymbol{q}_{\boldsymbol{ref}}) + \boldsymbol{J}(\boldsymbol{q}(\boldsymbol{\tau}))^{\boldsymbol{T}}\boldsymbol{h})\boldsymbol{d\tau} \tag{3.3}$$

To impose limits on joint positions, velocities and acceleration we will formulate a QP problem for the control signal computation. To achieve this, we will first express the desired dynamics in the form of equation 2.6 and then use the obtained H, g and joint limits as the inputs to qpOASES solver.

3.2 Predictive SMC

In many practical applications, time delay is often encountered and is a significant source of instabilities and unsatisfactory performance. Hence, the problem of time delay has received considerable attention and different approaches have been suggested [23, 24, 25]. It's strong sensitivity to uncertainties can drastically affect system performance. Although, SMC has intrinsic capability to keep the system insensitive to these uncertainties on the sliding surface but it's applicability has to be carefully investigated.

3.2.1 Delayed torque: response without prediction

Let's, consider the presence of a known delay (2 time steps) on the control signal (torque) of our 7-DOF manipulator model and implement directly the SMC control based on the σ defined in equation 3.3. We can clearly observe stable oscillatory behaviour both in the joint space position response as well as the control signal in figure 3.2. So, the trajectories start from origin and at steady state end up in a limit cycle rather than converging back to origin, see figure 3.1.

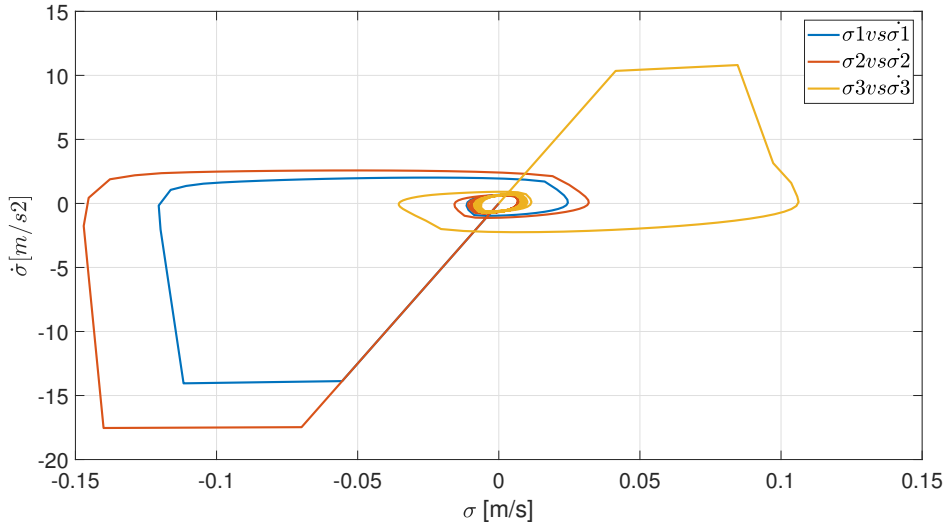

Figure 3.1: Phase diagram for sliding surface showing the presence of limit cycles

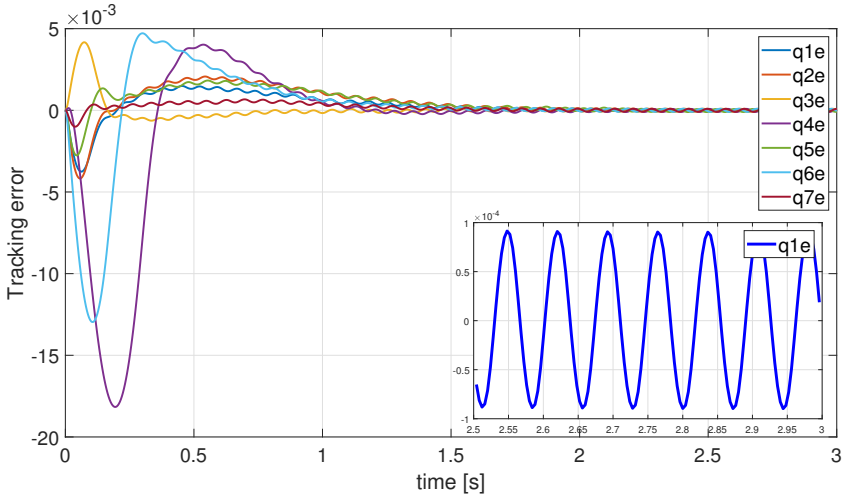

(a) Joint space tracking

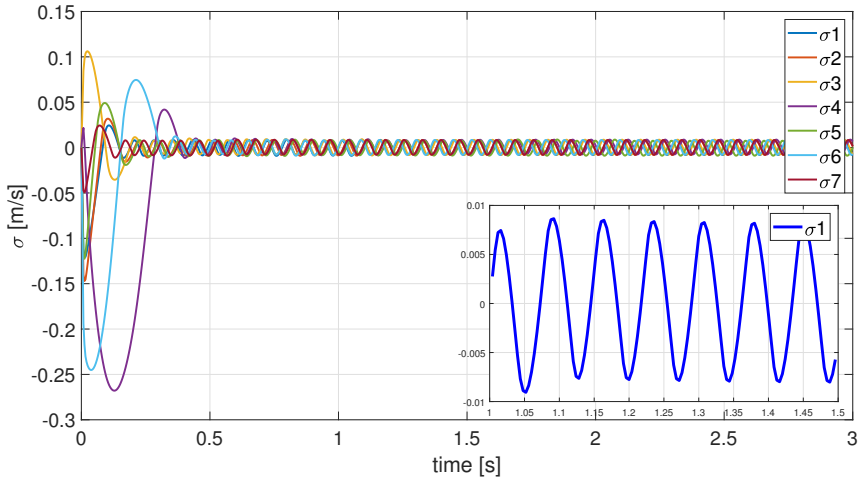

(b) Sliding surface

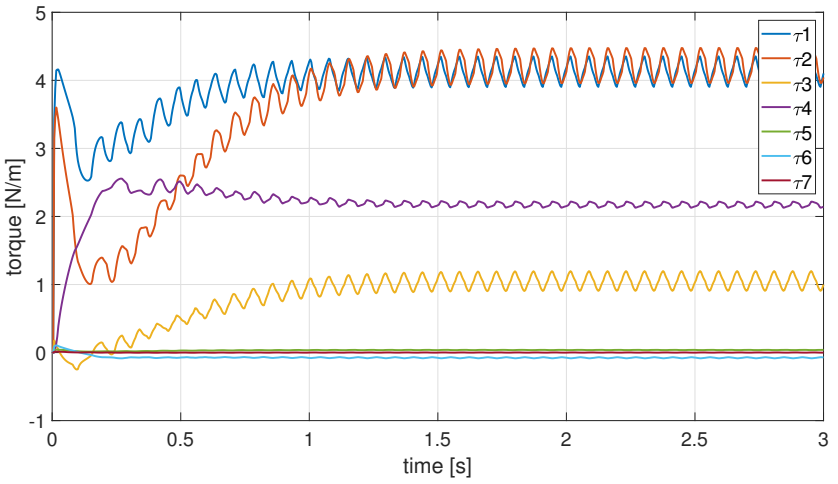

(c) Control signal

Figure 3.2: Joint space impedance control with 2-step delayed torque: 7-DOF YuMi model

3.2.2 Delayed torque: predictive SMC response

If there is a known constant delay d acting on the torque communication channel, it is possible to overcome this problem by using the predicted values of the joint variables and the sliding surface, say $\hat{\sigma}(t+d|t)$. The technique is called *Predictive SMC* and a general scheme of implementation is shown in figure 3.3.

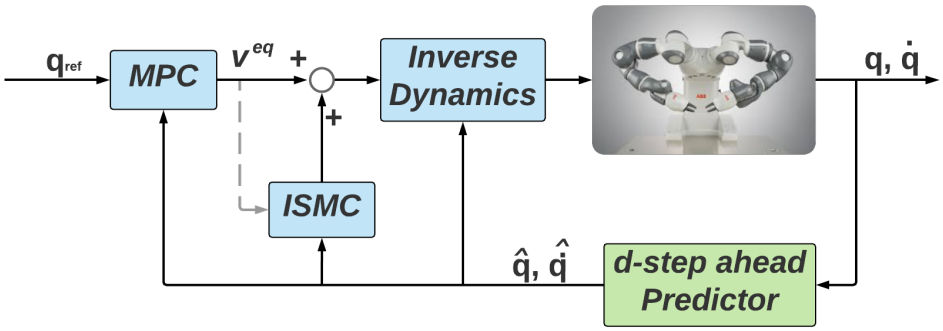

Figure 3.3: Predictive SMC: block diagram

For our second order robotic system we expect to have a chain of two integrators after all uncertainties and non-linearities are taken care off by SMC and inverse dynamics together, $\ddot{q} = v$. For a delay of d time steps, formulation of a d-step predictor is reported here which needs discretization of state evolution and for which we adopted *forward euler method* because of computational simplicity as it is explicit.

$$
\begin{aligned}
&\dot{\boldsymbol{z}}(\boldsymbol{t}) = \boldsymbol{v}(\boldsymbol{t} - \boldsymbol{d}.\boldsymbol{T_s}) \\
&\hat{\boldsymbol{z}}(\boldsymbol{k}+\boldsymbol{1}) = \boldsymbol{z}(\boldsymbol{k}) + \boldsymbol{T_s}\boldsymbol{v}(\boldsymbol{k}-\boldsymbol{d}) \\
&\hat{\boldsymbol{z}}(\boldsymbol{k}+\boldsymbol{2}) = \boldsymbol{z}(\boldsymbol{k}) + \boldsymbol{T_s}\boldsymbol{v}(\boldsymbol{k}-\boldsymbol{d}) + \boldsymbol{T_s}\boldsymbol{v}(\boldsymbol{k}-\boldsymbol{d}+\boldsymbol{1}) \\
&\textit{and so on} \\
&\hat{\boldsymbol{z}}(\boldsymbol{k}+\boldsymbol{d}) = \boldsymbol{z}(\boldsymbol{k}) + \boldsymbol{T_s}\boldsymbol{v}(\boldsymbol{k}-\boldsymbol{d}) + \ldots + \boldsymbol{T_s}\boldsymbol{v}(\boldsymbol{k}-\boldsymbol{1})
\end{aligned}
\tag{3.4a}
$$

$$
\begin{aligned}
&\dot{\boldsymbol{y}}(\boldsymbol{t}) = \boldsymbol{z}(\boldsymbol{t}) \\
&\hat{\boldsymbol{y}}(\boldsymbol{k+1}) = \boldsymbol{y}(\boldsymbol{k}) + \boldsymbol{T_s z}(\boldsymbol{k}) \\
&\hat{\boldsymbol{y}}(\boldsymbol{k+2}) = \boldsymbol{y}(\boldsymbol{k}) + \boldsymbol{2T_s z}(\boldsymbol{k}) + \boldsymbol{T_s^2 v}(\boldsymbol{k-d}) \\
&\textit{and so on} \\
&\hat{\boldsymbol{y}}(\boldsymbol{k+d}) = \boldsymbol{y}(\boldsymbol{k}) + \boldsymbol{d.T_s z}(\boldsymbol{k}) + \boldsymbol{(d-1)T_s^2 v}(\boldsymbol{k-d}) + \\
&\quad \dot{\boldsymbol{x}}(\boldsymbol{t}) = \boldsymbol{y}(\boldsymbol{t}) \quad \boldsymbol{(d-2)T_s^2 v}(\boldsymbol{k-d+1}) + \boldsymbol{...} + \boldsymbol{T_s^2 v}(\boldsymbol{k-2}) \\
&\quad \hat{\boldsymbol{x}}(\boldsymbol{k+1}) = \boldsymbol{x}(\boldsymbol{k}) + \boldsymbol{T_s y}(\boldsymbol{k}) \\
&\quad \hat{\boldsymbol{x}}(\boldsymbol{k+2}) = \boldsymbol{x}(\boldsymbol{k}) + \boldsymbol{2T_s y}(\boldsymbol{k}) + \boldsymbol{T_s^2 z}(\boldsymbol{k}) \\
&\quad \hat{\boldsymbol{x}}(\boldsymbol{k+3}) = \boldsymbol{x}(\boldsymbol{k}) + \boldsymbol{3T_s y}(\boldsymbol{k}) + \boldsymbol{3T_s^2 z}(\boldsymbol{k}) + \boldsymbol{T_s^3 v}(\boldsymbol{k-d}) \\
&\quad \textit{and so on} \\
&\quad \hat{\boldsymbol{x}}(\boldsymbol{k+d}) = \boldsymbol{x}(\boldsymbol{k}) + \boldsymbol{d.T_s y}(\boldsymbol{k}) + \frac{\boldsymbol{d(d-1)}}{\boldsymbol{2}}\boldsymbol{T_s^2 z}(\boldsymbol{k}) + \\
&\qquad \frac{\boldsymbol{(d-1)(d-2)}}{\boldsymbol{2}}\boldsymbol{T_s^3 v}(\boldsymbol{k-d}) + \ \boldsymbol{...} \\
&\qquad + \frac{\boldsymbol{3.2}}{\boldsymbol{2}}\boldsymbol{T_s^3 v}(\boldsymbol{k-4}) + \frac{\boldsymbol{2.1}}{\boldsymbol{2}}\boldsymbol{T_s^3 v}(\boldsymbol{k-3})
\end{aligned}
\tag{3.4b}
\tag{3.4c}
$$

replacing z, y, x in equation with $\dot{q}, q, \int q$, we can obtain the d-steps ahead predicted values of the joint position, velocities and integral of joint position respectively. To compare the results of predictive SMC from the results reported in figure 3.2, we have again considered a 2-step delayed torque signal. The equations for $\hat{\dot{q}}(k+2)$, $\hat{q}(k+2)$ and $\hat{\int} q(k+2)$ follow directly from equation 3.4.

$$\hat{\dot{\boldsymbol{q}}}(\boldsymbol{k+2}) = \dot{\boldsymbol{q}}(\boldsymbol{k}) + \boldsymbol{T_s v}(\boldsymbol{k-2}) + \boldsymbol{T_s v}(\boldsymbol{k-1}) \tag{3.5a}$$

$$\hat{\boldsymbol{q}}(\boldsymbol{k+2}) = \boldsymbol{q}(\boldsymbol{k}) + \boldsymbol{2T_s \dot{q}}(\boldsymbol{k}) + \boldsymbol{T_s^2 v}(\boldsymbol{k-2}) \tag{3.5b}$$

$$\hat{\int}\, \boldsymbol{q}(\boldsymbol{k+2}) = \int \boldsymbol{q}(\boldsymbol{k}) + \boldsymbol{2T_s q}(\boldsymbol{k}) + \boldsymbol{T_s^2 \dot{q}}(\boldsymbol{k}) \tag{3.5c}$$

Replacing $\dot{q}, q$ and $\int q$ in equation 3.3 by their predicted values from equation 3.5 we get:

$$\hat{\boldsymbol{\sigma}}(\boldsymbol{k+2}) = \bar{\boldsymbol{B}}\hat{\dot{\boldsymbol{q}}}(\boldsymbol{k+2}) + \bar{\boldsymbol{C}}(\hat{\boldsymbol{q}}(\boldsymbol{k+2}) - \boldsymbol{q_{ref}}) + \bar{\boldsymbol{g}}\hat{\int}\, \boldsymbol{q}(\boldsymbol{k+2}) \tag{3.6}$$

as it was reported in section 2.4 the system dynamics is approximated by $\dot{\boldsymbol{\sigma}} = \mathbf{0}$. The relation can then be expressed in the form $A(q)v = b(q)$ to finally determine the terms H, g using equation 2.16. Note: we use predicted values to formulate the QP problem as:

$$\begin{aligned} \hat{\boldsymbol{H}} &= \boldsymbol{H} = \boldsymbol{I} \\ \hat{\boldsymbol{g}} &= \bar{\boldsymbol{B}}^{-1}(\bar{\boldsymbol{C}}\hat{\dot{\boldsymbol{q}}}(\boldsymbol{k}+\mathbf{2}) + \bar{\boldsymbol{g}}(\hat{\boldsymbol{q}}(\boldsymbol{k}+\mathbf{2}) - \boldsymbol{q_{ref}})) \end{aligned} \tag{3.7a}$$

$$\begin{aligned} \boldsymbol{q_{min}} \leq \boldsymbol{q} &\leq \boldsymbol{q_{max}} \\ |\dot{\boldsymbol{q}}| &\leq \dot{\boldsymbol{q}}_{\boldsymbol{max}} \\ |\ddot{\boldsymbol{q}}| &\leq \ddot{\boldsymbol{q}}_{\boldsymbol{max}} \end{aligned} \tag{3.7b}$$

The joint limit formulation of equation 3.7b is not suitable to express the relationships between position, velocity and acceleration. A method that considers the dynamic properties of velocity provides a more suitable way of expressing joint limits by utilizing a quadratic relationship between position and velocity. Finally, we use these as inputs to qpOASES to solve an optimization problem to obtain $\hat{v}^{eq}$ and SMC contribution to the control signal $\hat{u}^{SMC}$ using $\hat{\sigma}$. The final torque to the robot model is the Sliding-mode Model Predictive Control (SMPC) control law, given by:

$$\boldsymbol{v}|_{\boldsymbol{PredictiveSMC}} = \hat{\boldsymbol{v}}^{\boldsymbol{eq}} + \hat{\boldsymbol{v}}^{\boldsymbol{SMC}} \tag{3.8}$$

The figure 3.4 compares the sliding surface and it's phase plane evolution. It verifies that predictive SMC successfully eliminates the presence of limit cycles. Note: the convergence of estimators used relies on the rejection capabilities of SMC. Also, notice that the sliding surface shown is actually integral sliding mode.

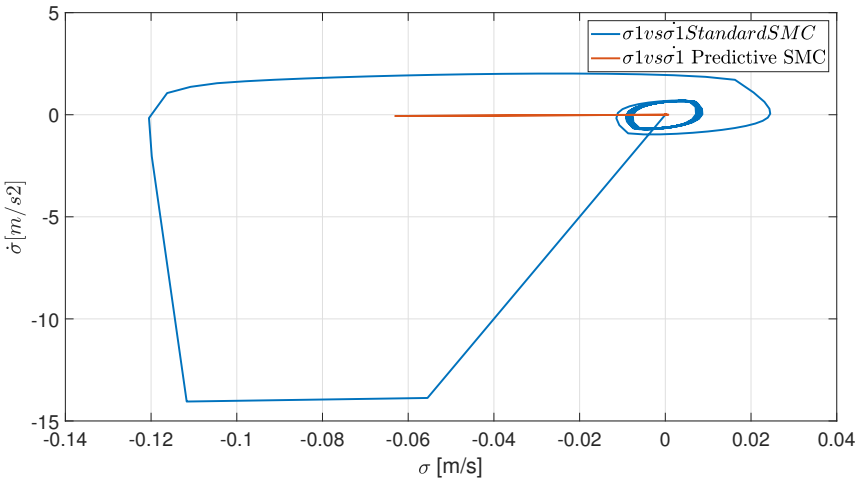

(a) Phase diagram

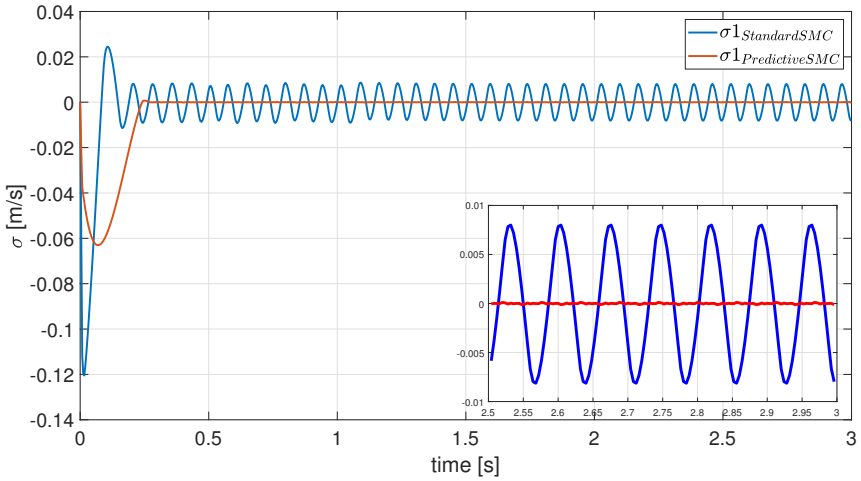

(b) Sliding surface

Figure 3.4: Standard SMC vs Predictive SMC

The figure 3.5 compares the simulations for standard SMC and predictive SMC via tracking error and control signal (torque) for the first joint position. The oscillatory behaviour due to the presence of delay on the torque channel is successfully eliminated providing smooth control signal as well as joint space tracking. Hence, predictive SMC evidently improves stability and sliding precision. Unfortunately, decentralized control presents some major drawbacks:

- It may require very **high SMC gains** to reject uncertainties due to inaccurate inverse dynamics. Also, the uncertainties depend on the robot

configuration which makes it difficult to set the value of SMC gain.

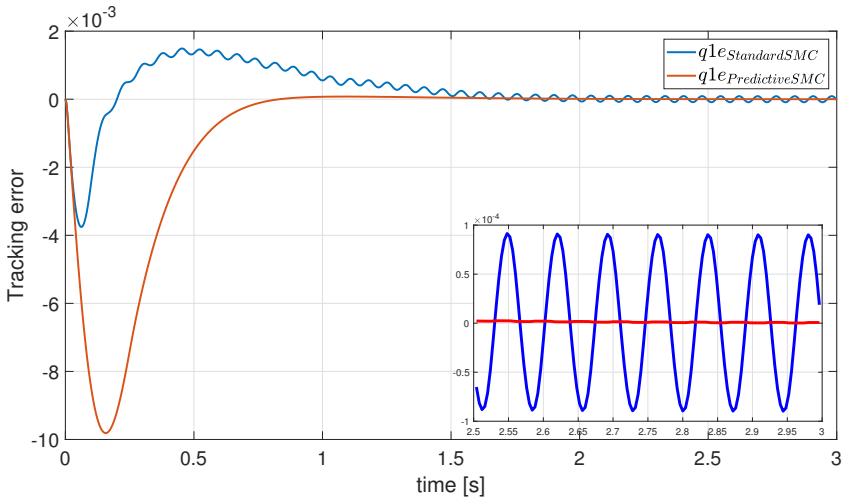

(a) Tracking error

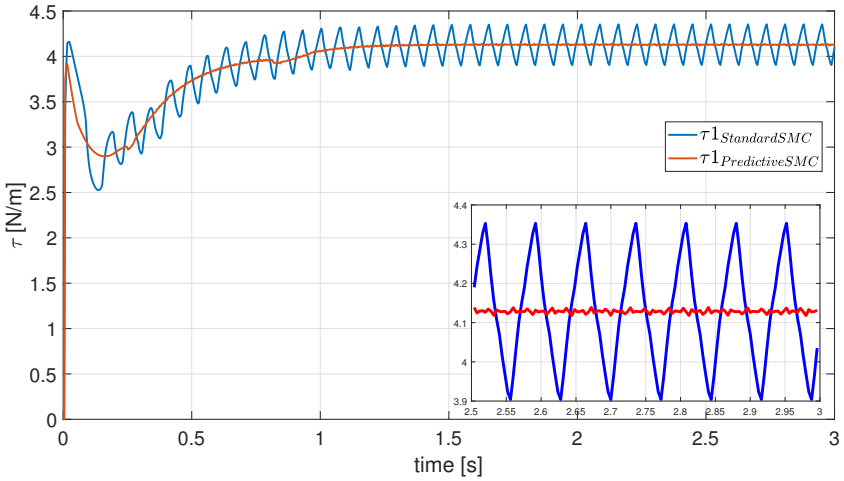

(b) Control signal

Figure 3.5: Standard SMC vs Predictive SMC

- It cannot impose desired dynamics directly to the end-effector and hence we have **configuration dependent impedance**. For many practical applications where we require dexterous manipulation of the end-effector e.g. robot teleoperation, we often desire constant impedance to enhance user experience. And this limits the applicability of the control architecture.

Chapter 4

Robust Centralized Control

With the growing interest about robot systems in interactive applications, the dexterity of manipulation is highly desirable and redundant manipulators offer potential advantages. In this chapter a detailed discussion about the operational space control architecture is reported.

Many robots are equipped with internal industrial controllers which can have filters on the control signal. And often they do not provide the freedom to modify it. Hence, the operational space control strategies have been divided in two categories viz. chapter 4: without the consideration of filter on the torque (control signal) channel and chapter 5: with filter on torque channel. In this chapter, the effect of uncertain robot dynamic model, delay on torque channel and joint friction on the system response is reported. The complexity or sources of instability are added step by step so as to clearly understand the affect of each source separately to finally address them together through a unified control strategy. An extensive analysis of the behaviour of robot redundancy has been performed by considering different optimization for the QP formulation to ensure desired dynamic behaviour while satisfying different constraints on the joint limits.

All the obtained results have been verified through simulations on 2-DOF manipulator and then on the 7-DOF YuMi right arm model.

4.1 Operational space SMC

By defining control objectives directly in the manipulator operational space the problems of decentralized control scheme can be resolved. It is able to enforce a known-constant dynamics to the end-effector which can be defined by mass, damping and stiffness parameters with clear physical interpretation.

As we did in decentralized scheme, we again start with inverse dynamics to get the equation $\ddot{q} = v - \eta$. Though we have the same equation, but the implementation for the control is completely different. For decentralized control scheme we assumed a complete decoupling of joints but for centralized scheme we will define v using all joint information. Also, we will define the desired dynamics directly in the manipulator operational space. The desired end-effector impedance can be a general n-dimensional (1-DOF, 3-DOF for (x,y,z), 6-DOF full end-effector position and orientation) formulation depending on the degrees of freedom of the manipulator.

$$\bar{\boldsymbol{M}}\ddot{\boldsymbol{x}} + \bar{\boldsymbol{D}}\dot{\boldsymbol{x}} + \bar{\boldsymbol{K}}\boldsymbol{x} = \boldsymbol{h} \tag{4.1}$$

where $\bar{\mathbf{M}} = diag(m_1, ..., m_n), \bar{\mathbf{D}} = diag(d_1, ..., d_n), \bar{\mathbf{K}} = diag(k_1, ..., k_n)$ and $\boldsymbol{h}$ is the external force acting on the end-effector. The definitions should be adapted as per the choice of degrees of freedom for the impedance. The objective is to obtain the desired dynamics rejecting the uncertainties and the coupling due to imperfect inverse dynamics (defined as disturbances in equation 3.1).

4.1.1 Operational space sliding surface

The steps to obtain the sliding surface will be similar to the ones adopted in section 3.1. The basic idea remains the same i.e. when the system evolves on the sliding manifold it follows the desired dynamics. This is possible by ensuring that $\dot{\sigma} = 0$ on the sliding surface. For the same reasons we will drop the term h as we can ensure a proper compensation for it in the control signal computation

through its estimation. The impedance profile can now be written as:

$$\boldsymbol{I} = \bar{\boldsymbol{M}}\ddot{\boldsymbol{x}} + \bar{\boldsymbol{D}}\dot{\boldsymbol{x}} + \bar{\boldsymbol{K}}\boldsymbol{x} - \boldsymbol{h} \tag{4.2}$$

and the sliding manifold can hence be expressed by the integration of 4.2:

$$\boldsymbol{S} = \int \boldsymbol{I} = \bar{\boldsymbol{M}}\dot{\boldsymbol{x}} + \bar{\boldsymbol{D}}\boldsymbol{x} + \bar{\boldsymbol{K}} \int \boldsymbol{x} - \int \boldsymbol{h} \tag{4.3}$$

using manipulator forward and differential kinematics we can express the Cartesian positions, velocities and acceleration in joint coordinates:

$$\boldsymbol{x} = \boldsymbol{T}(\boldsymbol{q}); \qquad \dot{\boldsymbol{x}} = \boldsymbol{J}(\boldsymbol{q})\dot{\boldsymbol{q}}; \qquad \ddot{\boldsymbol{x}} = \boldsymbol{J}(\boldsymbol{q})\ddot{\boldsymbol{q}} + \dot{\boldsymbol{J}}(\boldsymbol{q})\dot{\boldsymbol{q}} \tag{4.4}$$

where $T(q)$ represents direct kinematics and $J(q)$ is the Jacobian matrix. Substituting 4.4 in 4.3 we get:

$$\boldsymbol{S} = \bar{\boldsymbol{M}}\boldsymbol{J}(\boldsymbol{q})\dot{\boldsymbol{q}} + \bar{\boldsymbol{D}}\boldsymbol{T}(\boldsymbol{q}) + \bar{\boldsymbol{K}} \int \boldsymbol{T}(\boldsymbol{q}) - \int \boldsymbol{h} \tag{4.5}$$

The *kineto-static duality* of robotic manipulators i.e. $\tau = J(q)^T h$ is used to get $\boldsymbol{I_\tau} = \boldsymbol{J}(\boldsymbol{q})^{\boldsymbol{T}}\boldsymbol{I}$ as impedance is nothing but torque and force balance at the end-effector. But, due to the dependency on acceleration ($\ddot{x}$) it cannot be used as the sliding surface. An alternative operational space sliding surface is defined as:

$$\begin{aligned} \boldsymbol{\sigma_{op}} &= \boldsymbol{J}(\boldsymbol{q})^{\boldsymbol{T}}\boldsymbol{S} \\ &= \boldsymbol{J}(\boldsymbol{q})^{\boldsymbol{T}}\left[\bar{\boldsymbol{M}}\boldsymbol{J}(\boldsymbol{q})\dot{\boldsymbol{q}} + \bar{\boldsymbol{D}}\boldsymbol{T}(\boldsymbol{q}) + \bar{\boldsymbol{K}} \int \boldsymbol{T}(\boldsymbol{q}) - \int \boldsymbol{h}\right] \end{aligned} \tag{4.6}$$

Theoretical proof exists that guarantees desired dynamic convergence, it says if $\boldsymbol{\sigma_{op}} = \boldsymbol{0}\ \forall \boldsymbol{t} \geq \boldsymbol{t_f}$ then $\boldsymbol{I} = \boldsymbol{0}\ \forall \boldsymbol{t} \geq \boldsymbol{t_f}$ and hence, the correct impedance profile is traversed. The detailed theoretical discussion has been reported by Fabio Allevi [3]. Although $\int I_\tau$ is different from σ_{op} but they share the same sliding surface.

4.1.2 Centralized equivalent control

It is required to maintain the system on the sliding manifold and it will be computed by equating the derivative of sliding variable to zero. This was represented as v^{eq} in section 2.4. But, we can also directly use the impedance profile I as in sliding mode $\sigma_{op} = 0$ and $\dot{\sigma}_{op} = 0$ but also $I = 0$. Substituting the kinematic relationships 4.4 to get the desired impedance profile in terms of joint variables:

$$\bar{\boldsymbol{M}}\left(\boldsymbol{J}(\boldsymbol{q})\ddot{\boldsymbol{q}} + \dot{\boldsymbol{J}}(\boldsymbol{q})\dot{\boldsymbol{q}}\right) + \bar{\boldsymbol{D}}\boldsymbol{J}(\boldsymbol{q})\dot{\boldsymbol{q}} + \bar{\boldsymbol{K}}\boldsymbol{T}(\boldsymbol{q}) - \boldsymbol{h} = \boldsymbol{0} \tag{4.7}$$

The equivalent control law is computed for the system in nominal conditions and for our 2nd order system we consider a chain of two integrators $\ddot{q} = v$. Using this we finally can come up with a formulation that can be used as a cost function for the quadratic optimization.

$$\bar{\boldsymbol{M}}\left(\boldsymbol{J}(\boldsymbol{q})\boldsymbol{v} + \dot{\boldsymbol{J}}(\boldsymbol{q})\dot{\boldsymbol{q}}\right) + \bar{\boldsymbol{D}}\boldsymbol{J}(\boldsymbol{q})\dot{\boldsymbol{q}} + \bar{\boldsymbol{K}}\boldsymbol{T}(\boldsymbol{q}) - \boldsymbol{h} = \boldsymbol{0} \tag{4.8a}$$

$$\boldsymbol{A}(\boldsymbol{q})\boldsymbol{v} = \boldsymbol{b}(\boldsymbol{q}) \tag{4.8b}$$

where $\boldsymbol{A}(\boldsymbol{q}) = \bar{\boldsymbol{M}}\boldsymbol{J}(\boldsymbol{q})$ and $\boldsymbol{b}(\boldsymbol{q}) = \boldsymbol{h} - \bar{\boldsymbol{M}}\dot{\boldsymbol{J}}(\boldsymbol{q})\dot{\boldsymbol{q}} - \bar{\boldsymbol{D}}\dot{\boldsymbol{q}} - \bar{\boldsymbol{K}}\boldsymbol{T}(\boldsymbol{q})$. This leads us to following two conditions:

- A(q) is invertible square matrix i.e. $\boldsymbol{v^{eq}} = \boldsymbol{A(q)^{-1}b(q)}$
- A(q) is under-determined i.e. it's rank is less than the manipulator's DOFs. In other words dimension of desired impedance is lower than manipulator's DOFs. This is the typical case of redundant manipulators. It is possible to formulate the relation 4.8b as a quadratic optimization problem as: $\boldsymbol{C} = ||\boldsymbol{A}(\boldsymbol{q})\boldsymbol{v} - \boldsymbol{b}(\boldsymbol{q})||^{\boldsymbol{2}}$.

We are interested in the 2nd case as we can use MPC architecture to use full capabilities of redundant manipulators by imposing additional constraints to address our objective i.e. dexterous manipulation in operational space.

4.2 Kinematically redundant manipulators

The presence of obstacles/constraints in a robot workspace can effectively reduce the number of degrees of freedom but the associated loss of functionality can be avoided for kinematically redundant manipulators. A manipulator is considered to be kinematically redundant when it has more degrees of freedom than needed to execute the given task i.e. the dimension of joint space is greater than the dimension of the task space. The concept has been widely studied in the past, [28, 29, 30]. In the next section, a way to exploit robot redundancy by imposing constraints is reported in brief.

4.2.1 MPC equivalent control

As the redundant system is under-determined it can have infinite equivalent control vectors. To select one of these solutions, a standard method is to minimize additional cost function while retaining the main desired properties (equivalent control from nominal conditions for impedance tracking in our case). A typical choice for these additional cost functions can be minimization of joint velocities or penalization of control effort. It can be imposed by:

$$\boldsymbol{C_{additional}} = \frac{\mathbf{1}}{\mathbf{2}}\boldsymbol{x^T Q x} \tag{4.9}$$

where x can be velocity or control effort vector and Q is the positive diagonal weight matrix. Finally, to exploit the redundancy, constraints can be added to the quadratic optimization. The general form of the optimization formulation is:

$$\begin{aligned} &\min_{\boldsymbol{v}} \ ||\boldsymbol{A(q)v - b(q)}||^{\mathbf{2}} \\ s.t. \ &\boldsymbol{A_{low}} \leq \boldsymbol{Av} \leq \boldsymbol{A_{high}} \\ &\boldsymbol{v_{low}} \leq \boldsymbol{v} \leq \boldsymbol{v_{high}} \end{aligned} \tag{4.10}$$

The optimization that is used in the simulations in the next section uses a combination of two differently weighted cost functions. First, enforces the required

impedance relation on the robot dynamics and the second minimizes the joint velocities. Additional constraints on euler angles of the end-effector have been introduced to solve the problem of redundancy. Using equation 2.6 and 4.8b we can obtain the first cost function, say H_1 that is given by:

$$\boldsymbol{H_1 = A_q^T Q_1 A_q} \tag{4.11a}$$

$$\boldsymbol{g_1 = -A_q^T Q_1 b_q} \tag{4.11b}$$

$$\boldsymbol{Q_1 = 10^{10} I_3} \tag{4.11c}$$

The cost function for minimization of joint velocities can be derived by assuming a discrete-time manipulator model reduced to a dual-integrator system under the presence of SMC.

$$\begin{aligned} \boldsymbol{q_{k+1}} &= \boldsymbol{q_k + T_s \dot{q}_k + \frac{T_s^2}{2} \ddot{q}_k} \\ \boldsymbol{\dot{q}_{k+1}} &= \boldsymbol{\dot{q}_k + T_s \ddot{q}_k} \end{aligned} \tag{4.12}$$

From equation 4.12, $\boldsymbol{min||\dot{q}_{k+1}||}$ can be expressed as $\boldsymbol{A_{vel} v - b_{vel}}$ where $\boldsymbol{A_{vel} = T_s}$ and $\boldsymbol{b_{vel} = -\dot{q}}$. The second cost function H_2 can be expressed as:

$$\boldsymbol{H_2 = A_{vel}^T Q_1 A_{vel}} \tag{4.13a}$$

$$\boldsymbol{g_2 = -A_{vel}^T Q_1 b_{vel}} \tag{4.13b}$$

$$\boldsymbol{Q_2 = 10^{10} I_3} \tag{4.13c}$$

Finally, the constraints on the euler angles are defined so as to maintain the initial orientation of the end-effector. The *Grönwall's lemma* is used to define these constraints. First of all, we have:

$$\boldsymbol{\theta(t) = \theta_p(t) = \theta_{init}}; \qquad \boldsymbol{\dot{\theta}(t) = \dot{\theta}_p(t) = 0}; \qquad \boldsymbol{\ddot{\theta}(t) = \ddot{\theta}_p(t) = 0} \tag{4.14}$$

Using *Grönwall's lemma*, equalities (4.14) can be written as a unique stable differential equation given by:

$$\ddot{\boldsymbol{\theta}}(t) = \ddot{\boldsymbol{\theta}}_p(t) - (\boldsymbol{\lambda_1} + \boldsymbol{\lambda_2})(\dot{\boldsymbol{\theta}}(t) - \dot{\boldsymbol{\theta}}_p(t)) - \boldsymbol{\lambda_1}\boldsymbol{\lambda_2}(\boldsymbol{\theta}(t) - \boldsymbol{\theta}_p(t)) \tag{4.15}$$

This equality (4.15) has to be converted into the form $Av = b$ and in terms of joint variables before we can finally use it in the optimization problem. This is possible by using the differential kinematics, $\dot{\boldsymbol{\theta}} = \boldsymbol{J_A}\dot{\boldsymbol{q}}$ where J_A is analytical jacobian. This relation also enables the substitution of $\ddot{\theta}$ as $\ddot{\boldsymbol{\theta}} = \boldsymbol{J_A}\ddot{\boldsymbol{q}} + \dot{\boldsymbol{J}}_{\boldsymbol{A}}\dot{\boldsymbol{q}}$. The constraints are used in the optimization problem in the following form:

$$\boldsymbol{A} = \boldsymbol{J_A} \tag{4.16a}$$

$$\boldsymbol{lbA} = \boldsymbol{ubA} = -(\boldsymbol{\lambda_1} + \boldsymbol{\lambda_2})\boldsymbol{J_A}\dot{\boldsymbol{q}} - \boldsymbol{\lambda_1}\boldsymbol{\lambda_2}(\boldsymbol{\theta} - \boldsymbol{\theta_{init}}) \tag{4.16b}$$

Finally, the joint limits from equation 3.7b along with $H_{final} = H_1 + H_2$, $g_{final} = g_1 + g_2$ and the constraints (4.16) form the optimization problem that needs to be solved.

4.2.2 Null space sliding surface

Now we know, there exist an infinite number of control laws that can guarantee $I = 0$. This implies there exists a subset of joint space whose projection does not affect the task space. This is called the null space and it is this motion that accounts for the satisfaction of constraints while preserving the main objective.

In section 4.1.1 we defined $\boldsymbol{\sigma_{op}}$ without any knowledge of the robot null space as it was directly derived from the impedance relation in the cartesian space. From the standard theory of robot null space methods, we can write the sliding surface in operational space as a combination of a particular and homogeneous part where the later is the projection in null space.

$$\begin{aligned} \boldsymbol{\sigma} &= \boldsymbol{\sigma_{op}} + \boldsymbol{P}\boldsymbol{\sigma_0} \\ &= \boldsymbol{J^T} \int \boldsymbol{I} + \left(\boldsymbol{I} - \boldsymbol{J^T}(\boldsymbol{J}\boldsymbol{J^T})^{-1}\boldsymbol{J} \right) \boldsymbol{\sigma_0} \end{aligned} \tag{4.17}$$

where $\boldsymbol{P}$ is the projection matrix, $\boldsymbol{JJ^T}$ is a nxn invertible matrix (full rank), $\boldsymbol{\sigma_{op}}$ is the operational space sliding surface defined in section 4.1.1 and $\boldsymbol{\sigma_0}$ is a new sliding surface which is responsible for the disturbance rejection in the null space. A good choice for σ_0 will provide some sort of sensitivity to the null space disturbances. A typical choice is:

$$\begin{aligned} \boldsymbol{\dot{\sigma}_0} &= \boldsymbol{v} - \boldsymbol{v^{eq}} \\ \boldsymbol{\sigma_0} &= \boldsymbol{\dot{q}} - \boldsymbol{\dot{q}^{eq}} \end{aligned} \tag{4.18}$$

which represents the difference between the manipulator speed with disturbances and the one it would have if MPC control law was applied without uncertainty. With these developments, we are ready to apply SMC techniques to reject uncertainties in the entire joint space of the manipulator.

4.3 7-DOF simulations

The obtained results is implemented to the 7-DOF manipulator model under consideration. In contrary to the past studies, more realistic scenarios are analyzed without limiting the model complexity. The complexities will be added in steps so as to differentiate the corresponding behaviour of various system variables. These complexities are presence of uncertainties in the dynamic model, delayed torque and the friction in the manipulator joints. In contrast with the Chapter3 where we used decentralized SMC, now we have to deal with the redundancy issue and kinematic singularities which are difficult to compute a-priori. In Chapter 5, there is an additional consideration for the presence of a filter on the torque channel.

Equation (4.1) defines the impedance being enforced through the diagonal matrices $\bar{\boldsymbol{M}} = \boldsymbol{I_3}, \bar{\boldsymbol{D}} = \boldsymbol{10I_3}$ and $\bar{\boldsymbol{K}} = \boldsymbol{8I_3}$. Various continuous approximations for the switching function and Integral Sliding Mode Control (ISMC) are implemented to improve the performance of the control scheme. The imposed dynamics is that of an over-damped system where it forces the system to move from initial configuration $q_0 = 0$ to final position in the task space $(x, y, z) = (0.4, 0.1, 0.5)$.

4.3.1 Control with uncertain dynamic model

The uncertainty in the robot dynamic model often limits the robustness of control as it may lead to degraded performance or unpredictable responses. The level of uncertainty in the simulation has been defined in the simulation by underestimating the term $\boldsymbol{N}(\boldsymbol{q}, \dot{\boldsymbol{q}}) = \boldsymbol{C}(\boldsymbol{q}, \dot{\boldsymbol{q}})\dot{\boldsymbol{q}} + \boldsymbol{g}(\boldsymbol{q})$ in the inverse dynamics as $\hat{\boldsymbol{N}}(\boldsymbol{q}, \dot{\boldsymbol{q}}) = \mathbf{0.9}\boldsymbol{N}(\boldsymbol{q}, \dot{\boldsymbol{q}})$. The figure 4.1 reports the tracking in task space and the constraint error for the euler angles with SMC.

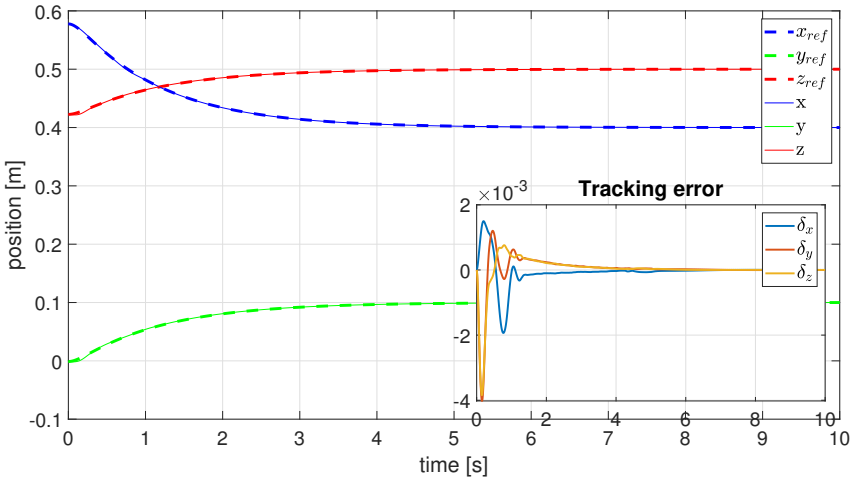

(a) Tracking in task space

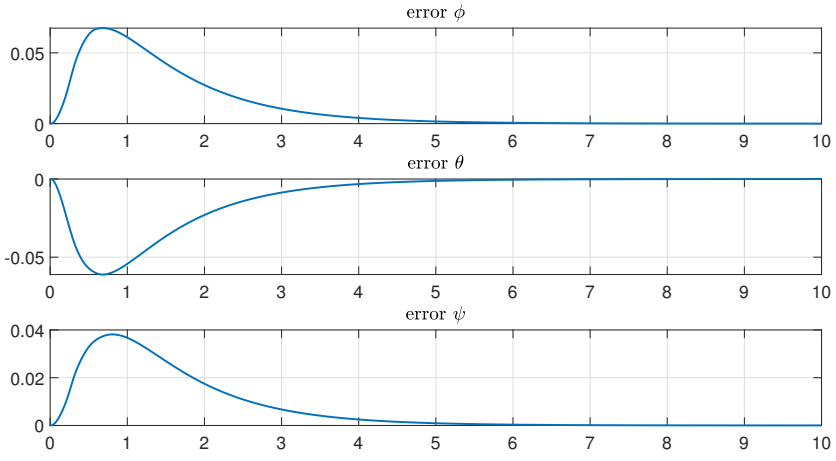

(b) Euler angle constraint error

Figure 4.1: Operational space control response with sliding mode control)

Figure 4.2 and 4.3 reports the position evolution in task space and other system variables like torque, sliding surface and it's evolution with Sliding Mode Control with and without uncertainty on the robot dynamic model. Note: in the absence of SMC the tracking accuracy is extremely bad which is expected as the combined impedance control and inverse dynamic scheme is highly model dependent. The results obtained here clearly displays the robustness property of SMC as there is only a slight drift in the tracking accuracy, only by a tenth order in the magnitude of tracking error as observed in figure 4.2.

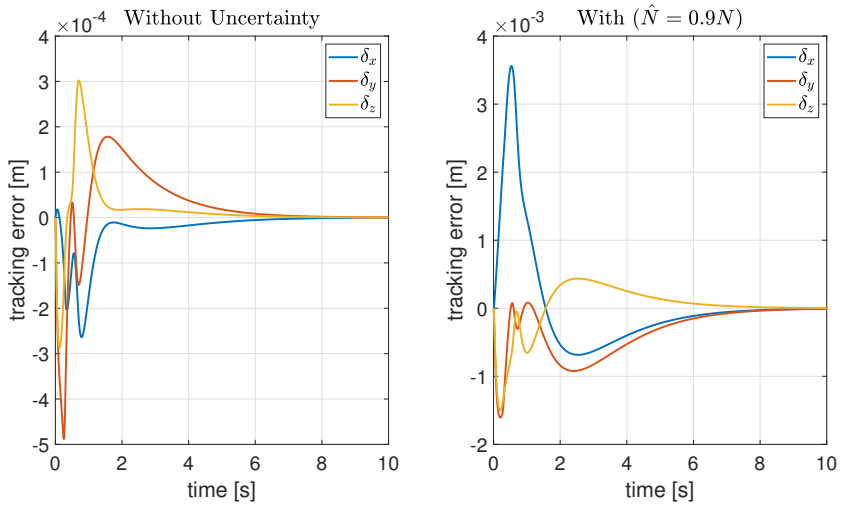

(a) Tracking error

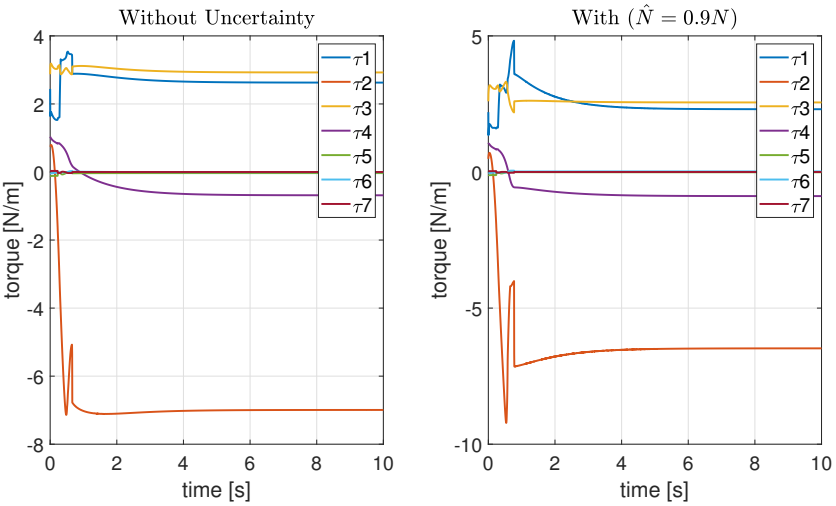

(b) Torque signal

Figure 4.2: Operational space control response with and without uncertain dynamic model (SMC with linear switching function)

The control signal are chatter free, thanks to continuous approximations of the switching function. The required torques are within the limits for each joint and hence are feasible to apply. The affect of uncertainty is easily noticeable from the sliding variable evolution. As mentioned in chapter 2, the linear approximation of SMC causes the loss of convergence properties i.e. it is not valid that the controlled system reaches $\sigma = 0$ in finite time. But as [8] proves that it is possible

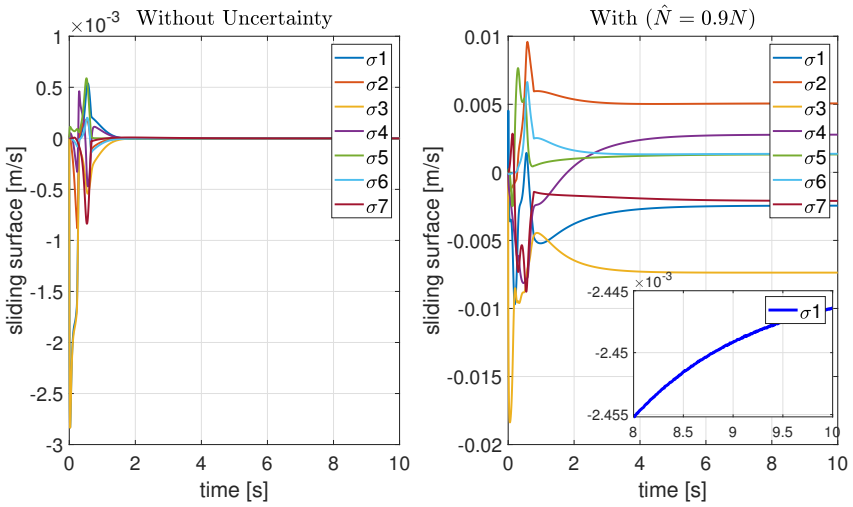

(a) Sliding surface

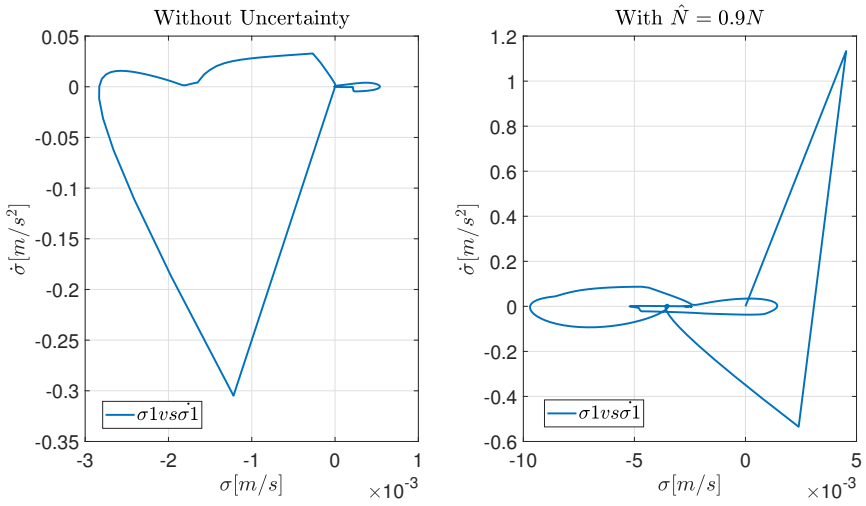

(b) Sliding variable evolution in $\sigma - \dot{\sigma}$ plane

Figure 4.3: Operational space control response with and without uncertain dynamic model (SMC with linear switching function)

to remain in the vicinity of the origin, without actual convergence. This is clearly

visible in figure 4.3b i.e. we do not see finite time convergence to the origin but the evolution of sliding variable remains in the vicinity of origin.

As it was reported in section 2.5.4 that Super Twisting Algorithm, a higher order sliding mode algorithm, makes it possible to derive uncertainty boundaries to guarantee finite time convergence of STA to the origin. The control law defined in equation 2.13, is implemented with parameters $k_1 = 1.1\sqrt{W}$ and $k_2 = 1.5\sqrt{W}$, W is gain. These parameters are tuned based on computer-numerical simulations.

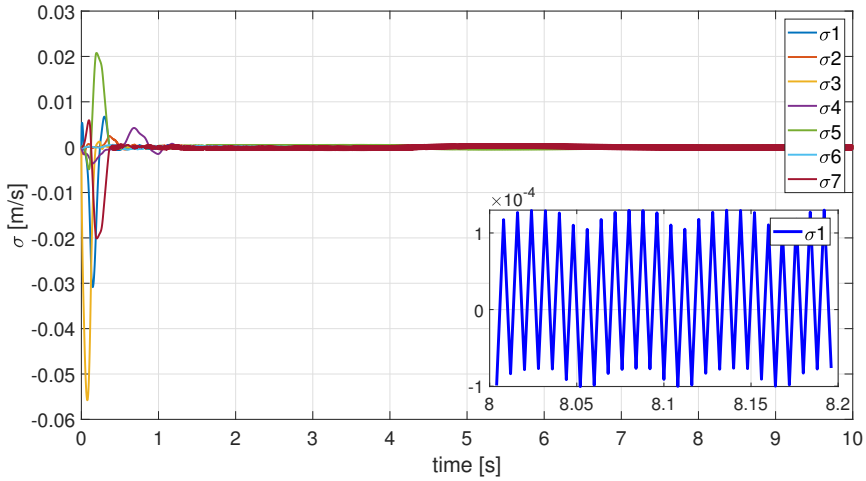

(a) Sliding surface

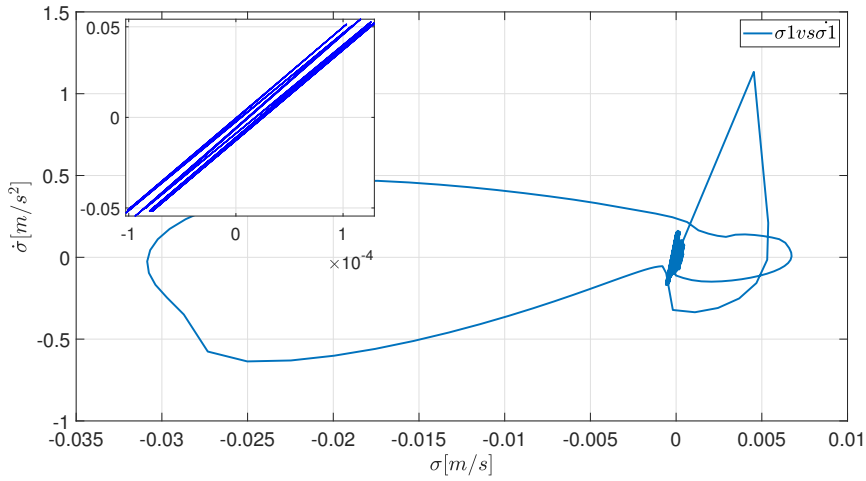

(b) Sliding variable evolution in $\sigma - \dot{\sigma}$ plane

Figure 4.4: Operational space control response with uncertain dynamic model (SMC with Super Twisting Algorithm)

The control parameters are reported in table 4.1. The parameters (K, ψ) describe the linear approximation for the switching function, (λ_1, λ_2) define the constraint and W is the gain for STA.

K	ψ	λ_1	λ_2	W
50	0.2	3	2	$\begin{bmatrix}100 & 20 & 120 & 20 & 120 & 20 & 120\end{bmatrix}^T$

Table 4.1: Control parameters: SMC with uncertain dynamic model

4.3.2 Control with uncertain dynamic model and delay

Accurate tracking in the control of robotic systems can be challenging in the presence of a time delay and especially detrimental when high accuracy and positioning is required. There can be various sources of this delay viz. mechanical latency, processing (signal) latency, communication latency etc. The focus of this section is to address the communication delay on the control channel. The control scheme for this step is similar to that of predictive SMC control scheme (figure 3.3) we used for decentralized control. The system is affected by uncertainty $\hat{N}(q, \dot{q}) = 0.9N(q, \dot{q})$ and now we know, it can be taken care of by using sliding mode control. The delay on the torque communication channel will be handled in a similar way as was done in section 3.2.1 using Sliding-mode Model Predictive Control (SMPC). Assuming that a known time delay (d=2) affects the control channel, we can use the results derived from equation 3.5 to compute the estimation of joint position and velocities using their corresponding d-step ahead predictors. The rejection capabilities of SMC defines the convergence of this estimator.

The figure 4.5 reports the tracking in the task space and the constraint error with Predictive SMC. The results are based on different constraints then the ones imposed in section 4.3.1, here the joints 5, 6 and 7 are constrained from any motion. The structure of the optimization remains same as in previous section, just the constraints are modified. A quick comparison between figure 4.1a and

4.5a shows higher tracking error when a delay is introduced on the torque channel. This is due to the added complexity that deviates the system from the nominal one. The system response without predictive SMC is a complete loss of control.

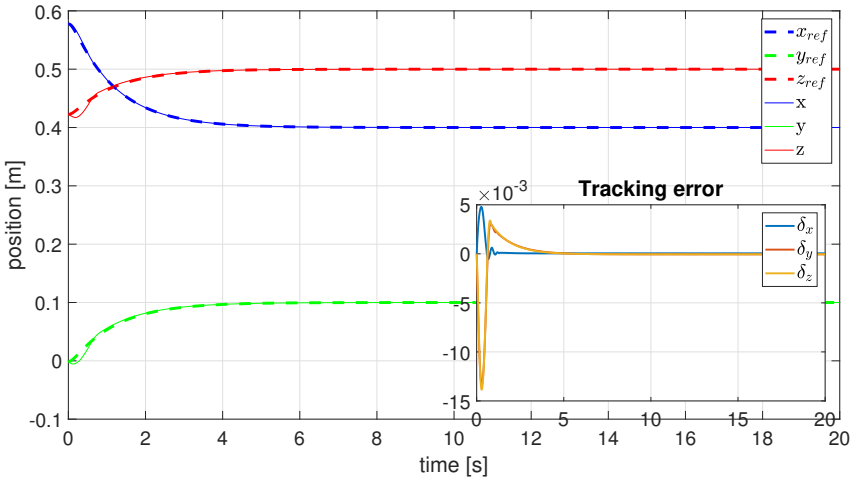

(a) Tracking in task space

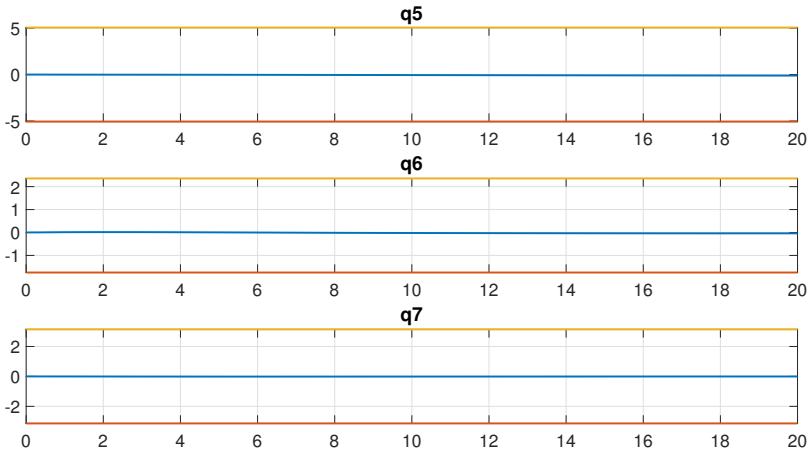

(b) Constrained joints 5,6 and 7

Figure 4.5: Operational space control response with predictive sliding mode control (Uncertainty + delayed torque)

Figure 4.6 and 4.7 compares the affect of delayed torque signal and uncertainty in the robot dynamic model with the results obtained in section 4.3.1 i.e. with only uncertainty in the dynamic model. The results reported in this comparison are based on the constraints on euler angles i.e. fixed orientation of the end-effector.

A lot depends on how the parameters reported in table 4.1 are tuned based on computer-numerical simulations. The comparison has been reported for Sliding Mode Control with Super Twisting Algorithm. Due to this additional deviation from the nominal system, an increase in transient tracking error can be observed in figure 4.6a. The control signal is fairly smooth, as expected with the STA. The sliding variables and it's evolution follows the expected behaviour i.e. a finite time convergence to the origin but with relatively more deviation from the sliding manifold.

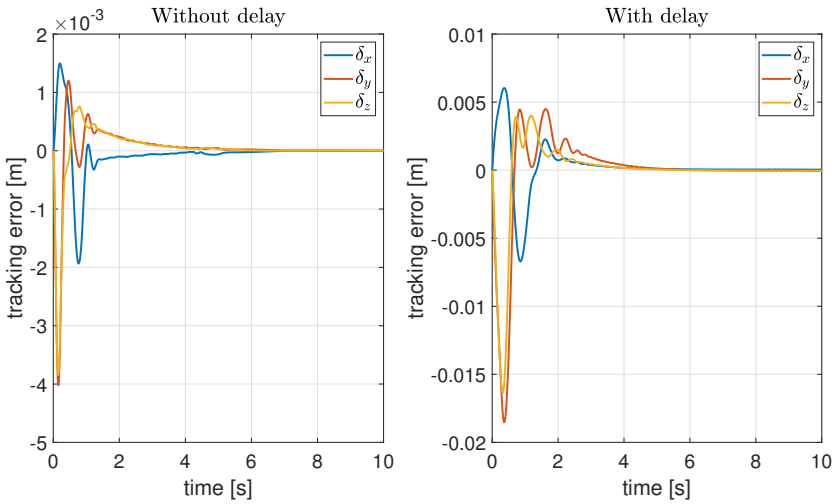

(a) Tracking error

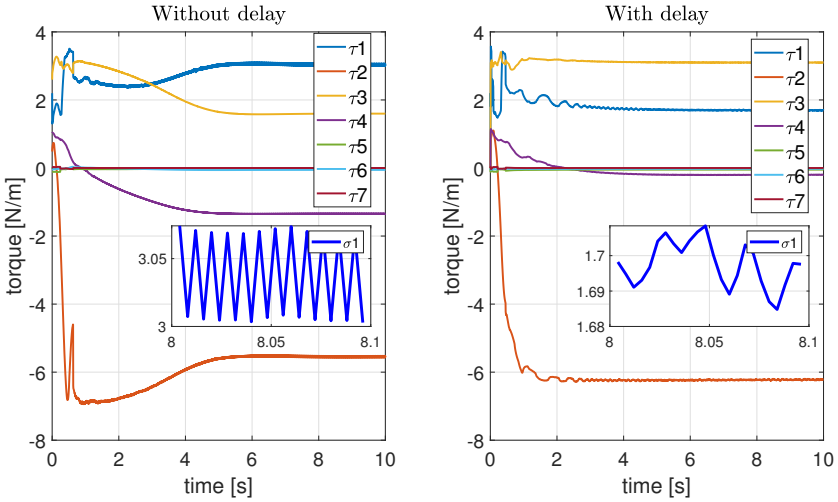

(b) Torque signal

Figure 4.6: Operational space control response comparison without and with delayed torque with uncertain dynamic model using SMC with STA

The tuning parameters for SMC control are reported in table 4.2. A trade-off exists with the gains (K for linear approximation and W for STA) i.e. higher values of gain result in better tracking accuracy but more oscillating control signal.

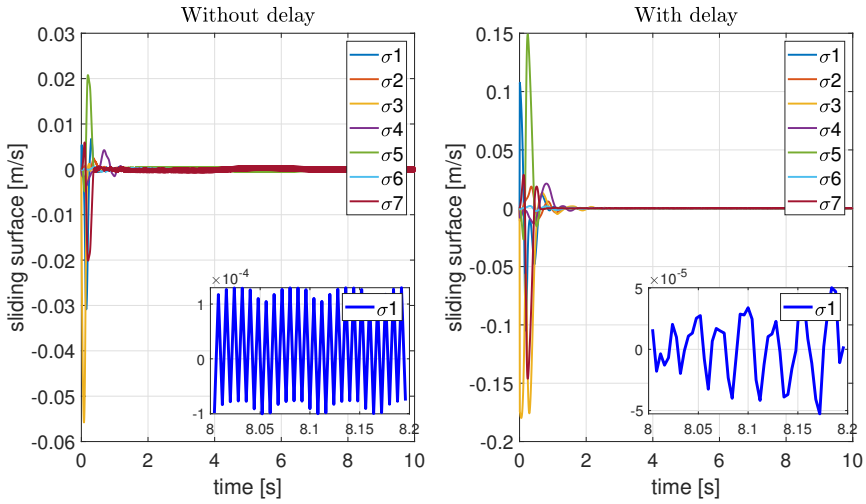

(a) Sliding surface

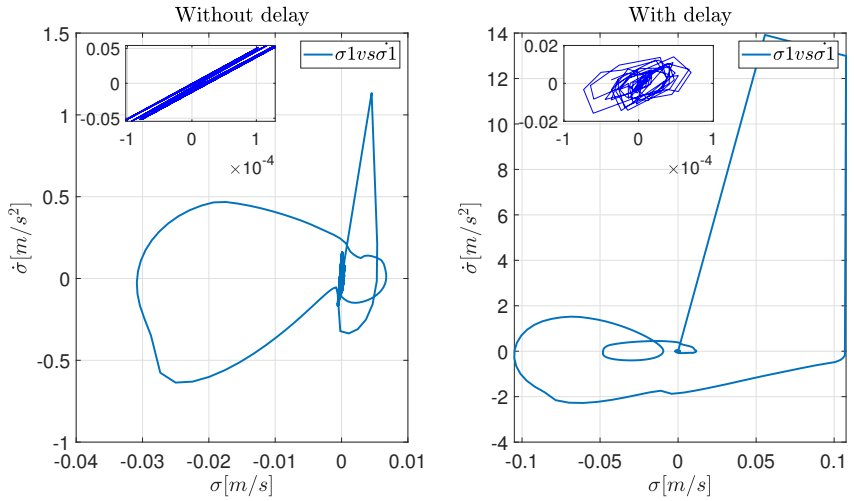

(b) Sliding variable evolution in $\sigma - \dot{\sigma}$ plane

Figure 4.7: Sliding variable comparison for system without & with delayed torque

K	ψ	λ_1	λ_2	W	Q_1	Q_2
60	0.2	25	5	$\begin{bmatrix}20 & 20 & 20 & 20 & 20 & 20 & 20\end{bmatrix}^T$	1e10.I_3	I_7

Table 4.2: Control parameters for Predictive SMC

4.3.3 Modified sliding surface

Modified null space sliding surface

We know that, there exist an infinite number of control laws that can guarantee $I = 0$ (refer 4.2.2). The choice $\sigma_0 = \dot{q} - \dot{q}^{eq}$ was made in order to ensure the sensitivity to disturbances acting on null space motion. With SMC the system evolves on the sliding manifold and it can be approximated by a chain of integrators as in equation 4.12. This gives us another possible choice for σ_0:

$$\boldsymbol{\sigma_0 = \dot{q} + T_s v^{eq}} \tag{4.19}$$

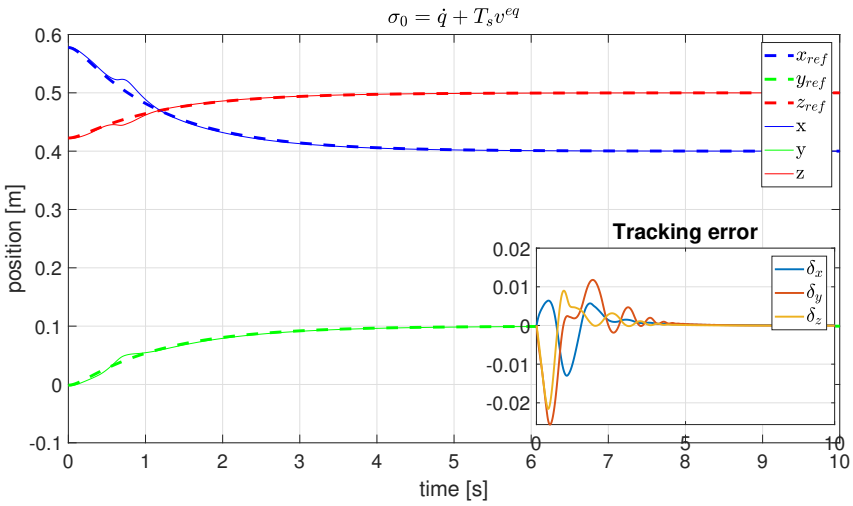

(a) Task space tracking

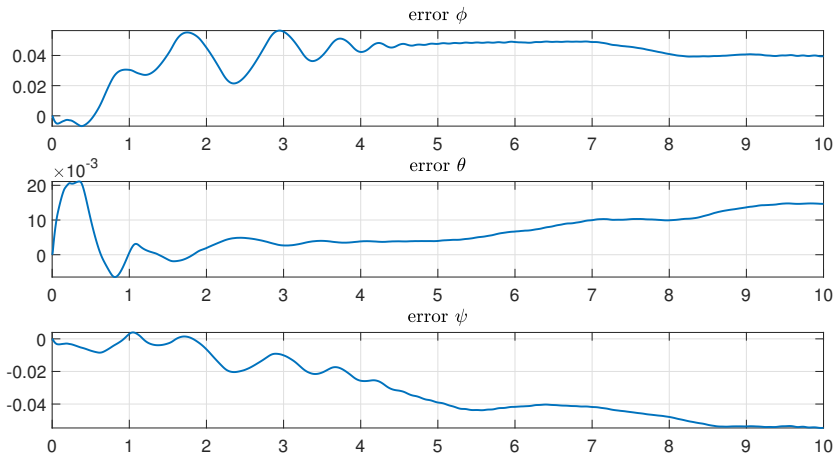

(b) End-effector orientation constraints

Figure 4.8: Operational space control with different null-space sliding surface

where v^{eq} is the acceleration computed by MPC control law and $\dot{q}$ is the actual manipulator joint velocities. The convergence to the origin implies that at steady state actual manipulator velocities tend to the ones from MPC control law. The first choice ensured that by considering the difference between the two and the later drives the system directly to the ones with MPC control law assuming the system behaves like a reduced dual-integrator system. Figure 4.8 reports tracking of x, y and z position of the end-effector in task space and the constraints on end-effector orientation through euler angles.

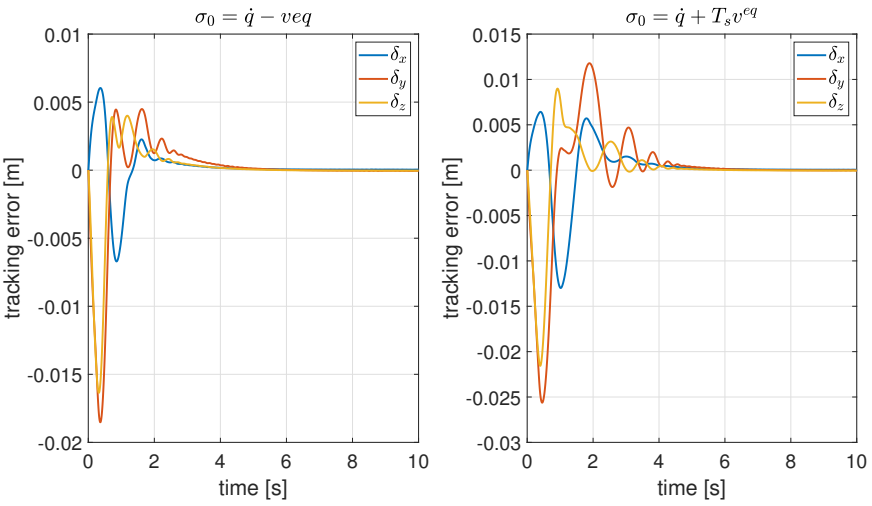

(a) Tracking error

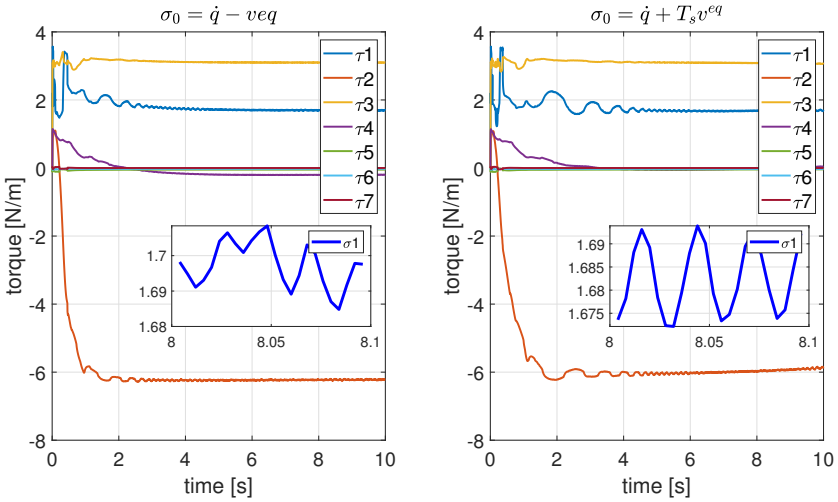

(b) Torque signal

Figure 4.9: Operational space control response with two different null-space sliding surface (uncertain dynamic model + delayed torque)

Figures 4.9 and 4.10 reports a comparison of the two considered choices for null-space sliding surface. Both perform equally well for the tracking accuracy in the task space and the system convergence (finite time convergence with STA). The control signal (torque) is smooth and within the specified limits and hence is safe for the application. The results have been obtained with same tuning parameters as reported in table 4.2.

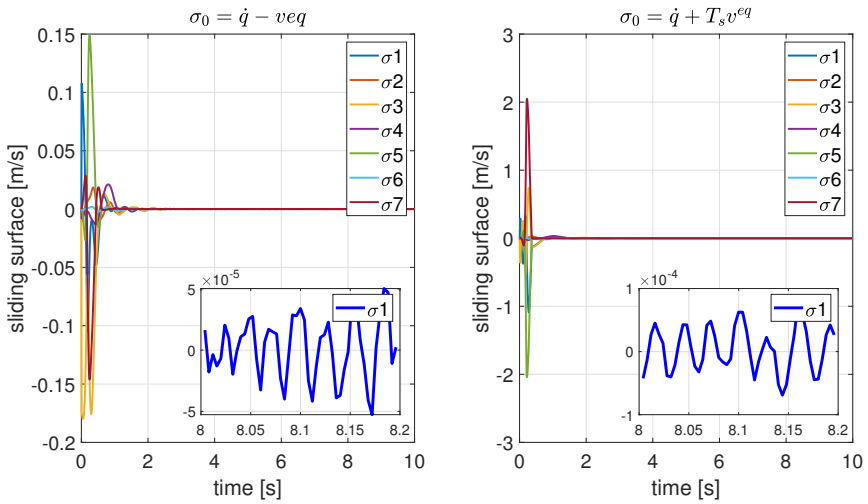

(a) Tracking error

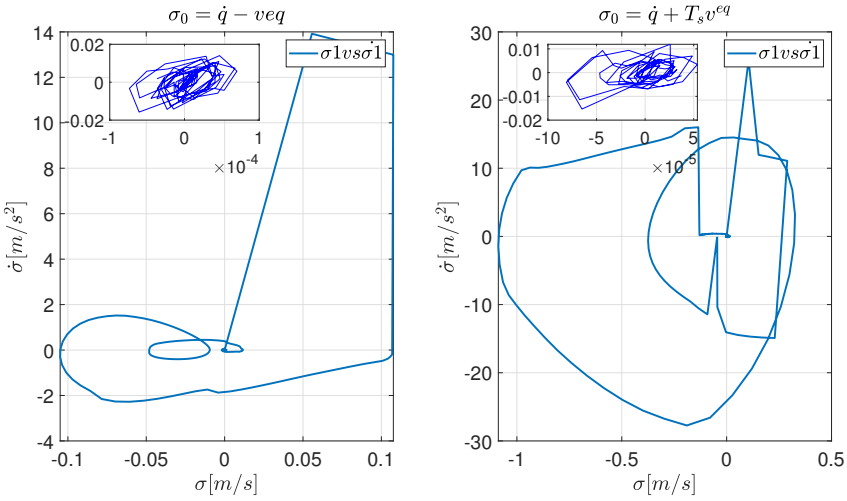

(b) Torque signal

Figure 4.10: Operational space control response with two different null-space sliding surface (uncertain dynamic model + delayed torque)

Simplified sliding surface

In section 4.2.2, the sliding surface was defined as a combination of particular and the homogeneous part that enabled that the system is able to follow the desired dynamics while rejecting the disturbances in the null space. To drive the actual manipulator joint velocities towards the ones computed by MPC control law, a simplified sliding surface $\boldsymbol{\sigma = \sigma_0 = \dot{q} - v^{eq}}$ has been evaluated in this section. Figure 4.11 reports the tracking in task space and constraints on the end-effector orientation with this modified sliding surface.

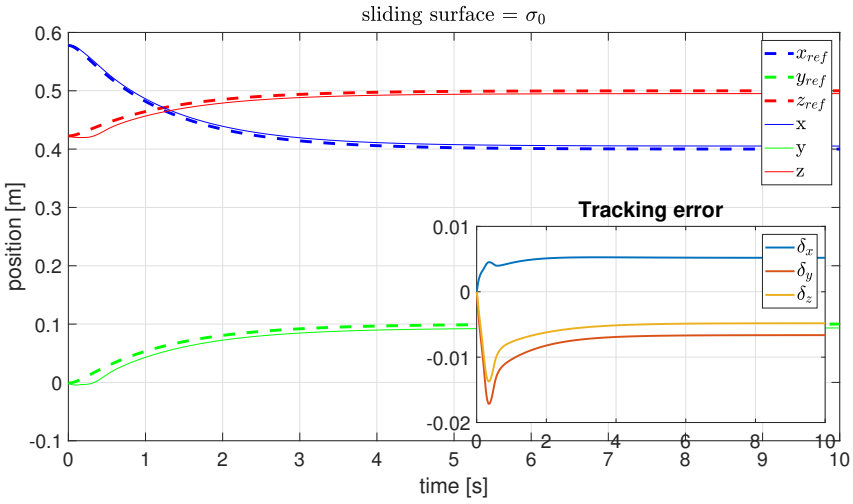

(a) Tracking error

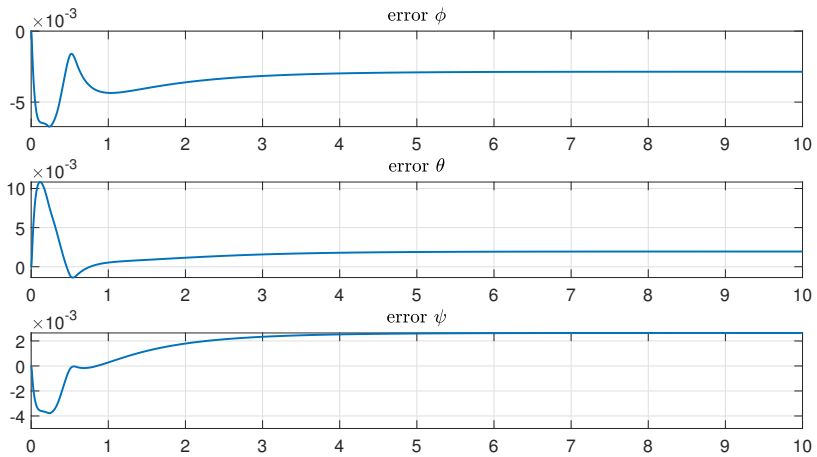

(b) Euler angle constraints

Figure 4.11: Operational space control response with simplified sliding surface (uncertain dynamic model + delayed torque)

The evolution of the sliding variables is reported in figure 4.12. As expected with the Super Twisting Algorithm a finite time convergence of sliding variables to the origin is observed. The results are quite satisfactory considering the simplicity of the method and the simplistic idea that on the sliding surface the system should evolve with the desired dynamics or impedance.

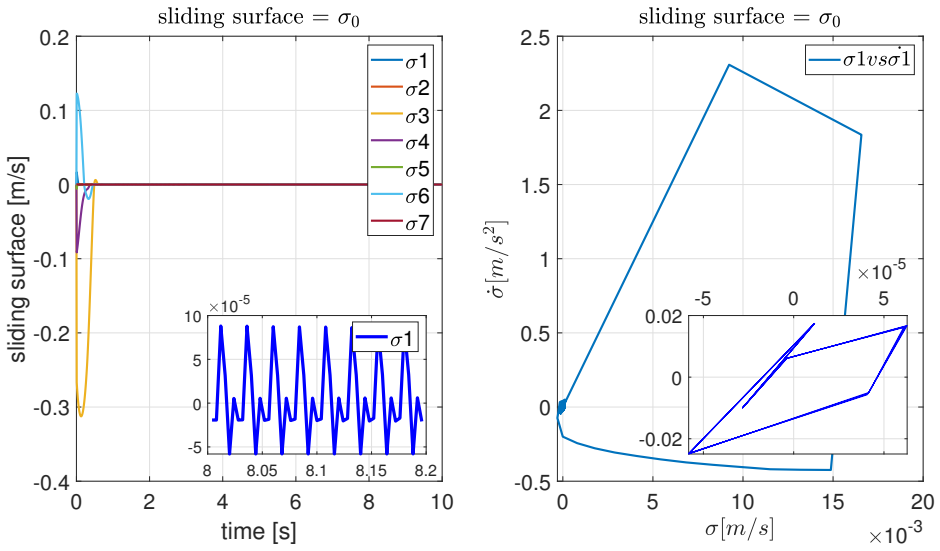

Figure 4.12: Operational space control response with simplified sliding surface (uncertain dynamic model + delayed torque)

4.3.4 Control with uncertainty, delay & friction

Friction is one of the most detrimental sources of instabilities especially when the magnitude of friction torque is comparable to the actuation torque (control signal). This usually happens at slow speeds. In fact, this was the motivation to consider the simulations with $5^{th}, 6^{th}$ and 7^{th} joints constrained from movement, as the wrist joints have high friction at slow speeds for the 7-DOF manipulator under consideration. The friction model is already obtained in the previous study [3] and is expressed as:

$$\boldsymbol{\tau_f} = \begin{cases} \left[\boldsymbol{\tau_c} + (\boldsymbol{\tau_s} - \boldsymbol{\tau_c})e^{-\alpha|\dot{q}|}\right] \boldsymbol{sgn}\dot{\boldsymbol{q}} + \boldsymbol{\kappa}\dot{\boldsymbol{q}} + \boldsymbol{\eta}(\boldsymbol{q} + \boldsymbol{q_0}), & |\dot{\boldsymbol{q}}| \geq \dot{\boldsymbol{q}}_{\boldsymbol{th}} \\ \frac{\tau_{th}^{+} - \tau_{th}^{-}}{2\dot{q}_{th}}\dot{\boldsymbol{q}} + \frac{\tau_{th}^{+} + \tau_{th}^{-}}{2}, & |\dot{\boldsymbol{q}}| \leq \dot{\boldsymbol{q}}_{\boldsymbol{th}} \end{cases} \tag{4.20}$$

The control scheme used for operational space control for this case is similar to the one for SMPC with an additional compensation for the joint friction and is shown in figure 4.13.

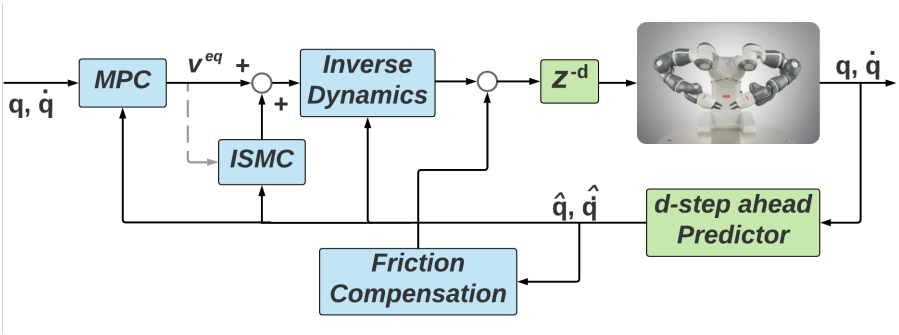

Figure 4.13: Operational space control scheme for manipulator with uncertain dynamic model, delayed torque and joint friction consideration

In figure 4.14a and 4.14b, the position evolution in task space and the constraints imposed on the end-effector orientation are reported. The figure 4.14c shows the control signal and the negative affect of the joint friction is noticeable. To analyze controller robustness, a 5% of uncertainty in the identified friction model is considered. The SMC is implemented with Super Twisting Algorithm. The results in figure 4.14 are obtained with value of the gain $W = 2$. A comparison of the effect of different gains is reported in figure 4.15. The gains k_1 and k_2 in equation 2.13 are defined as $u * \sqrt{W}$ and $v * \sqrt{W}$ respectively, where $u = 3.5$ and $v = 2.5$ are constant gains. There is a clear trade-off between the impedance tracking and the smoothness of the control signal. High gain ensures good response to the impedance tracking but higher amplitude of oscillations in the control signal. The same is also valid for the constants λ_1 and λ_2 that define the convergence of the constraints on the end-effector position (equation 4.15). High values of these constants will ensure effective fulfilment of these constraints but this will be at the expense of impedance tracking. This impact can be clearly observed in figure 4.15c where higher values result in faster convergence of the constraints. But, it also implies too much demand from the optimization that it affects the minimization of cost function that guarantees the desired dynamics.

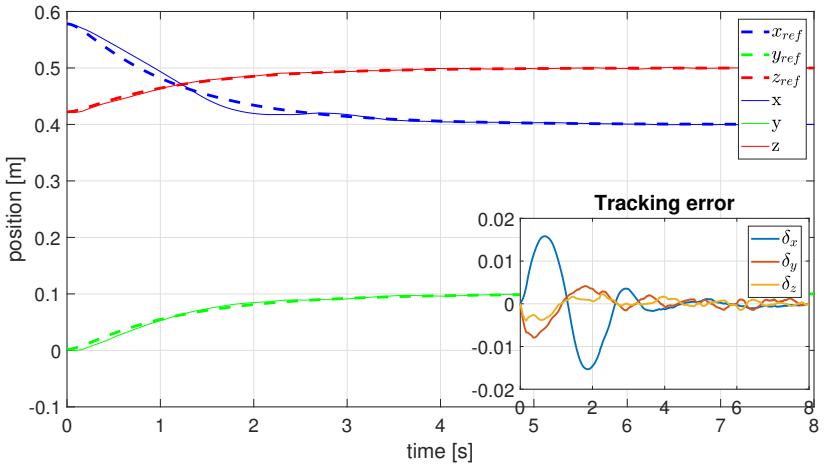

(a) Tracking error

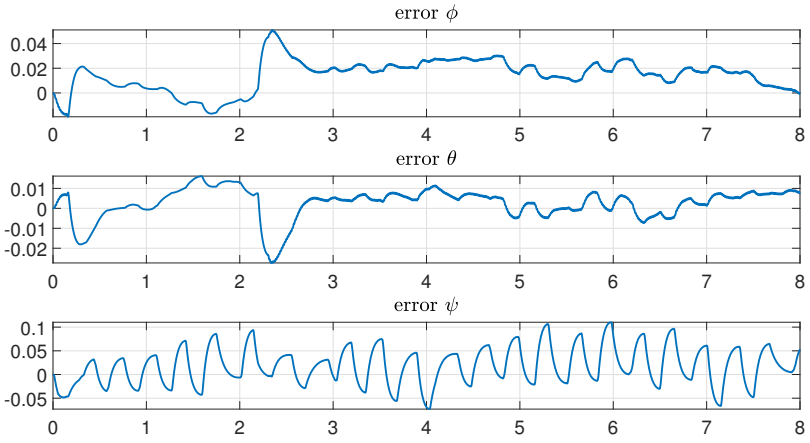

(b) End-effector orientation constraints (euler angles)

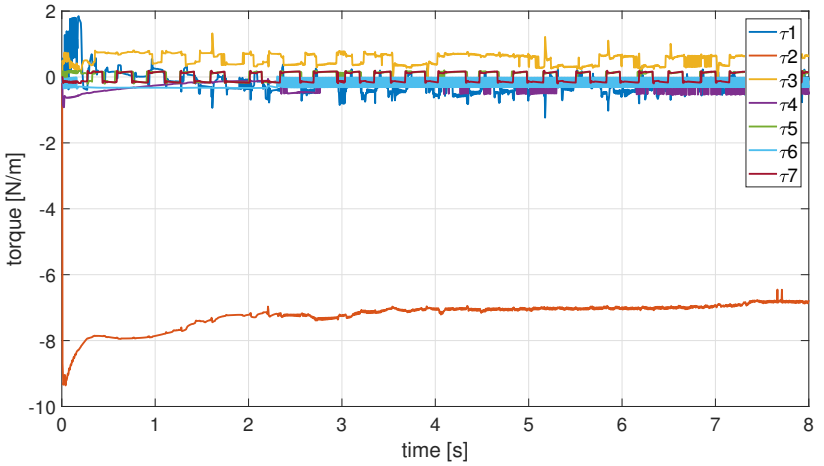

(c) Torques)

Figure 4.14: Operational space control response with uncertain dynamic model, delayed torque and joint friction consideration for the 7-DOF manipulator model

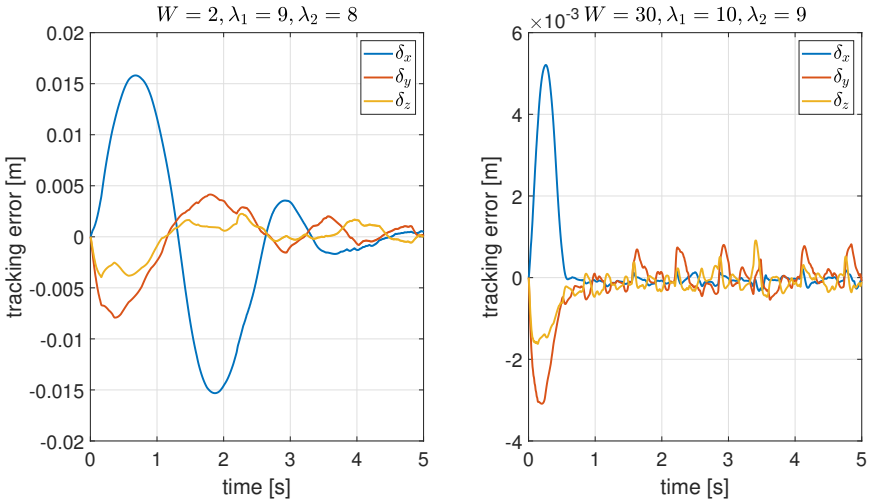

(a) Operational space tracking error

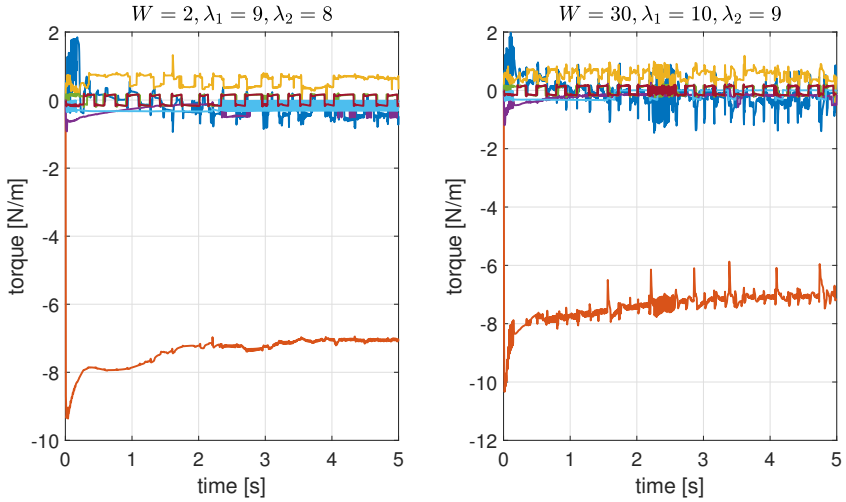

(b) Control signal (torque)

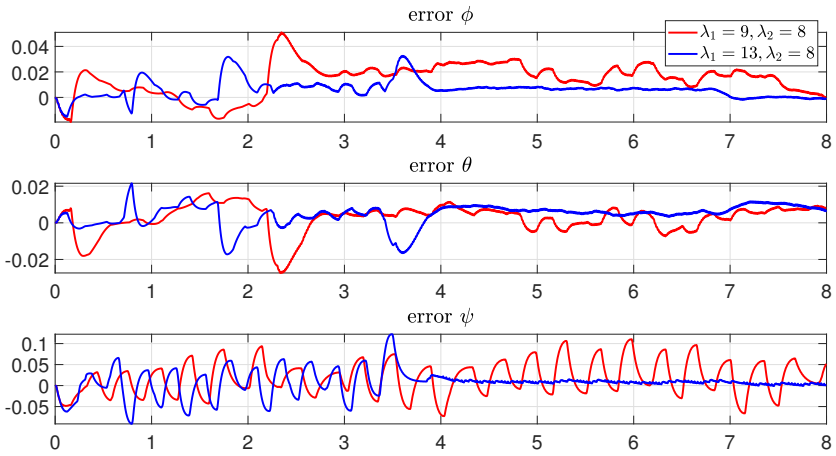

(c) End-effector constraints

Figure 4.15: Comparison of operational space impedance control variables for 7-DOF manipulator model with different tuning parameters

Approximation of Super Twisting Algorithm (STA)

In section 2.5.4, STA was introduced as one of the higher order algorithms with the objective to improve the quality of control signal. As observed in previous section, even with STA the amplitude of chattering is high. In this section an approximation of SMC is implemented. In it's basic form the presence of the term $sgn(\sigma)$ is a possible source of discontinuities. Smoothening of this term is reported in equation 4.21 where the term $sgn(\sigma)$ is replaced by a continuous approximation. The objective of these modifications is to improve the quality of the control signal.

$$\boldsymbol{v(t) = -k_1\sqrt{|\sigma|}\left(\frac{\sigma}{|\sigma| + \delta}\right) - k_2 \int \frac{\sigma}{|\sigma| + \delta}} \tag{4.21}$$

A comparison of torque profiles with standard STA and STA with sigmoid approximation for the *sign* function is reported in figure 4.16. Only the first 4 joint torques are reported here. It shows a considerable improvement in the quality of the control signal for the joint torques. Besides, there is also a slight improvement in their chattering amplitude.

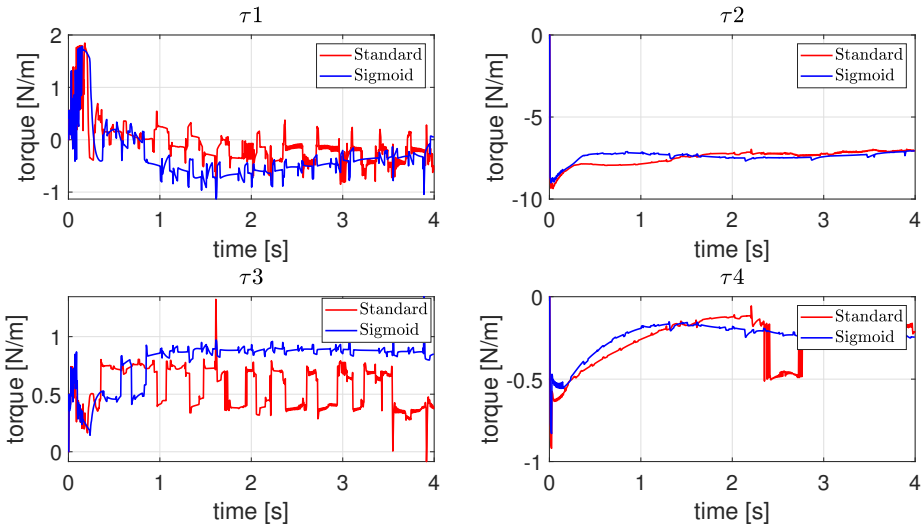

Figure 4.16: Control signal comparison of SMC between standard STA and STA smoothened by sigmoid approximation of *sign* function (first 4 joint torques)

It must be noted that, a trade-off exists between the impedance tracking accuracy and the quality of the control signal. Higher the value of δ more will be the deviation from the impedance profile in the transient. The tuning parameters for the controllers have to be assigned carefully based on computer-numerical simulations. It is a highly iterative method. It may appear that the designed impedance controller is highly dependent on the identified friction model or highly model dependent. These ambiguities are clarified in the next chapter when the robustness of the controller is validated.

Chapter 5

Impedance Control with Torque Filtering

The effect of uncertainty in the robot dynamic model, delay in the communication of control signal and joint friction was analyzed in the previous chapter. Now, the analysis is extended to the presence of a FIR-filter on the torque channel. It critically affects the stability of the entire system operation as it introduces additional dynamics that significantly lowers the allowable bandwidth of the control action. It is shown how sliding mode controllers can be implemented to a system affected by these sources of deviations from the nominal system.

The concept of feedback linearization control is already well explored [32, 33] and forms a starting point for our approach to the problem of torque filtering. An extensive analysis of the robot redundancy is performed by considering different optimization in the QP formulation. Estimated models of the torque filter present in the ABB YuMi robot is used to perform MATLAB-Simulink experiments. The controller is developed considering a simple first order low pass filter. The performance of the designed controller is then evaluated against a second order filter model on the torque channel. An analysis of different prediction horizons for the estimation of joint positions and joint velocities is also performed to better counter the affect of delay on the torque channel during the implementation of SMPC.

The objective is to enforce desired impedance (robot dynamics) under the presence of the aforementioned instabilities. The simulation results are reported

for 2-DOF planar manipulator model and 7-DOF ABB FRIDA model.

5.1 New system (Robot with torque FIR-filter)

In section 2.1, the dynamic model of a generic manipulator was introduced. As we mentioned earlier the system is highly non-linear with coupled dynamics. The presence of filter introduces additional dynamics to the original system that limits the available bandwidth and in turn serves as an additional source of instability. The previous work [3] has reported various filter models through experimental validation. The theory is developed using a generic first order filter while for simulations, a 1st order low pass filter given in equation 5.1a will be considered. The 2nd order transfer function in equation 5.1b will be later used to validate the designed impedance controller for robustness. The final impedance controller is developed for the system summarized in figure 5.1.

$$\hat{F}_1(s) = \frac{74.93}{s + 72.9} \tag{5.1a}$$

$$\hat{F}_2(s) = \frac{-24.42s + 2.486 \times 10^4}{s^2 + 304.3s + 2.486 \times 10^4} \tag{5.1b}$$

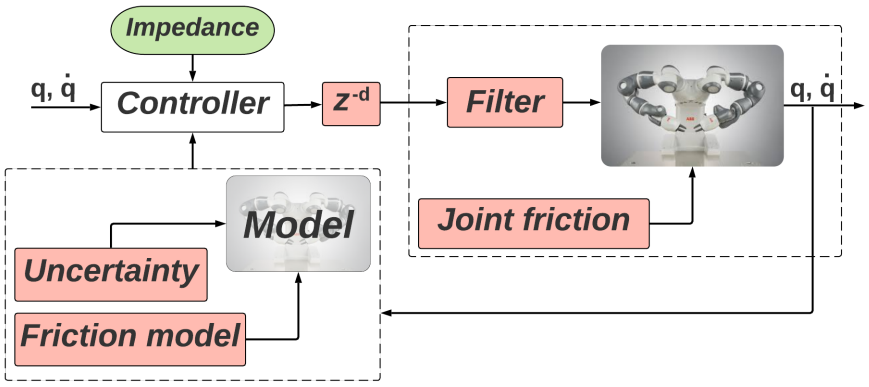

Figure 5.1: Overview: system and sources of instabilities

5.2 Feedback linearization: Classical approach

Feedback linearization is a common approach for the control of non-linear systems. It allows to transform a non-linear system into an equivalent linear system through a change of variables and an appropriate control input. An outer control loop strategy can then be applied on the resulting linear system. In this chapter, the strategy will be to implement feedback linearization to the new system (robot + torque filter) and then use the already established Sliding Mode Control as the outer control loop. With feedback linearization linear tracking performance with desired dynamics can be imposed to the non-linear system at hand. The robot dynamic equation 2.1 with filtered torque can be expressed as:

$$\dot{\boldsymbol{x}}_{\boldsymbol{1}} = \boldsymbol{x}_{\boldsymbol{2}} \tag{5.2a}$$

$$\dot{\boldsymbol{x}}_{\boldsymbol{2}} = -\boldsymbol{B}^{-\boldsymbol{1}}(\boldsymbol{x}_{\boldsymbol{1}})\Big(\boldsymbol{N}(\boldsymbol{x}_{\boldsymbol{1}}, \boldsymbol{x}_{\boldsymbol{2}}) + \boldsymbol{\tau}_{\boldsymbol{f}}(\boldsymbol{x}_{\boldsymbol{1}}, \boldsymbol{x}_{\boldsymbol{2}}) + \boldsymbol{x}_{\boldsymbol{3}}\Big) \tag{5.2b}$$

$$\dot{\boldsymbol{x}}_{\boldsymbol{3}} = \boldsymbol{\alpha\tau} - \boldsymbol{\beta x}_{\boldsymbol{3}} \tag{5.2c}$$

where $\boldsymbol{x}_{\boldsymbol{1}}$, $\boldsymbol{x}_{\boldsymbol{2}}$ and $\boldsymbol{x}_{\boldsymbol{3}}$ are robot joint position, joint velocities and the filtered torque respectively. Here, τ is the input torque signal that is filtered before acting on the manipulator. These are the three states of the obtained new system under the assumption of a 1st order FIR-filter on the torque channel.

The system prior to the presence of the torque filter was simply a 2nd order system. In section 2.2, general form of non-linear affine system was defined. A non-linear system is affine if it is linear in terms of input. Feedback linearization can be applied to the systems of that form. To ensure that the transformed system is an equivalent representation of the original system the transformation should be a *diffeomorphism* i.e. it should be invertible and also it's inverse must be smooth to preserve the differentiability of original coordinate system in the new coordinate system. The equation 5.2c comes from a generic first order filter $\alpha/(s+\beta)$ being used for mathematical demonstrations. The above equations can be expressed in the general form of non-linear affine system as:

$$\begin{bmatrix} \dot{\boldsymbol{x}}_1 \\ \dot{\boldsymbol{x}}_2 \\ \dot{\boldsymbol{x}}_3 \end{bmatrix} = \begin{bmatrix} \boldsymbol{x_2} \\ -\boldsymbol{B^{-1}}\Big(\boldsymbol{N} + \boldsymbol{\tau_f} - \boldsymbol{x_3}\Big) \\ -\boldsymbol{\beta x_3} \end{bmatrix} + \begin{bmatrix} \boldsymbol{0} \\ \boldsymbol{0} \\ \boldsymbol{\alpha} \end{bmatrix} \boldsymbol{\tau}$$
$$\boldsymbol{y} = \begin{bmatrix} \boldsymbol{1} & \boldsymbol{0} & \boldsymbol{0} \end{bmatrix} \begin{bmatrix} \boldsymbol{x_1} \\ \boldsymbol{x_2} \\ \boldsymbol{x_3} \end{bmatrix} \tag{5.3}$$

The system of equations 5.3 is in the form $\dot{x} = a(x) + b(x)u$ and $y = c(x)$ where $x = \begin{bmatrix} x_1 & x_2 & x_3 \end{bmatrix}$ is the state vector. As reported in 2.2, feedback linearization produces a transformed system has the output y and it's $n-1$ derivatives for a generic n^{th} order system. The notion of relative degree gives a way for the input u to the original system, to enter in this new transformed system. It can be verified using equations 2.3 that the relative degree of the system is 3 at x_0 i.e. origin. Hence, for the analysis of the system at hand the relative degree is equal to order of the system. The proof exists to demonstrate the existence of a state feedback control law through which a (locally) linear i/o map can be obtained. The control law has the following form determined from equation 2.4:

$$\begin{aligned} \boldsymbol{\tau} &= \frac{\boldsymbol{v} - \boldsymbol{L_a^3 c(x)}}{\boldsymbol{L_b L_a^2 c(x)}} \\ \boldsymbol{v} &= \boldsymbol{y^{(3)}} = \frac{\boldsymbol{d^3 y}}{\boldsymbol{dt^3}} \end{aligned} \tag{5.4}$$

The Lie derivatives are used to give the structure to the problem. They serve as a very convenient way to deal with multiple derivatives with respect to either same or different vector fields. Note: the denominator of the control law will be matrices for multiple inputs or multiple outputs system, so we will have to use inverses instead in the given expression. These derivatives can be computed by using the chain rule as in equations 5.5.

$$L_a c(x) = x_2 \tag{5.5a}$$

$$L_a^2 c(x) = L_a L_a c(x) = -B^{-1}\Big(N + \tau_f - x_3\Big) = \zeta \tag{5.5b}$$

$$L_a^3 c(x) = L_a L_a^2 c(x) = \left[\frac{\partial \zeta}{\partial x_1} x_2 + \frac{\partial \zeta}{\partial x_2}\zeta + \frac{\partial \zeta}{\partial x_3}(-\beta x_3)\right] \tag{5.5c}$$

$$L_b c(x) = c_x b = 0 \tag{5.5d}$$

$$L_b L_a c(x) = L_b\Big(c_x a(x)\Big) = 0 \tag{5.5e}$$

$$L_b L_a^2 c(x) = \frac{\partial \zeta}{\partial x_3}\alpha = \alpha B^{-1} \tag{5.5f}$$

using the results of above expressions in equation 5.4, we can obtain the expression of the control law from feedback linearization:

$$\tau = \frac{B}{\alpha}\left(v - \frac{\partial \zeta}{\partial x_1} x_2 - \frac{\partial \zeta}{\partial x_2}\zeta - \frac{\partial \zeta}{\partial x_3}(-\beta x_3)\right) \tag{5.6}$$

where $\zeta = -B^{-1}(x_1)(N(x_1, x_2) + \tau_f(x_1, x_2) - x_3)$, a variable introduced for simplification of mathematical expressions. It should be noted that, $\dot{x_2} = \zeta$. A scheme of the proposed controller is depicted in figure 5.2.

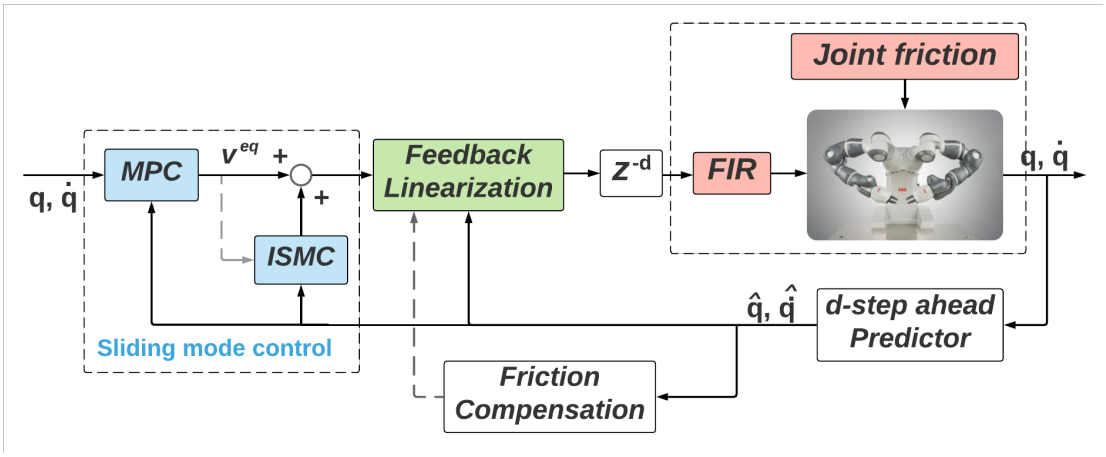

Figure 5.2: Feedback linearization control scheme with an outer loop for SMC

5.2.1 2-DOF simulation: Feedback Linearization

To illustrate the impact of feedback linearization, a simulation setup in MATLAB-Simulink is devised. A 2-dof planar manipulator is considered as the objective

is just to demonstrate the impact of feedback linearization control strategy in the presence of torque filtering. This simple manipulator has simple expressions for the dynamic matrices B, C, g and this allows analytical computation of the feedback linearization control law. The computation for the control law reported in equation 5.6 is computationally very intensive and is performed using *MATLAB - Symbolic Math Toolbox*.

Let's briefly recall the analytical model of this manipulator. The expressions computed by feedback linearization are not reported here due to their exorbitant length.

$$B = \begin{bmatrix} m_1 l_1^2 + I_1 + m_2(a_1^2 + l_2^2 + 2a_1 l_2 cos\theta_2) + I_2 & m_2(l_2^2 + a_1 l_2 cos\theta_2) + I_2 \\ m_2(l_2^2 + a_1 l_2 cos\theta_2) + I_2 & m_2 l_2^2 + I_2 \end{bmatrix}$$

$$C = \begin{bmatrix} -2m_2 a_1 l_2 \dot{\theta}_2 sin\theta_2 & -m_2 a_1 l_2 \dot{\theta}_2 sin\theta_2 \\ m_2 a_1 l_2 \dot{\theta}_1 sin\theta_2) & 0 \end{bmatrix}$$

$$g = \begin{bmatrix} (m_1 l_1 + m_2 a_1) g cos\theta_1 + m_2 g l_2 cos(\theta_1 + \theta_2) \\ m_2 l_2 g cos(\theta 1 + \theta_2) \end{bmatrix}$$

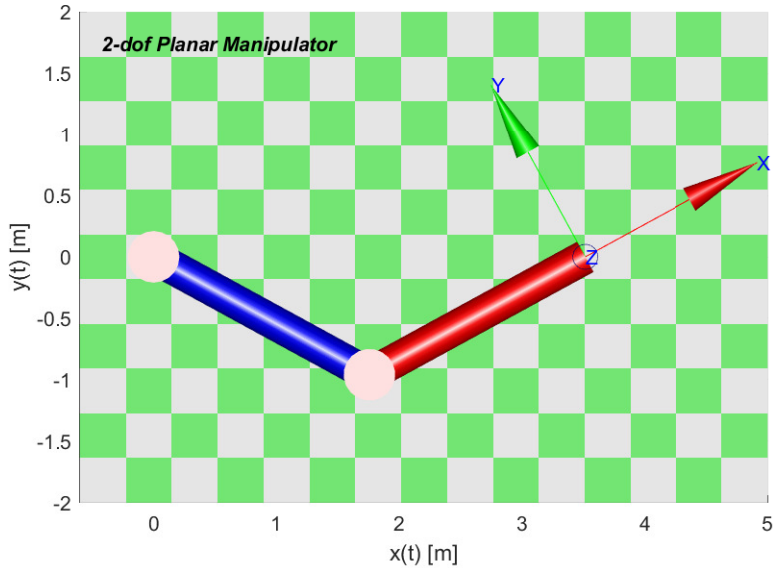

Figure 5.3: 2-DOF planar manipulator model

where θ_1 and θ_2 are the joint positions. a_1 and a_2 represent the link lengths, l_1 and l_2 identify the centre of mass position for each link, m_1 and m_2 are the link masses and I_1 and I_2 are the moments of inertia. A graphical representation of the manipulator is reported in figure 5.3. The simulation enforces desired joint impedance to this manipulator and moves it from initial configuration $q_0 = \begin{bmatrix} -0.5 & 1 \end{bmatrix}$ to the final configuration $q_{final} = \begin{bmatrix} 0 & 1.5 \end{bmatrix}$. Owing to the disturbance rejection property of SMC, the enforced joint impedance is independent of each other and is defined by $\bar{\boldsymbol{B}} = \boldsymbol{diag}(\mathbf{4}, \mathbf{1})$, $\bar{\boldsymbol{C}} = \boldsymbol{diag}(\mathbf{4}, \mathbf{4})$ and $\bar{\boldsymbol{g}} = \boldsymbol{diag}(\mathbf{4}, \mathbf{4})$. The system eigenvalues are assigned to have an approximate second order system with one very fast pole while other two of comparable magnitudes. Super Twisting Algorithm is implemented on both joint impedance control.

The figure 5.4 reports a comparison of joint space impedance control for the 2-dof manipulator model when a FIR (estimated 1st order model) is present on the torque channel. The feedback linearized system when controlled by the exact same SMC controller as an outer loop gives evidently better results. Note: the SMC control law for 3rd order impedance tracking for decentralized control is derived in next subsection. Our objective in this simulation was to validate the analytical expression obtained through feedback linearization. And this allowed us to use the formulations for decentralized SMC reported in chapter 3. The input v in the feedback linearized control law (equation 5.6 is a linear controller and it's structure will be discussed in the next section for centralized control which is our main objective.

5.2.2 Decentralized SMC: 3rd Order Impedance

Following the standard steps for the decentralized control for enforcing joint space impedance as in chapter 3, an extension of the discussion can be made for imposing a 3rd order dynamics in joint-space. This is obvious as the new system i.e. robot with the considered FIR-filter estimation, is a 3rd order system. Taking the advantage of SMC to reject disturbance, we can specify the desired joint dynamics independently for each joint:

$$\bar{\boldsymbol{P}}\tilde{\boldsymbol{q}}^{[3]} + \bar{\boldsymbol{Q}}\ddot{\tilde{\boldsymbol{q}}} + \bar{\boldsymbol{R}}\dot{\tilde{\boldsymbol{q}}} + \bar{\boldsymbol{T}}\tilde{\boldsymbol{q}} = \boldsymbol{J}^{\boldsymbol{T}}\boldsymbol{h} \tag{5.7}$$

where $\bar{\boldsymbol{P}} = diag(p_1, ..., p_n)$, $\bar{\boldsymbol{Q}} = diag(q_1, ..., q_n)$, $\bar{\boldsymbol{R}} = diag(r_1, ..., r_n)$ and $\bar{\boldsymbol{T}} = diag(t_1, ..., t_n)$ represents the desired dynamics of a generic n-dof system. The variable $\tilde{\boldsymbol{q}}$ defines the tracking error in joint space.

$$\tilde{\boldsymbol{q}} = \boldsymbol{q} - \boldsymbol{q_{ref}} \tag{5.8}$$

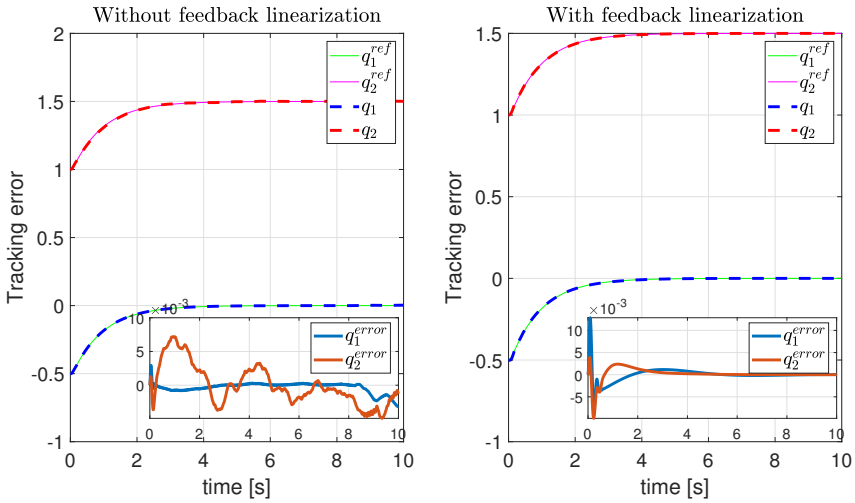

(a) Joint space impedance tracking and tracking error

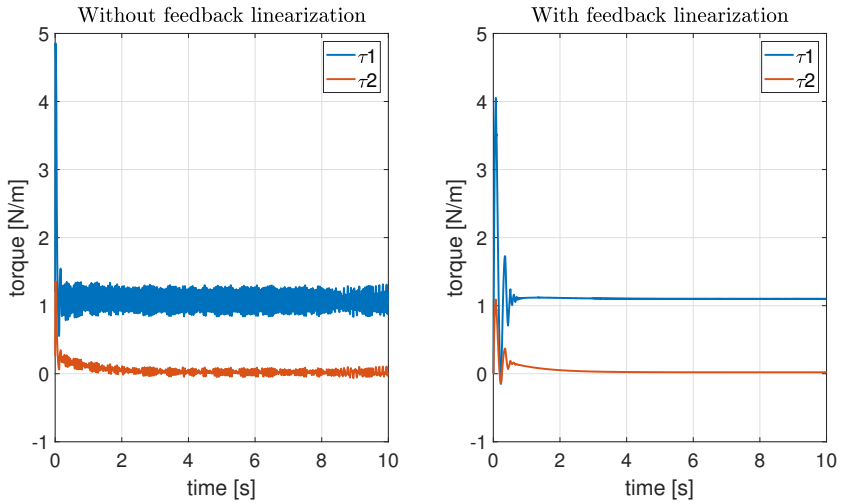

(b) Torque (control signal)

Figure 5.4: Comparison of joint space impedance control with & without feedback linearization in the presence of torque FIR-filter for 2-dof manipulator

It must be noted that the equation 5.7 is not fully decoupled due to the presence of the term $J^T h$, the force from the external environment. However, if the differential kinematic is known with a sufficient accuracy, this term can be calculated easily. The resultant sliding surface σ can then be defined as:

$$\boldsymbol{\sigma = \bar{P}\ddot{\tilde{q}} + \bar{Q}\dot{\tilde{q}} + \bar{R}\tilde{q} + \int_0^t \bar{T}\tilde{q}(\tau)d\tau} \tag{5.9}$$

while the equivalent control law can be simply obtained as the standard impedance control law:

$$\boldsymbol{v^{eq} = -\bar{P}^{-1}\big(\bar{Q}\ddot{\tilde{q}} + \bar{R}\dot{\tilde{q}} + \bar{T}\tilde{q} - J^T h\big)} \tag{5.10}$$

The objective of the results reported in figure 5.5 is to demonstrate third order impedance tracking in a decentralized control setting. For these 2-dof simulations, the affect due to joint friction and communication delay is not considered. But, in the next section an all-inclusive analysis of these sources of instabilities is considered for the impedance tracking in the operational space which is capable to fulfil our objective of dexterous manipulation. Note: in the next sections advantages of 3rd order over 2nd order impedance tracking will be demonstrated with simulations on 7-DOF manipulator model.

It must be noted that the computation of analytical expression for the feedback linearization is too intensive and for a 7-dof freedom case it is not possible to do this computation. Also, it is not scalable or extendable as for the accommodation of any change, the entire computation has to be repeated again. The expressions are exorbitantly lengthy and makes it difficult to comprehend the model. The numerical approximation of the spatial derivatives present in the feedback linearized control law seems to be a possible alternative, but a simplistic approximation for these vectorial derivatives result in infeasible computation due to numerical errors. So, in the next section an alternative approach to implement the feedback linearization is introduced. The overall control scheme for the implementation of feedback linearization is also explained in the next section.

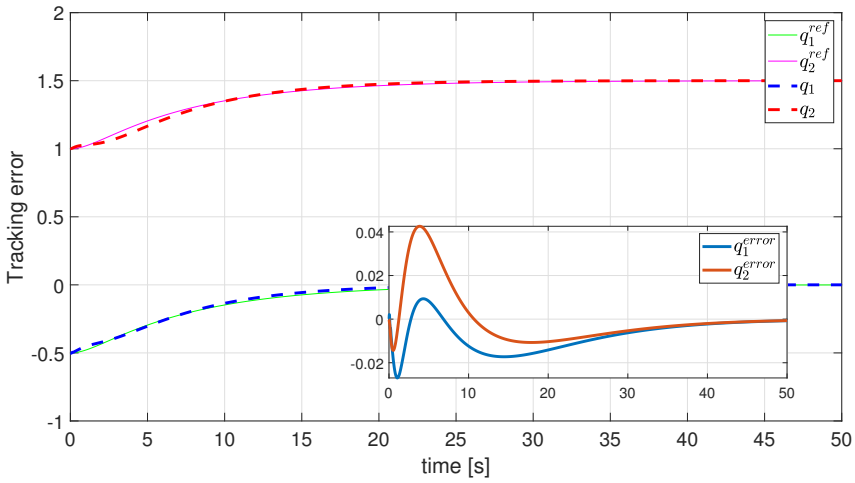

(a) Joint space impedance tracking and tracking error

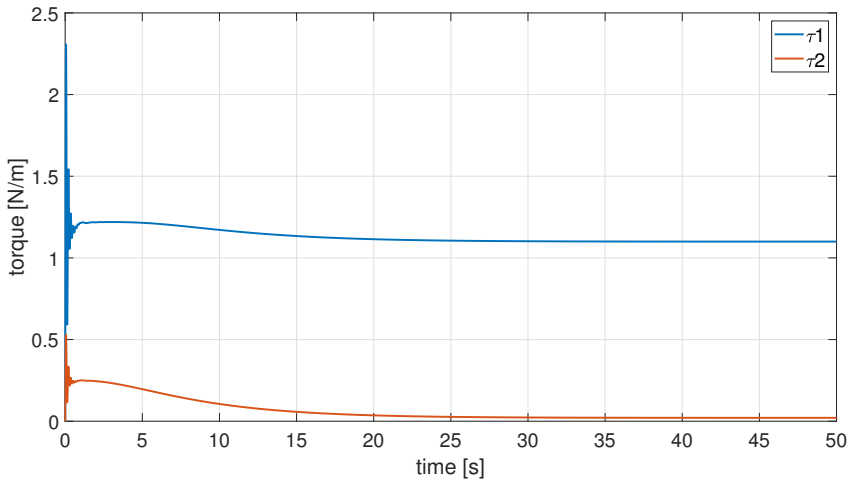

(b) Torque (control signal)

Figure 5.5: 3rd Order joint space impedance control with feedback linearization (2-dof robot model with the 1^{st} order filter model for torque FIR-filter)

5.3 Feedback Linearization: Simplified Method

Let's consider the system defined by equations 5.2. It is possible to see the vector relative degree of the system is 3. Let's rewrite the equation 5.2b replacing x_1 and x_2 by $\dot{q}$ and $\ddot{q}$ respectively.

$$\boldsymbol{B(q)\ddot{q} + N(q,\dot{q}) + \tau_f = x_3} \tag{5.11}$$

differentiating this equation once, we have:

$$\dot{\boldsymbol{B}}(\boldsymbol{q})\ddot{\boldsymbol{q}} + \boldsymbol{B}(\boldsymbol{q})\boldsymbol{q}^{[\mathbf{3}]} + \dot{\boldsymbol{N}}(\boldsymbol{q},\dot{\boldsymbol{q}}) + \dot{\boldsymbol{\tau}}_{\boldsymbol{f}}(\boldsymbol{q},\dot{\boldsymbol{q}}) = \dot{\boldsymbol{x}}_{\mathbf{3}} \tag{5.12}$$

replacing the term $\dot{x}_3$ using equation 5.2c, we have:

$$\dot{\boldsymbol{B}}(\boldsymbol{q})\ddot{\boldsymbol{q}} + \boldsymbol{B}(\boldsymbol{q})\boldsymbol{q}^{[\mathbf{3}]} + \dot{\boldsymbol{N}}(\boldsymbol{q},\dot{\boldsymbol{q}}) + \dot{\boldsymbol{\tau}}_{\boldsymbol{f}}(\boldsymbol{q},\dot{\boldsymbol{q}}) = -\boldsymbol{\beta}\boldsymbol{x}_{\mathbf{3}} + \boldsymbol{\alpha}\boldsymbol{\tau} \tag{5.13}$$

The state feedback control law can then be defined as:

$$\begin{aligned} \boldsymbol{q}^{[\mathbf{3}]} &= -\boldsymbol{B}^{-\mathbf{1}}\Big(\dot{\boldsymbol{B}}(\boldsymbol{q})\ddot{\boldsymbol{q}} + \dot{\boldsymbol{N}}(\boldsymbol{q},\dot{\boldsymbol{q}}) + \dot{\boldsymbol{\tau}}_{\boldsymbol{f}}(\boldsymbol{q},\dot{\boldsymbol{q}}) + \boldsymbol{\beta}\boldsymbol{x}_{\mathbf{3}}\Big) + \boldsymbol{B}^{-\mathbf{1}}\boldsymbol{\tau}\boldsymbol{\alpha} \\ \boldsymbol{\tau} &= \frac{\boldsymbol{B}}{\boldsymbol{\alpha}}\Big[\boldsymbol{B}^{-\mathbf{1}}\Big(\dot{\boldsymbol{B}}(\boldsymbol{q})\ddot{\boldsymbol{q}} + \dot{\boldsymbol{N}}(\boldsymbol{q},\dot{\boldsymbol{q}}) + \dot{\boldsymbol{\tau}}_{\boldsymbol{f}}(\boldsymbol{q},\dot{\boldsymbol{q}}) + \boldsymbol{\beta}\boldsymbol{x}_{\mathbf{3}}\Big) + \boldsymbol{v}\Big] \end{aligned} \tag{5.14}$$

Hence, the obtained control law transforms the original system to the form $q^{[3]} = v$. This basically makes the transformed system a chain of integrators. In fact this was exactly the final result of the classical approach of feedback linearization reported in section 2.2 that we applied in the previous section to the 2-dof manipulator model. This allows us to control the system by the means of linear controller composed of state feedback and feedforward action. A scheme of the proposed controller is depicted in figure 5.6.

$$\boldsymbol{v} = \boldsymbol{q}_{\boldsymbol{d}}^{[\mathbf{3}]} + \sum_{\boldsymbol{i}=\mathbf{0}}^{\mathbf{2}} \boldsymbol{K}_{\boldsymbol{qi}}(\boldsymbol{q}_{\boldsymbol{ref}}^{[\boldsymbol{i}]} - \boldsymbol{q}^{[\boldsymbol{i}]}) \tag{5.15}$$

where K_{qi} are diagonal gain matrices, $i = 0, ..., 2$ such that:

$$\boldsymbol{\lambda}^{\mathbf{3}} + \boldsymbol{\lambda}^{\mathbf{2}}\boldsymbol{k}_{\boldsymbol{q}\mathbf{2}_{\boldsymbol{j}}} + \boldsymbol{\lambda}\boldsymbol{k}_{\boldsymbol{q}\mathbf{1}_{\boldsymbol{j}}} + \boldsymbol{k}_{\boldsymbol{q}\mathbf{0}_{\boldsymbol{j}}} = \mathbf{0} \tag{5.16}$$

are Hurwitz polynomials with $j = 1, ..., n$, where k_{qi_j} are the j-th term of the diagonal gain matrices K_{qi} and $q_{ref}^{[i]}$ are the desired joint position and their time derivatives up to the 2-nd order. By means of this linear controller, it is possible to achieve the asymptotic tracking of the trajectories as it is basically driven by

how far the actual joint variables are form the desired ones. The state of the linearized system is $\boldsymbol{z} = \begin{bmatrix} \boldsymbol{q} & \dot{\boldsymbol{q}} & \ddot{\boldsymbol{q}} \end{bmatrix}^{\boldsymbol{T}}$.

It must be noted that the method saves us from the analytical computations of the classical approach to feedback linearization. But, the simplified method requires the information of joint acceleration and computation of derivatives of dynamic matrices. This problem is handled through numerical differentiation of joint velocity and dynamic matrices.

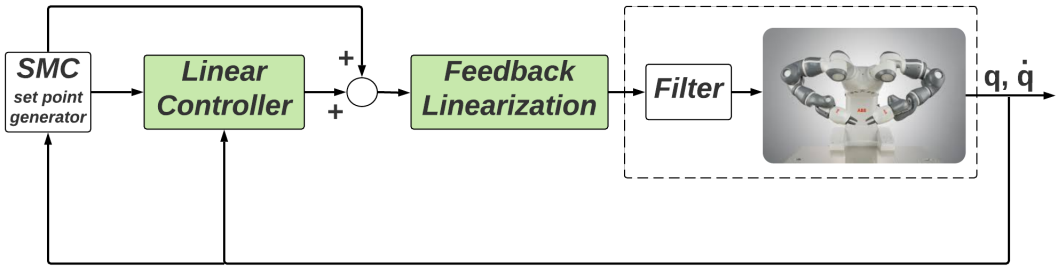

Figure 5.6: Feedback Linearization control scheme summary

The gain matrices K_{qi} are obtained from the solution of the Continuous Algebraic Ricatti Equation (CARE). To proceed with this computation, let's rewrite the transformed system in a matrix form:

$$\begin{aligned} \begin{bmatrix} \dot{\boldsymbol{q}} \\ \ddot{\boldsymbol{q}} \\ \boldsymbol{q}^{[3]} \end{bmatrix} &= \begin{bmatrix} \boldsymbol{0} & \boldsymbol{1} & \boldsymbol{0} \\ \boldsymbol{0} & \boldsymbol{0} & \boldsymbol{1} \\ \boldsymbol{0} & \boldsymbol{0} & \boldsymbol{0} \end{bmatrix} \begin{bmatrix} \boldsymbol{q} \\ \dot{\boldsymbol{q}} \\ \ddot{\boldsymbol{q}} \end{bmatrix} + \begin{bmatrix} \boldsymbol{0} \\ \boldsymbol{0} \\ \boldsymbol{1} \end{bmatrix} \boldsymbol{v} \\ &= \boldsymbol{A}\boldsymbol{z} + \boldsymbol{B}\boldsymbol{v} \end{aligned} \tag{5.17a}$$

$$\begin{aligned} \boldsymbol{y} = \boldsymbol{q} &= \begin{bmatrix} \boldsymbol{1} & \boldsymbol{0} & \boldsymbol{0} \end{bmatrix} \begin{bmatrix} \boldsymbol{q} \\ \dot{\boldsymbol{q}} \\ \ddot{\boldsymbol{q}} \end{bmatrix} \\ &= \boldsymbol{C}\boldsymbol{z} \end{aligned} \tag{5.17b}$$

The MATLAB function *care* allows us to find the unique stabilizing solution to the continuous-time algebraic Ricatti equation knowing the matrices A, B and C. It also computes the gain matrix directly.

5.3.1 7-DOF simulation: Simplified feedback linearization for 2nd order operational space impedance tracking

The simulations have been performed on the 7-dof manipulator model that was also used in section 4.3. The dynamic matrices and vectors $\boldsymbol{B}(\boldsymbol{q})$, $\boldsymbol{C}(\boldsymbol{q}, \dot{\boldsymbol{q}})$ and $\boldsymbol{g}(\boldsymbol{q})$ are computed directly using the *Peter Corke's Robotics for MATLAB* as a *MATLAB-Simulink* library.

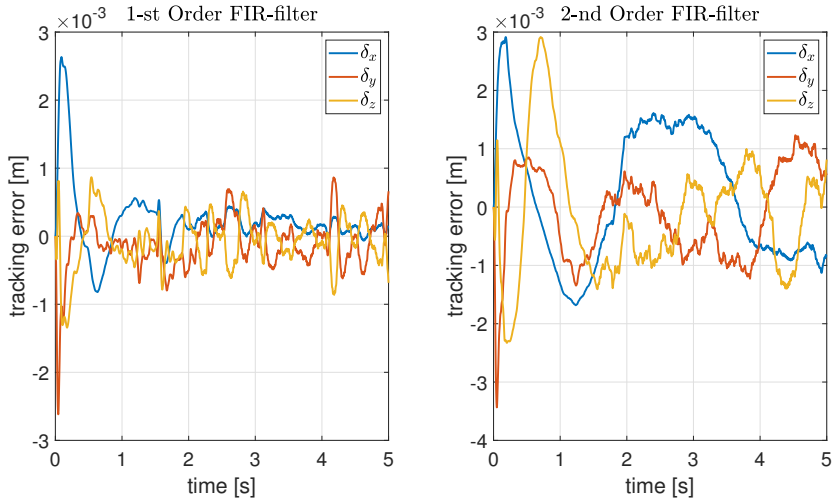

(a) Tracking error

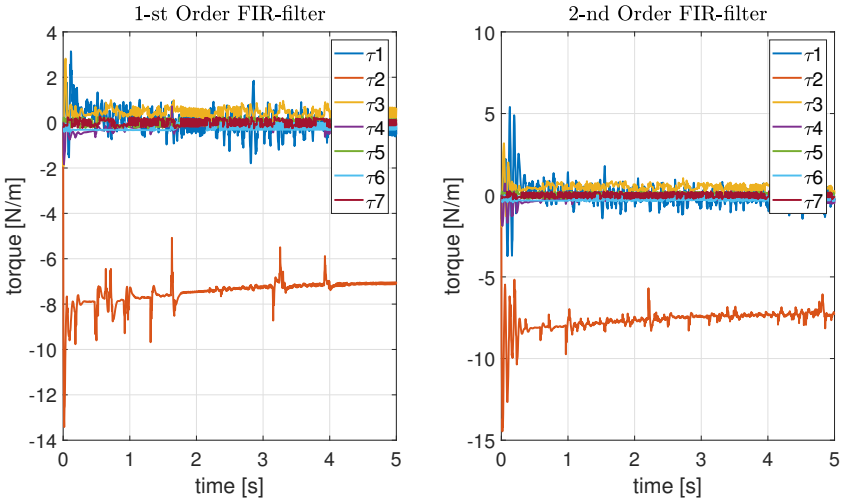

(b) Torques)

Figure 5.7: Operational space impedance tracking (2nd Order dynamics): SMC with linear approximation, feedback linearization simplified method

The uncertainty in the manipulator dynamics model is introduced by underestimating the dynamic vector $\boldsymbol{N}(\boldsymbol{q}, \dot{\boldsymbol{q}}) = \boldsymbol{C}(\boldsymbol{q}, \dot{\boldsymbol{q}})\dot{\boldsymbol{q}} + \boldsymbol{g}(\boldsymbol{q})$ in the feedback linearization control law as $\hat{\boldsymbol{N}}(\boldsymbol{q}, \dot{\boldsymbol{q}}) = \mathbf{0.9}\boldsymbol{N}(\boldsymbol{q}, \dot{\boldsymbol{q}})$. The desired 2nd order dynamics is defined with the diagonal matrices $\bar{\boldsymbol{M}} = \boldsymbol{I_3}$, $\bar{\boldsymbol{D}} = \mathbf{10}\boldsymbol{I_3}$ and $\bar{\boldsymbol{K}} = \mathbf{8}\boldsymbol{I_7}$. Thus, the imposed impedance relation is that of a over-damped system.

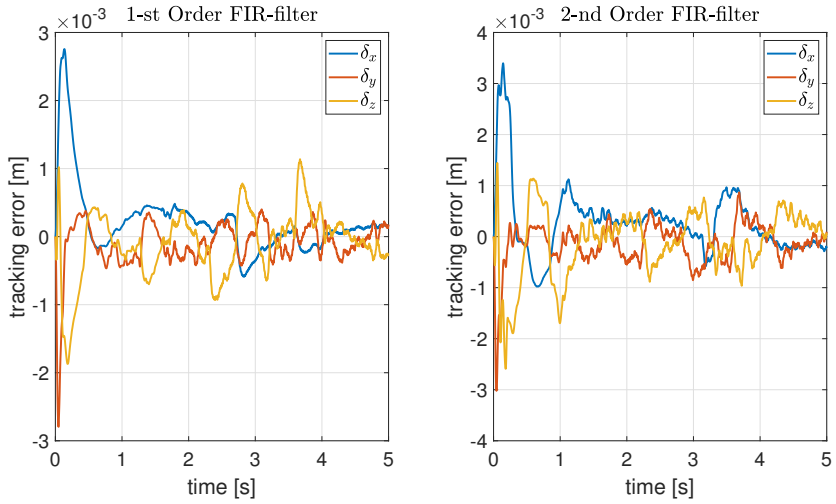

(a) Tracking error

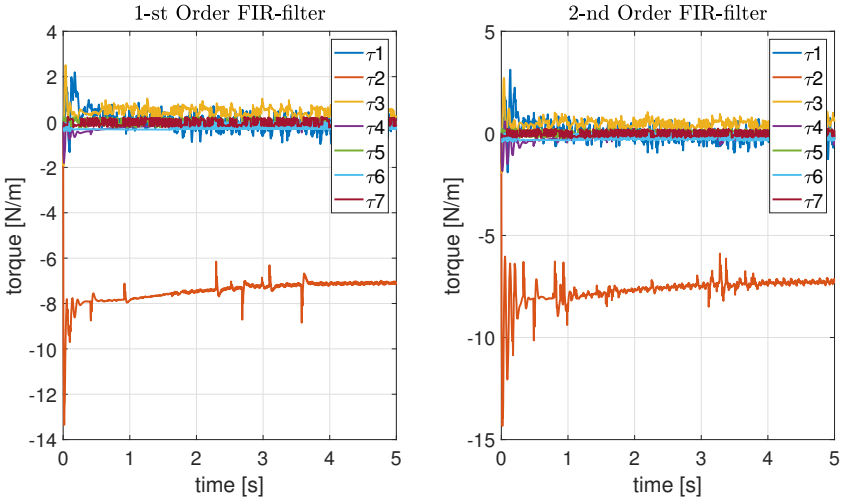

(b) Torques)

Figure 5.8: Operational space control: SMC with sigmoid approximation

The control effort and the tracking error for centralized SMC for each joint is reported in figures 5.7, 5.8 and 5.9. The results account for all the considered sources of instability viz. uncertain dynamic model, delay, joint friction and filter

on the torque channel. The MPC equivalent control law is computed with the constraint of constant end-effector orientation expressed through euler angles. They provide a comprehensive comparison of various SMC approximations for the switching function viz. linear approximation, sigmoid approximation and Super Twisting Algorithm.

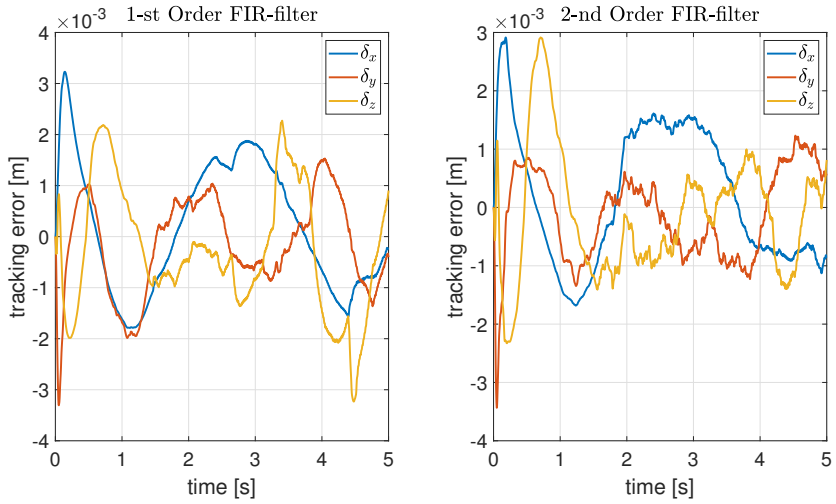

(a) Tracking error

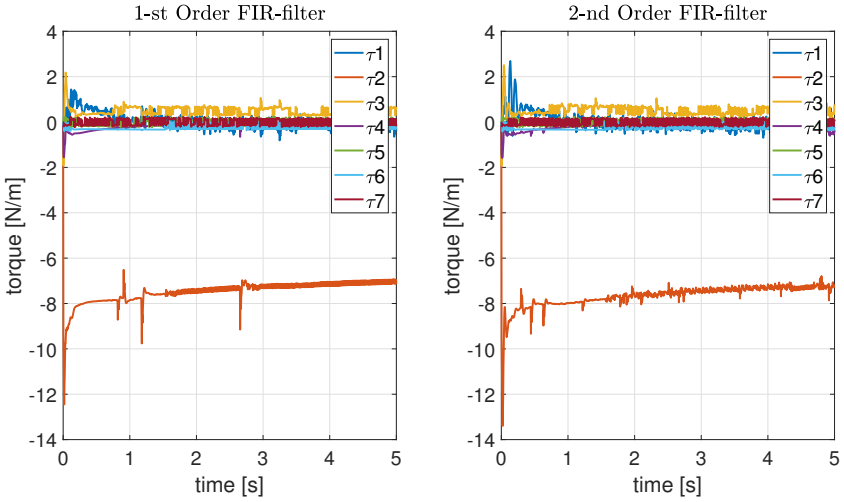

(b) Torques)

Figure 5.9: Operational space control: SMC with STA

The state feedback linearized control law is designed considering the 1-st order FIR model. Recalling the estimated joint friction model reported in equation 5.1a and 5.1b, the results also reflect on the robustness of the designed controller by

presenting the operational space impedance tracking when the FIR-filter model is different from the one on which the controller is designed. Note: the torque signals reported are the filtered by 1-st order FIR-filter. To summarize the above results, a progressive improvement in the torque profile is observed while using linear to STA approximation of SMC. But, this improvement is at the expense of tracking error.

5.3.2 Predictive SMC analysis: Operational space control

We saw that implementation of predictive SMC in section 3.2 for decentralized control and it has significantly better results. The predictive control scheme was then implemented for operational space control in chapter 4. Now, let's explore further how a change in prediction horizon for the estimation of joint position and joint velocities affect the operational space impedance control. In equation 3.4, we reported the d-step ahead predictors for joint variables. Using equation 3.4a and 3.4b, we can obtain the expression for 4-step ahead predictors for joint position and joint velocity. Note: these general equations can also be used for the case of 3rd order impedance tracking but in this section we will impose a second order dynamics and we will only use the first two set of equations.

$$\hat{\dot{\boldsymbol{q}}}(\boldsymbol{k+4}) = \dot{q}(k) + T_s\big(v(k-4) + v(k-3) + v(k-2) + v(k-1)\big) \quad (5.18a)$$

$$\hat{\boldsymbol{q}}(\boldsymbol{k+4}) = q(k) + 4T_s\dot{q}(k) + T_s^2\big(3v(k-4) + 2v(k-3) + v(k-2)\big) \quad (5.18b)$$

As we used an explicit numerical approximation (Forward Euler Method), we can directly use them as estimators using the information till the current time step i.e the the quanitities are a-priori known. The rejection capabilities of SMC dictates the convergence of these estimators. The figure 5.10 and 5.11 presents a comparison of 2-step and 4-step prediction horizons for the SMC with Super Twisting Algorithm. There is an evident improvement in the tracking error and the quality of the control signal. Besides, a faster convergence to the sliding manifold is observed with the 4-step ahead prediction.

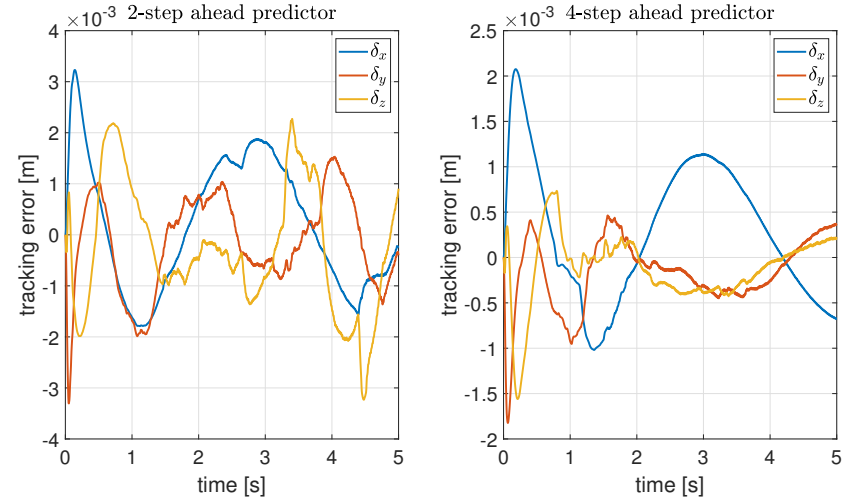

(a) Tracking error

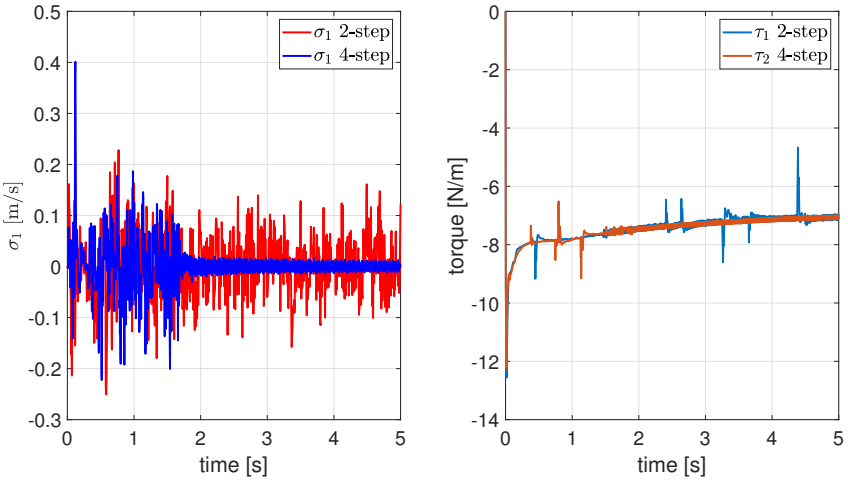

(b) Sliding surface and control signal of first joint

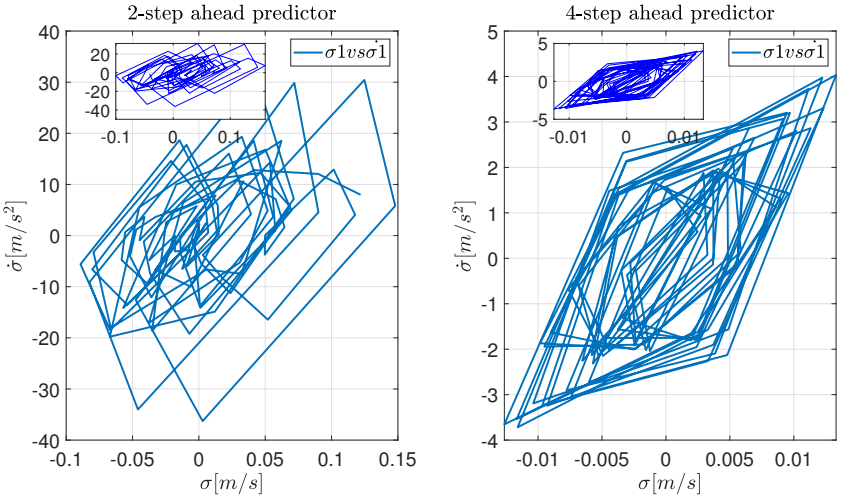

(c) Convergence to the sliding manifold

Figure 5.10: Comparison of 2nd order operational space impedance tracking with 2-step and 4-step ahead prediction (Predictive SMC with Feedback Linearization)

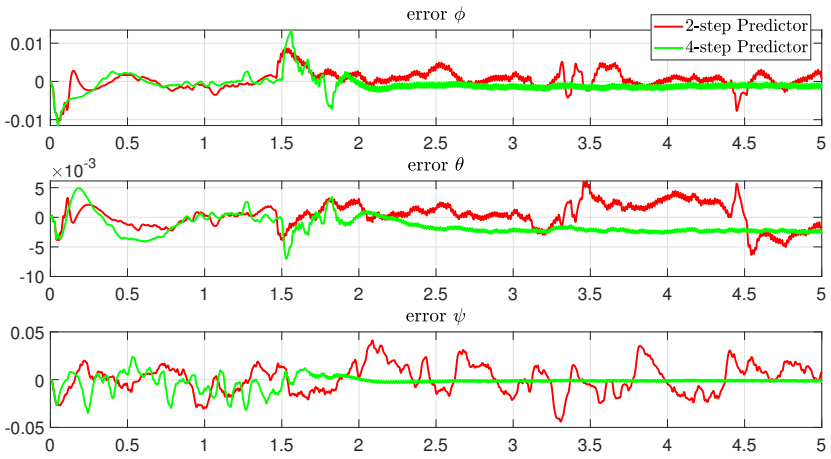

(a) End-effector orientation constraints (Euler angles)

Figure 5.11: Comparison of centralized control with 2-step and 4-step ahead prediction for joint variables (Predictive SMC with Feedback Linearization)

There is also a significant improvement in the satisfaction of enforced constraints in the MPC formulation for centralized equivalent control law.

5.4 Centralized SMC: Extension to 3rd Order Impedance Tracking

The filter on the torque channel of the manipulator system results into a 3rd order dynamical system. So let's extend the theory of operational space control for imposing a 3rd order dynamics given by:

$$\bar{\boldsymbol{P}}\boldsymbol{x}^{[3]} + \bar{\boldsymbol{Q}}\ddot{\boldsymbol{x}} + \bar{\boldsymbol{R}}\dot{\boldsymbol{x}} + \bar{\boldsymbol{T}}\boldsymbol{x} = \boldsymbol{h} \tag{5.19}$$

where $\bar{\boldsymbol{P}} = diag(p_1, ..., p_n)$, $\bar{\boldsymbol{Q}} = diag(q_1, ..., q_n)$, $\bar{\boldsymbol{R}} = diag(r_1, ..., r_n)$ and $\bar{\boldsymbol{T}} = diag(t_1, ..., t_n)$ are diagonal matrices that define the impedance profile. Depending on the requirement the value of n can be 1 for single spatial coordinate, 3 for x, y, z position or 6 for full end-effector position and orientation. External force h will not be considered during the simulations while for the practical implementation

this external force will be estimated. The desired impedance profile can then be expressed as:

$$\boldsymbol{I} = \bar{\boldsymbol{P}}\boldsymbol{x}^{[3]} + \bar{\boldsymbol{Q}}\ddot{\boldsymbol{x}} + \bar{\boldsymbol{R}}\dot{\boldsymbol{x}} + \bar{\boldsymbol{T}}\boldsymbol{x} - \boldsymbol{h} \tag{5.20}$$

Performing integration on both sides we get:

$$\boldsymbol{S} = \int \boldsymbol{I} = \bar{\boldsymbol{P}}\ddot{\boldsymbol{x}} + \bar{\boldsymbol{Q}}\dot{\boldsymbol{x}} + \bar{\boldsymbol{R}}\boldsymbol{x} + \bar{\boldsymbol{T}}\int \boldsymbol{x} - \int \boldsymbol{h} \tag{5.21}$$

This step in case of 2nd order dynamics resulted in an expression independent of acceleration. But now, we have dependency on the acceleration as well. So, we will use the joint variable prediction equations to compute the prediction of joint accelerations. Using manipulator forward and differential kinematics, we can express the obtained expression in terms of joint variables:

$$\boldsymbol{x} = \boldsymbol{T}(\boldsymbol{q}) \tag{5.22a}$$

$$\dot{\boldsymbol{x}} = \boldsymbol{J}(\boldsymbol{q})\dot{\boldsymbol{q}} \tag{5.22b}$$

$$\ddot{\boldsymbol{x}} = \dot{\boldsymbol{J}}(\boldsymbol{q})\dot{\boldsymbol{q}} + \boldsymbol{J}(\boldsymbol{q})\ddot{\boldsymbol{q}} \tag{5.22c}$$

$$\boldsymbol{x}^{[3]} = \boldsymbol{J}(\boldsymbol{q})\boldsymbol{q}^{[3]} + 2\dot{\boldsymbol{J}}(\boldsymbol{q})\ddot{\boldsymbol{q}} + \ddot{\boldsymbol{J}}(\boldsymbol{q})\dot{\boldsymbol{q}} \tag{5.22d}$$

Using the same arguments as in section 4.1.1, we can finally derive the operational space sliding surface as a function of joint space coordinates:

$$\boldsymbol{\sigma_{op}} = \boldsymbol{J}^{\boldsymbol{T}}(\boldsymbol{q})\Big[\bar{\boldsymbol{P}}\ddot{\boldsymbol{x}} + \bar{\boldsymbol{Q}}\dot{\boldsymbol{x}} + \bar{\boldsymbol{R}}\boldsymbol{x} + \bar{\boldsymbol{T}}\int \boldsymbol{x} - \int \boldsymbol{h}\Big] \tag{5.23}$$

The defined sliding surface still guarantees I as the sliding manifold and that can be verified through following theorem that is based on *Rouche-Capelli Theorem.*

Theorem: *(Dynamics convergence) Consider an n-dof manipulator, with Jacobian rank equal to dimension of impedance relation operating in a set defined by joint positions far away from kinematic singularities. If* $\boldsymbol{\sigma_{op}} = \boldsymbol{0} \quad \forall t \geq t_f$, *then* $\boldsymbol{I} = \boldsymbol{0} \quad \forall t \geq t_f$ *and correct impedance profile is tracked.*

Proof: Let's write the hypothesis: $\boldsymbol{\sigma_{op} = J^T(q) \int I = 0}$, then if the matrix $J^T(q)$ fulfills the assumption:

$$\text{rank } \boldsymbol{J^T(q)} = n = dim\boldsymbol{I} \qquad \forall \boldsymbol{q \in Q}$$

then, there exists a unique solution which corresponds to:

$$\int \boldsymbol{I = 0} \qquad \forall \boldsymbol{t \geq t_f} \implies \boldsymbol{I = 0} \qquad \forall \boldsymbol{t \geq t_f}$$

This is a sufficient condition. Although, σ_{op} is different from $\int J^T I$ but they share the same sliding manifold. Note: the theorem is valid also when the manipulator is redundant.

Centralized equivalent control

Now, let's transform the sliding surface as the function of joint variables using equation 5.22. As we have defined the sliding surface, we need to compute the equivalent control law v^{eq} by equating the sliding variable to zero. Note: we can use directly $I = 0$ as it is valid on the sliding manifold. For simplification dependency on q is not shown in the following expressions.

$$\bar{\boldsymbol{P}}\Big(\boldsymbol{J q^{[3]} + 2\dot{J}\ddot{q} + \ddot{J}\dot{q}}\Big) + \bar{\boldsymbol{Q}}\Big(\boldsymbol{J\ddot{q} + \dot{J}\dot{q}}\Big) + \bar{\boldsymbol{R}}\boldsymbol{J\dot{q}} + \bar{\boldsymbol{T}}\boldsymbol{T(q)} - \boldsymbol{h} = \boldsymbol{0} \quad (5.24)$$

with nominal condition for the manipulator model as $q^{[3]=v}$, we can compute equivalent control by substituting this in equation 5.24 and we will have the following form:

$$\boldsymbol{A(q)v = b(q)} \quad (5.25)$$

where,

$$\begin{aligned} \boldsymbol{A(q)} &= \bar{\boldsymbol{P}}\boldsymbol{J(q)} \\ \boldsymbol{b(q)} &= -\bar{\boldsymbol{T}}\boldsymbol{T(q)} - \bar{\boldsymbol{R}}\boldsymbol{J\dot{q}} - \bar{\boldsymbol{Q}}\Big(\boldsymbol{J\ddot{q} + \dot{J}\dot{q}}\Big) - \bar{\boldsymbol{P}}\Big(\boldsymbol{2\dot{J}\ddot{q} + \ddot{J}\dot{q}}\Big) \end{aligned} \quad (5.26)$$

The matrix $A(q)$ can be invertible or under-determined. But, we will use MPC formulation ($||A(q)v - b(q)||^2$) which can accomplish our objective of dexterous manipulation. This can then be used to express in a compatible qp formulation using equation 4.11 to define $\boldsymbol{H_{eq}}$ and $\boldsymbol{g_{eq}}$.

5.4.1 Predictive SMC

The 2-step and 4-step predictors for joint variables will be different from the ones we used so far. As the centralized equivalent control is now $q^{[3]} = v$ which was earlier $\ddot{q} = v$ when we were imposing a second order dynamics. The predictor equations can be obtained directly from the d-step ahead predictor equations 3.4.

2-step ahead predictor equations

$$\hat{\ddot{\boldsymbol{q}}}(\boldsymbol{k+2}) = \ddot{q}(k) + T_s\Big(v(k-2) + v(k-1)\Big) \tag{5.27a}$$

$$\hat{\dot{\boldsymbol{q}}}(\boldsymbol{k+2}) = \dot{q}(k) + 2T_s\ddot{q}(k) + T_s^2 v(k-2) \tag{5.27b}$$

$$\hat{\boldsymbol{q}}(\boldsymbol{k+2}) = q(k) + 2T_s\dot{q}(k) + T_s^2\ddot{q}(k) \tag{5.27c}$$

4-step ahead predictor equations

$$\hat{\ddot{\boldsymbol{q}}}(\boldsymbol{k+4}) = \ddot{q}(k) + T_s\Big(v(k-4) + v(k-3) + v(k-2) + v(k-1)\Big) \tag{5.28a}$$

$$\hat{\dot{\boldsymbol{q}}}(\boldsymbol{k+4}) = \dot{q}(k) + 4T_s\ddot{q}(k) + T_s^2\Big(3v(k-4) + 2v(k-3) + v(k-2)\Big) \tag{5.28b}$$

$$\hat{\boldsymbol{q}}(\boldsymbol{k+4}) = q(k) + 4T_s\dot{q}(k) + 6T_s^2\ddot{q}(k) + T_s^3\Big(3v(k-4) + v(k-3)\Big) \tag{5.28c}$$

As mentioned earlier the predictors are explicit numerically and hence can be implemented with the a-priori known information. It must be noted that as the equivalent control represents $q^{[3]}$, we also need an estimator for acceleration in addition to the position and velocity.

5.4.2 MPC formulation

In section 2.7.1, the general form of the QP formulation was introduced. We already formulated the centralized equivalent control requirements as the cost

function for this optimization. But, to deal with redundancy we to introduce some constraints or additional cost functions to be minimized. The procedure we adopted involves the consumption of the remaining degrees of freedom through minimization of joint velocities. Mathematically, this goal translates into:

$$\min_{q^{[3]}} ||\dot{q}_{k+1}||$$

Assuming to work within the pass band of the controller, the discrete time manipulator is reduced to chain of integrator system:

$$\begin{aligned} q_{k+1} &= q_k + T_s\dot{q}_k + \frac{T_s^2}{2}\ddot{q}_k + \frac{T_s^3}{6}q_k^{[3]} \\ \dot{q}_{k+1} &= \dot{q}_k + T_s\ddot{q}_k + \frac{T_s^2}{2}q_k^{[3]} \\ \ddot{q}_{k+1} &= \ddot{q}_k + T_s q_k^{[3]} \end{aligned} \tag{5.29}$$

Using this discrete form, finally we obtain a form compatible with the QP formulation:

$$\begin{aligned} H_{vel} &= A_{q\ vel}^T Q_{vel} A_{q_{vel}} \\ g_{vel} &= -A_{q\ vel}^T Q_{vel} b_{q_{vel}} \\ &where, \\ A_{q_{vel}} &= \frac{T_s^2}{2} \\ b_{q_{vel}} &= -\left(\dot{q}_k + T_s\ddot{q}_k\right) \end{aligned} \tag{5.30}$$

The problem of overall optimization is then defined by:

$$\begin{aligned} H_{total} &= H_{eq} + H_{vel} \\ g_{total} &= g_{eq} + g_{vel} \end{aligned} \tag{5.31}$$

Constraint formulation

In chapter 4 we used two different constraints for the optimization viz. end-effector orientation and constraint on the motions of 5th, 6th and 7th joints.

Let's formulate the end-effector orientation constraint (through euler angles) when a third order impedance tracking is performed. The constraint is being applied directly in the cartesian space while the minimization problem is in the joint space. This conversion is performed using the *Grönwall's lemma*. The constraints can be defined as:

$$\begin{aligned} \boldsymbol{\Theta} &= \begin{bmatrix} \boldsymbol{\phi} & \boldsymbol{\theta} & \boldsymbol{\psi} \end{bmatrix} \\ \boldsymbol{\Theta(t)} &= \boldsymbol{\Theta_0} \\ \dot{\boldsymbol{\Theta}} &= \boldsymbol{0} \\ \ddot{\boldsymbol{\Theta}} &= \boldsymbol{0} \end{aligned} \tag{5.32}$$

where Θ_0 can be initial orientation of the end-effector or any other desired value. Using *Grönwall's lemma*, these equalities can be written as the solution of the differential equation:

$$\begin{aligned} \boldsymbol{\Theta^{[3]}} = \boldsymbol{\Theta_0^{[3]}} &- (\boldsymbol{\lambda_1} + \boldsymbol{\lambda_2} + \boldsymbol{\lambda_3})(\ddot{\boldsymbol{\Theta}} - \ddot{\boldsymbol{\Theta}}_{\boldsymbol{0}}) \\ &-(\boldsymbol{\lambda_1\lambda 2} + \boldsymbol{\lambda_2\lambda_3} + \boldsymbol{\lambda_1\lambda_3})(\dot{\boldsymbol{\Theta}} - \dot{\boldsymbol{\Theta}}_{\boldsymbol{0}}) - \boldsymbol{\lambda_1\lambda_2\lambda_3}(\boldsymbol{\Theta} - \boldsymbol{\Theta_0}) \end{aligned} \tag{5.33}$$

where $\lambda_1, \lambda_2, \lambda_3$ are positive scalar coefficients that define the reaching transient. Using the following relations from differential kinematics of the manipulator we can convert this differential equation in terms of joint coordinates. The explicit dependency of the constraint on v is finally expressed in the form 2.15c ($lbA \leq Av \leq ubA$) as expressed in equation 5.35.

$$\begin{aligned} \dot{\boldsymbol{\Theta}} &= \boldsymbol{J_A}\dot{\boldsymbol{q}} \\ \ddot{\boldsymbol{\Theta}} &= \boldsymbol{J_A}\ddot{\boldsymbol{q}} + \dot{\boldsymbol{J}}_{\boldsymbol{A}}\dot{\boldsymbol{q}} \\ \boldsymbol{\Theta^{[3]}} &= \ddot{\boldsymbol{J}}_{\boldsymbol{A}}\dot{\boldsymbol{q}} + 2\dot{\boldsymbol{J}}_{\boldsymbol{A}}\ddot{\boldsymbol{q}} + \boldsymbol{J_A}\boldsymbol{q^{[3]}} \end{aligned} \tag{5.34}$$

$$
\begin{aligned}
\boldsymbol{ubA = lbA} = \boldsymbol{\Theta^{[3]} - (\ddot{J}_A\dot{q} + 2\dot{J}_A\ddot{q}) - (\lambda_1 + \lambda_2 + \lambda_3)*} \\
&\boldsymbol{(J_A\ddot{q} + \dot{J}_A\dot{q} - \ddot{\Theta}_0) - (\lambda_1\lambda 2 + \lambda_2\lambda_3 + \lambda_1\lambda_3)*} \\
&\boldsymbol{(J_A\dot{q} - \dot{\Theta}_0) - \lambda_1\lambda_2\lambda_3(\Theta - \Theta_0)} \\
\boldsymbol{A} &= \boldsymbol{J_A}
\end{aligned}
\tag{5.35}
$$

where J_A is of dimension (3x7) for the 7-DOF manipulator in consideration. This gives us the constraints in the form of equation 2.15c.

Joint-limits: complementary constraints

Besides, the constraints described earlier, there are constraints due to robot capabilities due to it's mechanical characteristics. These are constraints on the joint accelerations, velocities and positions. We defined these limits in equation 3.7 and in section 4.2.1 we mentioned their importance in computation of MPC equivalent control law. But the transformation of nominal system from $v = \ddot{q}$ to $v = q^{[3]}$ also demands a modification in their formulation. The formulation used prior to third order impedance is:

$$
\begin{aligned}
\boldsymbol{lb} &= \boldsymbol{max}\left(-\ddot{\boldsymbol{q}}_{\boldsymbol{max}}, \frac{-\dot{\boldsymbol{q}}_{\boldsymbol{max}} - \dot{\boldsymbol{q}}_{\boldsymbol{k}}}{\boldsymbol{T_s}} \right) \\
\boldsymbol{ub} &= \boldsymbol{min}\left(\ddot{\boldsymbol{q}}_{\boldsymbol{max}}, \frac{\dot{\boldsymbol{q}}_{\boldsymbol{max}} - \dot{\boldsymbol{q}}_{\boldsymbol{k}}}{\boldsymbol{T_s}} \right)
\end{aligned}
\tag{5.36}
$$

where the maximum and minimum operators are applied element by element. The parameters $q_{min_i}, \dot{q}_i$ are defined as equation 3.7b. It also impose a quadratic relationship between position and speed as in figure 5.12. Note: the actual configuration bounds are defined by this new quadratic relationship.

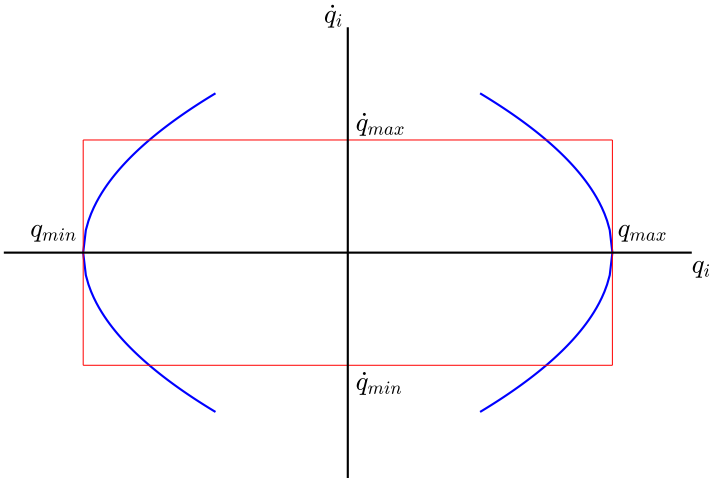

Figure 5.12: Quadratic relation $(q_i, \dot{q}_i)$ to set joint limits

Finally, a similar form of equation 5.36 is used to enforce the joint limits when $q^{[3]}$ is the control signal. We ensure this by replacing $\ddot{q}_{max}$, $\dot{q}_{max/min}$ and $\dot{q}_k$ by $q^{[3]}_{max}$, lb/ub (as computed above) and $\ddot{q}_k$ respectively.

5.4.3 7-DOF Simulation: 3^{rd} Order Impedance Tracking

Without joint friction

To verify the results obtained in section 5.4, simulations are performed on the 7-DOF manipulator model used earlier in chapter 3 and 4. Sliding Mode Control is implemented with Super Twisting Algorithm. ISMC is implemented to guarantee the desired reaching phase. The *sign* function in STA is approximated with a sigmoid function with $\delta = 0.1$. The MPC formulation uses the optimization with constraints on the end-effector orientation defined by euler angles. The three constant parameters that define the convergence of these constraints using *Grönwall's lemma* are $\lambda_1 = 3.5, \lambda_2 = 2.5, \lambda_3 = 1.1$. The approach to feedback linearization defined in section 5.3 has been adopted. A first order FIR filter is used as an estimated model of the filter. The diagonal matrices $\bar{\boldsymbol{P}} = I_3$, $\bar{\boldsymbol{Q}} = 4I_3$, $\bar{\boldsymbol{R}} = 5I_3$ and $\bar{\boldsymbol{T}} = 2I_3$ define the desired impedance profile, which is an over-damped system.

Figure 5.13 reports the position evolution and the tracking error for the task space. The effectiveness of SMC to reject model uncertainties is verified. Besides, predictive SMC is able to counter the instabilities due to delay and from our conclusion of section 5.3.2 we have implemented using 4-step prediction horizon. **All sources of instabilities except joint friction** have been considered.

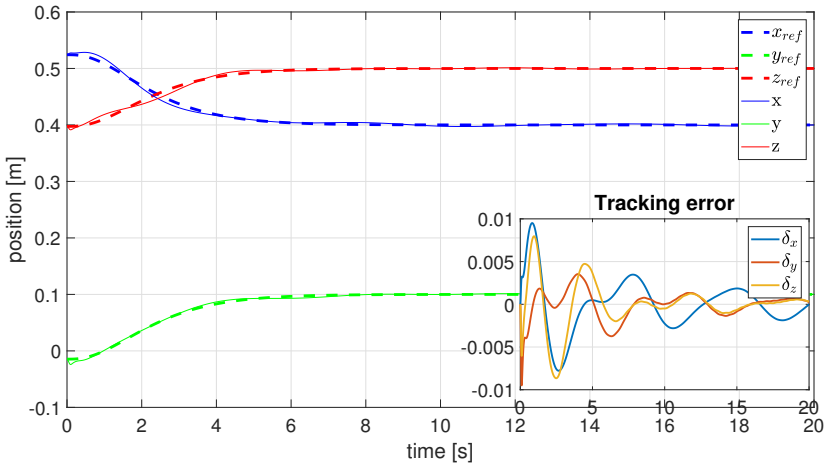

(a) Tracking error

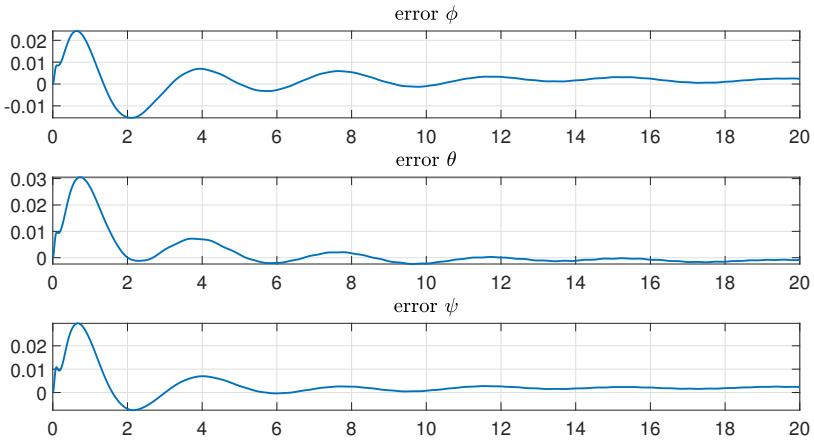

(b) End-effector orientation constraints (using Euler angles)

Figure 5.13: Centralized control: 3^{rd} order impedance tracking on 7-DOF Yumi Model (Feedback linearization with SMC as the outer loop)

It is worth mentioning here that the approach adopted in chapter 4 (section 4.3) is also implemented here to get the final control parameters i.e. step by step

consideration of each source of instability. There is a significant improvement in the tracking of the desired operational space impedance over the results reported for second order dynamic relation fulfilment using feedback linearization. This can be attributed to the fact that it involves intrinsic approximation while assigning the second order robot dynamics to a third order system. This is ensured by setting the appropriate eigenvalues in the compuation of gains during the solution of Continuous Algebraic Ricatti Equation (CARE) for the linear controller that was introduced in the feedback linearization control scheme 5.6.

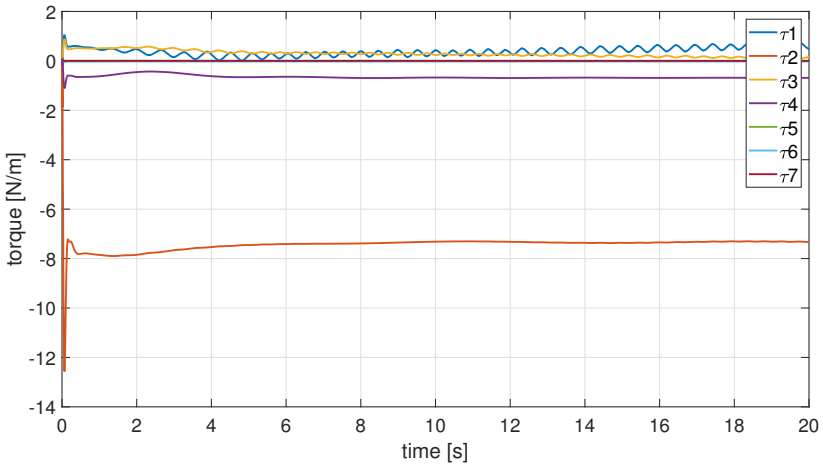

(a) Control signal: torque

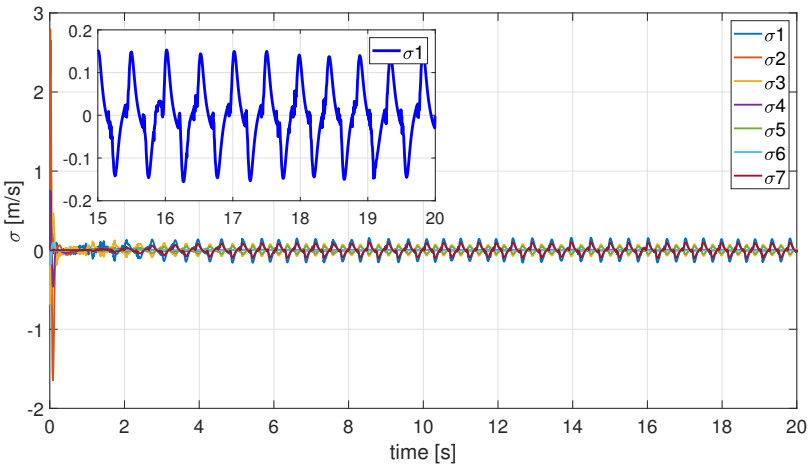

(b) Sliding surface

Figure 5.14: Centralized control: 3^{rd} order impedance tracking on 7-DOF Yumi Model (Feedback linearization with SMC as the outer loop)

With joint friction

Finally, to observe the affect of joint friction a comparison of results with and without joint friction consideration for operational space impedance tracking is reported in figure 5.15 and 5.16.

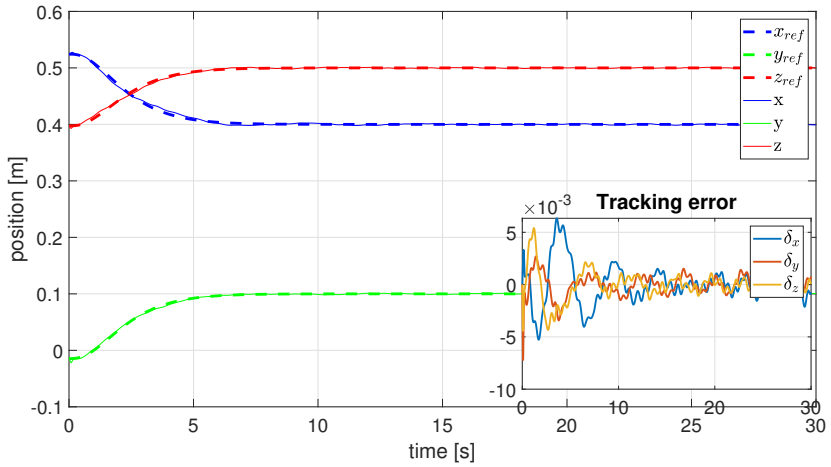

(a) Impedance tracking and tracking error without joint friction

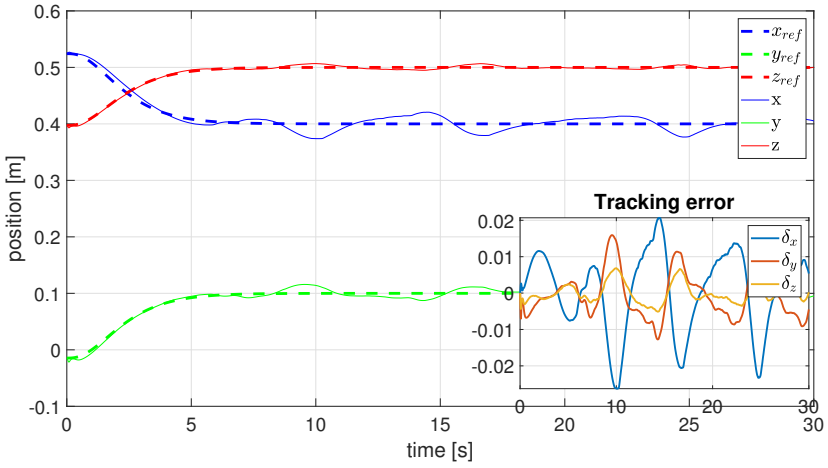

(b) Impedance tracking and tracking error with joint friction

Figure 5.15: Centralized control: 3^{rd} order impedance tracking on 7-DOF Yumi Model with and without joint friction

In this experiment, only first four joints of the 7-DOF manipulator are used to enforce the desired third order impedance while the remaining are constrained from motion. It significantly affects the quality of the control signal and impedance

tracking. This can be observed by increased chattering in the torque signals, higher tracking error and evolution of sliding variable.

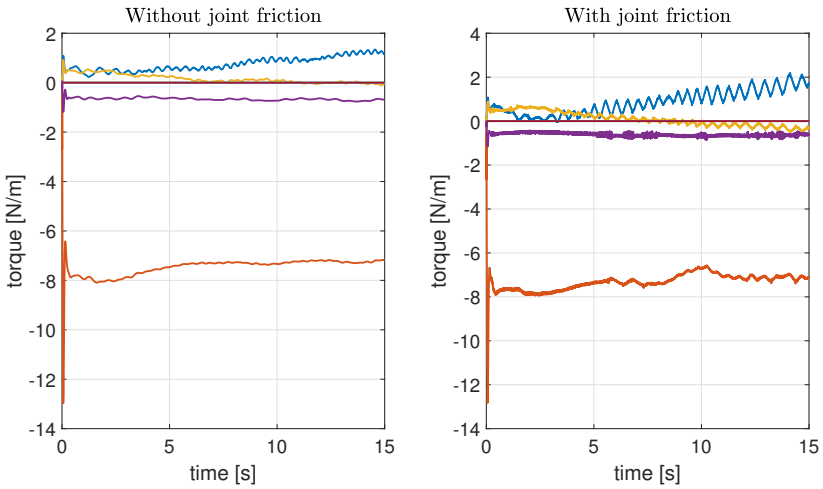

(a) Control signal: torque

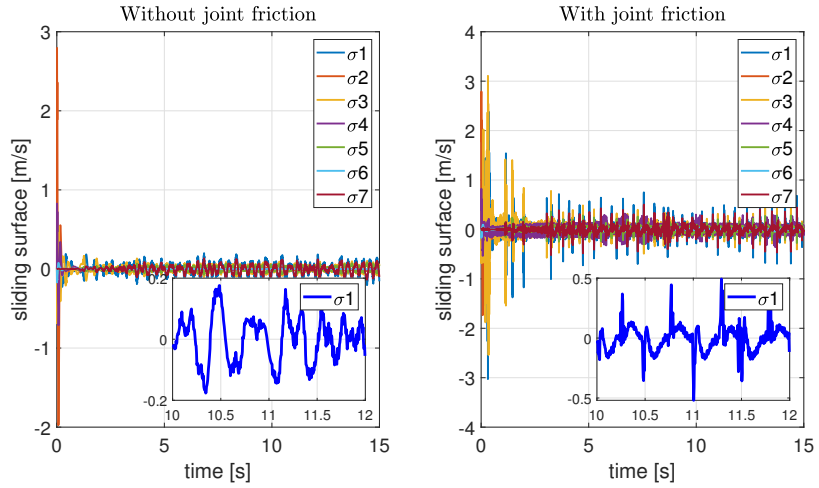

(b) Sliding surface

Figure 5.16: Centralized control: 3^{rd} order impedance tracking on 7-DOF Yumi Model with and without joint friction

A comparison between results of section 5.3.1 and 5.4 shows that 3rd order impedance tracking is better in all aspects with respect to the 2nd order impedance tracking. This is because the system with torque FIR-filter is actually a 3rd order system. There is a clear improvement in system evolution to the sliding manifold and quality of the control signal.

Chapter 6

Experimental Results

6.1 Experimental Set-up

The strategies developed in this study will be implemented on a dual arm robotic manipulator but using only a single arm. It is a 7-DOF manipulator, *ABB FRIDA*. A visual representation of the manipulator is shown in figure 6.1.

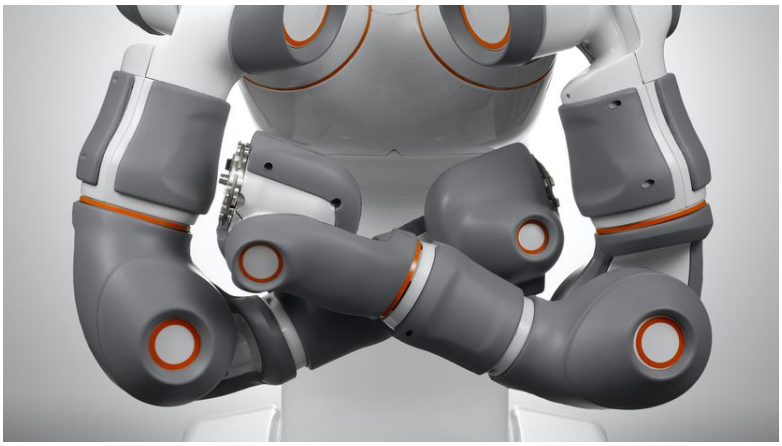

Figure 6.1: ABB FRIDA: experimental set-up

It is also equipped with an internal industrial controller that allows it to perform both in joint and operational (Cartesian) space. The control architecture is constituted by independent PID controllers. The feedback of encoders provides angular positions $q(t)$ and its derivative to get $\dot{q}(t)$, which is used to close the con-

trol loops. A research interface named *OPCOM* provides a means to interact with this internal controller directly through *MATLAB-Simulink Libraries*. In order to exploit full freedom the internal controller will be deactivated by using all gains as zero and using directly the torque feed-forward channel. A major concern is the presence of a FIR-filter that limits the maximum input frequency.

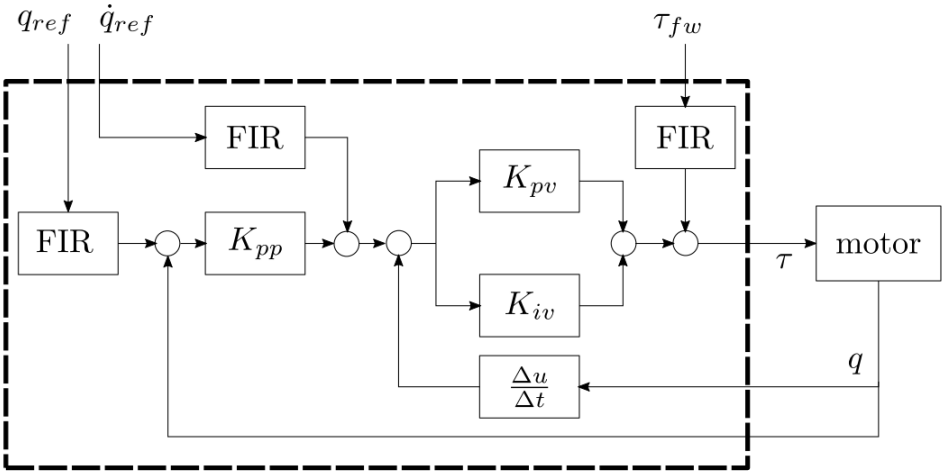

Figure 6.2: Block diagram of Yumi-FRIDA internal control structure

6.2 2nd Order: Impedance Tracking

In this section, the operational space controller results are presented for the left arm of the ABB FRIDA robot. The experiments are performed with the following considerations:

- The sequence of task execution is summarized in the state machine, figure 6.3. Only the left arm is used for the impedance control implementation. Open loop implies that YuMi internal controller is active while closed loop implies the use of external controller. In closed loop the internal PID is disabled and the control is performed directly through the torques, $\boldsymbol{\tau_{fw}}$. The abbreviation OTG stands for online trajectory generation.

- The control scheme presented in figure 5.2 is implemented with SMC as impedance control applied to the feedback linearized system (robot + filter).

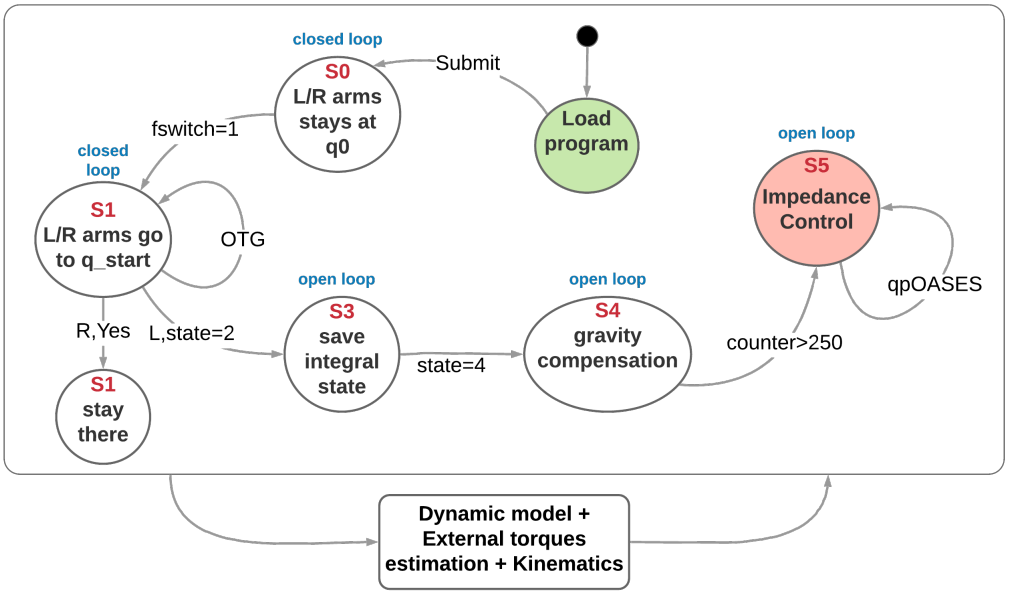

Figure 6.3: Finite state machine for the impedance control program

- The optimization performed for the compuation of centralized equivalent control law is based on the first 4 joints while joints 5, 6 and 7 are constrained from motion. In fact, joint 6 is mechanically fixed.

- The tuning parameters defining for the sliding mode control (via. super twisting algorithm) and the imposed dynamics in the experiment are reported in table 6.1. The impedance controller is tuned so as to achieve the 2 stable poles in -5. The initial condition of the left arm is defined as $q_{start} = \begin{bmatrix} 0 & 0 & 0 & 0 & 0 & \pi/2 & 0 \end{bmatrix}^T$ while for the right arm any position far away from the desired working space of the left arm is chosen.

$\begin{bmatrix} M & D & K \end{bmatrix}$	k_{CARE}	δ	u	v	W
$\begin{bmatrix} 1 & 10 & 25 \end{bmatrix}$	$\begin{bmatrix} 4000 & 800 & 80 \end{bmatrix}$	0.1	3.5	1.5	$\begin{bmatrix} 10 & 15 & 15 & 5 & 5 & 5 & 5 \end{bmatrix}^T$

Table 6.1: Tuning parameters chosen for the STA implementation for operational space impedance tracking with the 2nd order dynamics

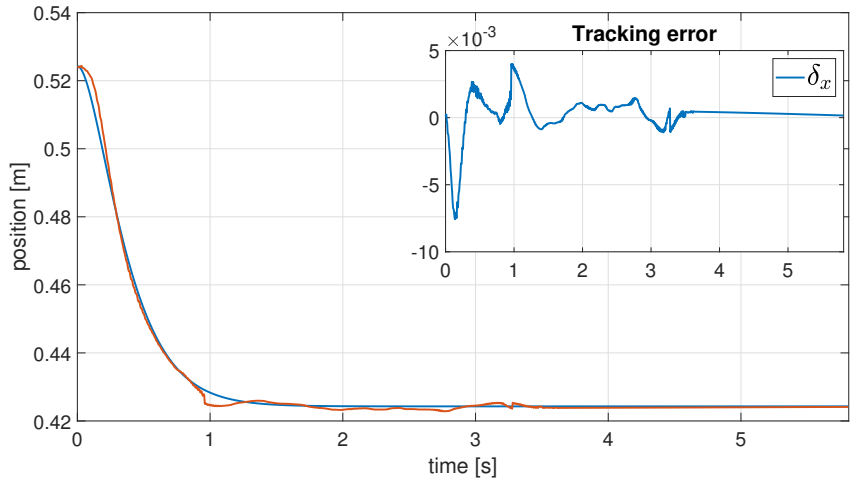

(a) Impedance tracking along x-axis

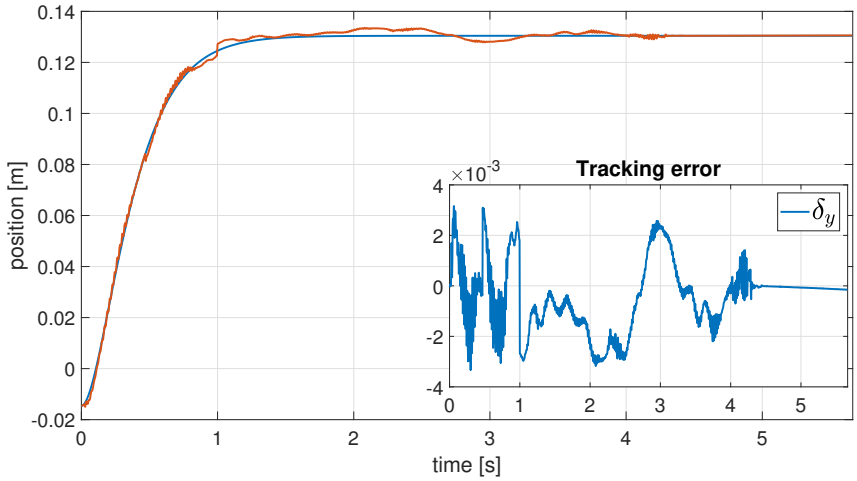

(b) Impedance tracking along y-axis

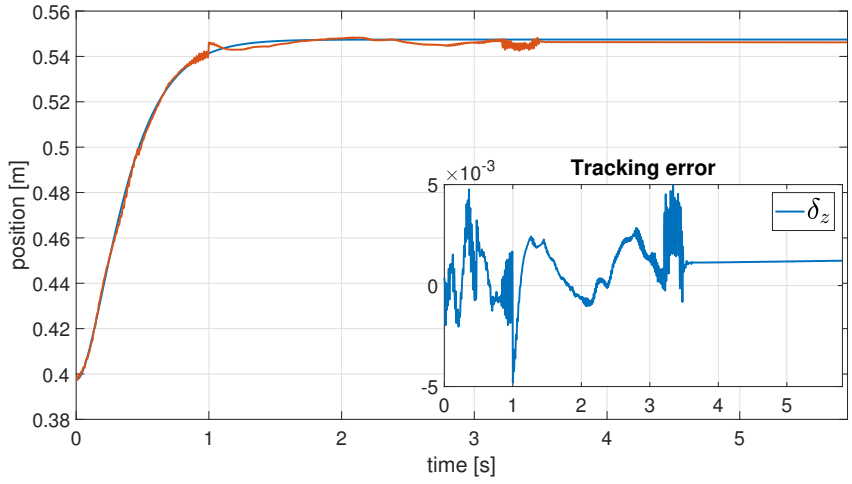

(c) Impedance tracking along z-axis

Figure 6.4: 2nd Order operational space impedance tracking with SMC applied as outer control loop to feedback linearized system

Figure 6.4 shows the tracking of desired dynamics for x, y and z axes. The obtained results validate the robustness of the obtained impedance controller based on a simple estimated model of the torque filter. The results are significantly affected by joint friction. When the desired dynamics is defined by slower poles i.e. relatively slow velocities the joint friction may become comparable to the actuation torques to perform the necessary control and that results in poor tracking.

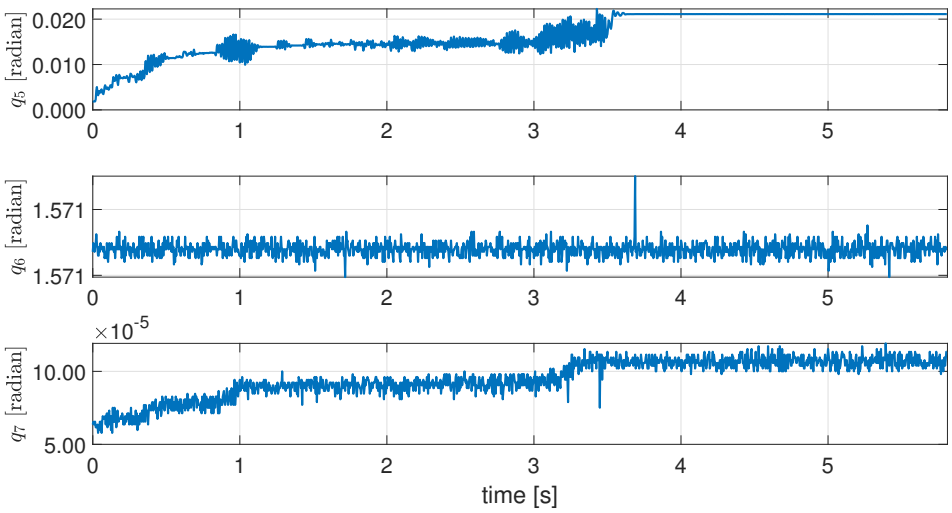

(a) Constraints on the motion of joints 5, 6 and 7

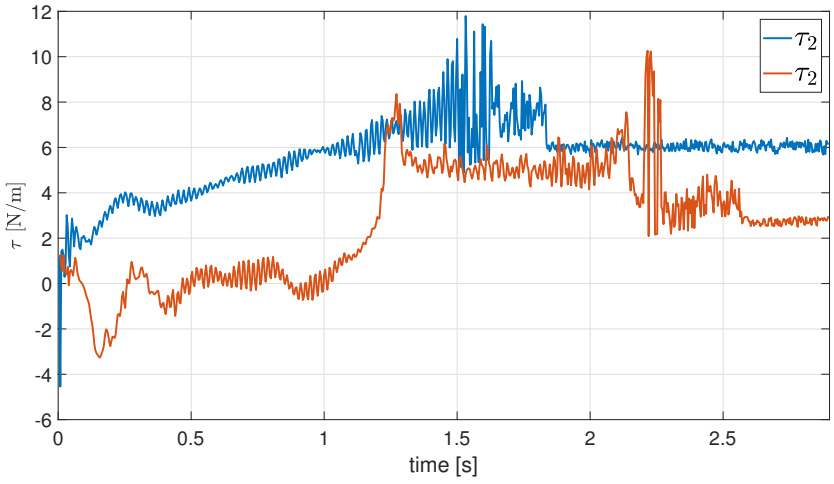

(b) Torques for joints 1 and 2

Figure 6.5: Constraints and control signal for 2nd Order operational space impedance tracking experiment

Figure 6.6 shows the joint position evolution for 5, 6 and 7th joints as they were constrained from movement and its evident it is satisfied adequately. The joint torques for first two joints show some oscillations in the transient but that is mainly due to the joint friction model considered for control design which is a highly simplistic one. The evolution of sliding variable is reported in the figure below. Note: there is always a trade-off between satisfying the constraints, impedance tracking or the quality of control signal.

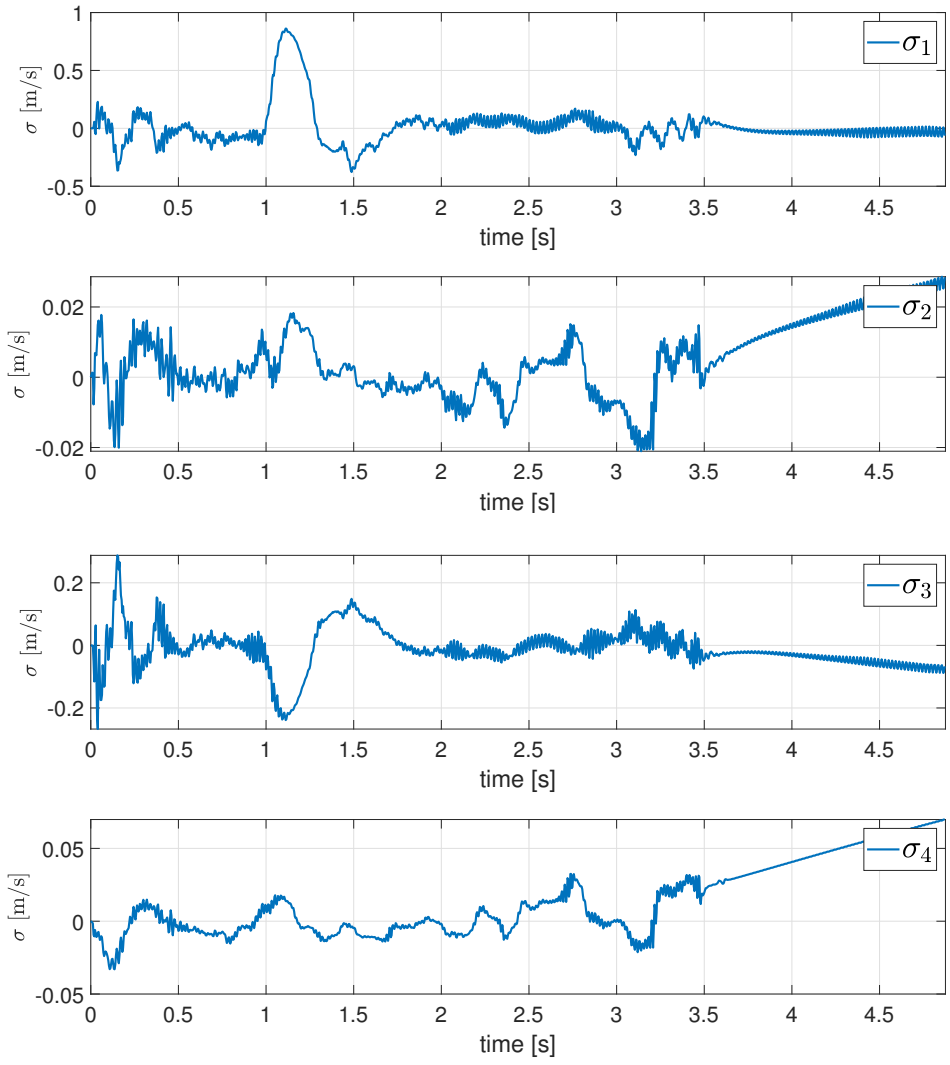

Figure 6.6: Sliding surfaces for the first four joints for the 2nd Order operational space impedance tracking experiment

Chapter 7

Conclusions

In this thesis, a comprehensive analysis was made for the operational space control using various non-linear control strategies. An operational space impedance controller has been developed and the theory is validated through simulations. The main objective of this thesis i.e. dexterous manipulation, in general refers to the variety of tasks that a system can accomplish and how well these tasks can be performed. The designed impedance controller is based on Sliding-mode Model Predictive Control (SMPC) that uses an optimization of various cost functions and constraints to find an optimal solution. Thus, fulfilling our objective of dexterous manipulation of robots.

From the work, it emerged how to integrate non-linear techniques namely feedback linearization and sliding mode control with an optimization problem to realize operational space impedance shaping with robustness to various uncertainties. It is shown particularly, the effectiveness of SMC to counter system uncertainties. A variation of STA with sigmoid approximation of sign function proved particularly effective in obtaining smooth torques. The choice of controller parameters that define the optimization have clear physical interpretation and this enables an insightful tuning procedure. This is applicable to either the chosen dynamic relation, weights of the cost function or the controller gains. Furthermore, the definition of finite state machine allowed the usage of both internal and external

controllers and extendability for further adaptation. The robustness of the proposed controller is validated through simulations with a different friction model and FIR-filter estimated model. Finally, the developed results are implemented on one of the world's first collaborative robot, ABB YuMi FRIDA.

Although the results achieved corroborate the proposed methods, the excessive demand on SMC can be reduced by a better estimation of joint friction. Also, an exact computation of feedback linearization control law has a potential to produce better results which needs to be further explored for implementations with higher degrees of freedom. Finally, the implementation needs to be extended to tasks of practical significance.

As research in dexterous manipulation continues to advance, we look for further evolution of concepts and ideas presented in this thesis.

BIBLIOGRAPHY

[1] Raymond R. Ma and Aaron M. Dollar. *"On Dexterity and Dexterous Manipulation"*. In: 15th International Conference on Advanced Robotics (ICAR), DOI:10.1109/ICAR.2011.6088576, Tallinn, Estonia, June 20-23, 2011.

[2] Bruno Siciliano, Oussama Khatib. *"Springer Handbook of Robotics"*. In: Springer International Publishing (2016), DOI 10. 1007/ 978- 3- 319- 32 55 2-1, Springer-Verlag Berlin Heidelberg 2016.

[3] Fabio Allevi. *"Impedance shaping and Model Predictive Sliding Mode Control for stable bilateral robot teleoperation"*. Master Thesis: Politecnico di Milano, 2016 -2017

[4] Uri Itkis. *"Control systems of variable structure"*. Wiley New York, 1976.

[5] S.Spurgeon. *"Sliding mode control: a tutorial"*. In: European Control Conference (ECC). July 2014, pp.2272–2277. doi: 10.1109/ECC.2014.6862622.

[6] John Y. Hung, Weibing Gao. *"Variable Structure Control: A Survey "*. In: IEEE Transactions on Industrial Electronics, VOL.40, No. 1, February 1993

[7] A. Calanca et al. *"Improving continuous approximation of Sliding Mode Control"*. In: 2013 16th International Conference on Advanced Robotics (ICAR). Nov. 2013, pp. 1–6. doi: 10.1109/ICAR.2013.6766486.

[8] Yuri Shtessel et al. *"Introduction: Intuitive Theory of Sliding Mode Control"*. In: Sliding Mode Control and Observation. New York, NY: Springer New York, 2014, pp. 1–42. isbn: 978-0-8176-4893-0. doi: 10.1007/978-0-8176-4893-01.

[9] A Levant. *"Introduction to high-order sliding modes"*. In: School of Mathematical Sciences, Israel 58.6 (2003), p. 1.

[10] G. Bartolini, A. Ferrara, and E. Usai. *"Chattering avoidance by second-order sliding mode control"*. In: IEEE Transactions on Automatic Control 43.2 (Feb. 1998), pp. 241–246. doi: 10.1109/9.661074.

[11] Mirza Tariq Hamayun, Christopher Edwards, Halim Alwi. *"Fault tolerant control schemes using integral sliding modes"*. Springer, 2016

[12] A. Ferrara and G. P. Incremona. *"Design of an Integral Suboptimal SecondOrder Sliding Mode Controller for the Robust Motion Control of Robot Manipulators"*. In: IEEE Transactions on Control Systems Technology 23.6 (Nov. 2015), pp. 2316–2325. issn: 1063-6536. doi: 10.1109/TCST.2015.2420624.

[13] Salah Laghrouchea, Franck Plestanb, Alain Glumineau. *"Higher order sliding mode control based on integral sliding mode"*. Automatica 43 (2007) 531 – 537. doi:10.1016/j.automatica.2006.09.017.

[14] Davide Nicolis, Andrea Maria Zanchettin, Paolo Rocco. *"A Hierarchical Optimization Approach to Robot Teleoperation and Virtual Fixtures Rendering."* IFAC PapersOnLine 50-1 (2017) 5672–5679.

[15] A. Ferrara, G. P. Incremona, and L. Magni. *"A robust MPC/ISM hierarchical multi-loop control scheme for robot manipulators"*. In: 52nd IEEE Conference on Decision and Control. Dec. 2013, pp. 3560–3565. doi: 10.1109/CDC.2013.6760430.

[16] Guido O. Guardabassi, Sergio M. Savaresi. *"Approximate feedback linearization of discrete-time non-linear systems using virtual input direct design"*. In: Systems & Control Letters 32 (1997) 63-74. PII S0167-6911(97)00063-7.

[17] M. Rubagotti et al. *"Robust Model Predictive Control With Integral Sliding Mode in Continuous-Time Sampled-Data Nonlinear Systems"*. In: IEEE Transactions on Automatic Control 56.3 (Mar. 2011), pp. 556–570. issn: 0018-9286. doi: 10.1109/TAC.2010.2074590.

[18] Andrea Maria Zanchettin and Paolo Rocco. *"Path-consistent safety in mixed human-robot collaborative manufacturing environments."* 2013 IEEE/RSJ International Conference on Intelligent Robots and Systems (IROS) November 3-7, 2013. Tokyo, Japan.

[19] A. de Luca, P. Lucibello. *"A general algorithm for dynamic feedback linearization of robots with elastic joints"*. In: 1998 IEEE International Conference on Robotics and Automation (Cat. No.98CH36146). DOI: 10.1109, ROBOT.1998.677024.

[20] M.W. Spong, R. Ortega. *"On adaptive inverse dynamics control of rigid robots"*. In: IEEE Transactions on Automatic Control (Volume: 35, Issue: 1, Jan 1990). DOI: 10.1109/9.45152.

[21] J.S. Chen, Y.H. Chen. *"Robust control of non-linear uncertain systems: A feedback linearization approach"*. In: Proceeding of the 30th Conference on Decision & Control, Brighton, England. CH3076-7/91/0000-2515 IEEE.

[22] Andrea Maria Zanchettin and Paolo Rocco. *"Robust constraint-based control of robot manipulators: an application to a visual aided grasping task"*. In: 2016 IEEE/RSJ International Conference on Intelligent Robots and Systems (IROS). 978-1-5090-3762-9/16.

[23] W. García-Gabín and E. F. Camacho. *"Sliding mode model based predictive control for non minimum phase systems"*. In: 2003 European Control Conference (ECC). Sept. 2003, pp. 904–909.

[24] Yuanqing Xia, Yingmin Jia. *"Robust sliding-mode control for uncertain time-delay systems: an LMI approach"*. In: IEEE Transactions on Automatic Control (Volume: 48 , Issue: 6 , June 2003). DOI: 10.1109/TAC.2003.812815.

[25] Matteo Rubagotti, Davide Martino Raimondo, Antonella Ferrara, Lalo Magni. *"Robust Model Predictive Control With Integral Sliding Mode in Continuous-Time Sampled-Data Nonlinear Systems"*. In: IEEE Transactions on Automatic Control 2011. DOI: 10.1109/TAC.2010.2074590.

[26] Marco Palumbo. *"Generazione del moto con sensori di visione per un manipolatore robotico a due bracci parzialmente teleoperato"*. Master thesis: Politecnico di Milano 2016-17.

[27] Christopher Kitts, Ignacio Mas. "Centralized and decentralized multirobot control methods using the cluster space control framework". In: 2010 IEEE/ASME International Conference on Advanced Intelligent Mechatronics. DOI: 10.1109/AIM.2010.5695768.

[28] J. Baillieul. *"Avoiding obstacles and resolving kinematic redundancy"*. In: 1986 IEEE International Conference on Robotics and Automation. DOI: 10.1109/ROBOT.1986.1087464.

[29] D.P. Martin, J. Baillieul, J.M. Hollerbach. *"Resolution of kinematic redundancy using optimization techniques"*. In: IEEE Transactions on Robotics and Automation (Volume: 5, Issue: 4, Aug 1989). DOI: 10.1109/70.88067.

[30] Ian D. Walker. *"The Use of Kinematic Redundancy in Reducing Impact and Contact Effects in Manipulation"*. In: IEEE International Conference on Robotics and Automation. DOI: 10.1109/ROBOT.1990.126016.

[31] Ivan Buzurovic, Dragutin Lj. Debeljkovic, Vladimir Misic, Goran Simeunovic. *"Stability of the Robotic System with Time Delay in Open Kinematic Chain Configuration"*. In: Acta Polytechnica Hungarica, Vol. 11, No. 8, 2014.

[32] G. Palli and C. Me lc h io rri. *"On the Feedback Linearization of Robots with Variable Joint Stiffness"*. In: 2008 IEEE International Conference on Robotics and Automation Pasadena, CA, USA, May 19-23, 2008. 978-1-4244-1647-9/08.

[33] Xiaoping Yun. *"Dynamic state feedback control of constrained robot manipulators"*. In: Proceedings of the 27th IEEE Conference on Decision and Control. DOI: 10.1109/CDC.1988.194384.

[34] Peter Corke. *"Robotics, Vision and Control: Fundamental Algorithms In MATLAB"*. R Second, Completely Revised. Vol. 118. Springer, 2017.

[35] R.J. Anderson , M.W. Spong. *"Hybrid impedance control of robotic manipulators"*. In: IEEE Journal on Robotics and Automation (Volume: 4 , Issue: 5 , Oct 1988). DOI: 10.1109/56.20440.

[36] O. Khatib, J. Burdick. *"Motion and force control of robot manipulators"*. Proc. 1986 Int. Conf on Robotics and Automation, pp. 1381-1386.

[37] Neville Hogan. *"Impedance Control: An Approach to Manipulation"*. In: 1984 American Control Conference. DOI: 10.23919/ACC.1984.4788393.

[38] Pyung-Hun Chang, Ki Cheol Park, Sukhan Lee. *"An Extension to Operational Space for Kinematically Redundant Manipulators: Kinematics and Dynamics"*. In: IEEE TRANSACTIONS ON ROBOTICS AND AUTOMATION, VOL. 16, NO. 5, OCTOBER 2000.

[39] Oussama Kanoun, Florent Lamiraux, Pierre-Brice Wieber. *"Kinematic Control of Redundant Manipulators: Generalizing the Task-Priority Framework to Inequality Task"*. IEEE TRANSACTIONS ON ROBOTICS, VOL. 27, NO. 4, AUGUST 2011 78. DOI: 10.1109/TRO.2011.2142450.

[40] Andrea Maria Zanchettin, Paolo Rocco. *"Path-consistent safety in mixed human-robot collaborative manufacturing environments"*. In: 2013 IEEE/RSJ International Conference on Intelligent Robots and Systems (IROS) Nov 3-7, 2013. Tokyo, Japan.

[41] Kuo-Kai Shyu, J.Y. Hung, J.C. Hung. *"Total sliding mode trajectory control of robotic manipulators"*. In: 25th Annual Conference of the IEEE Industrial Electronics Society (Cat. No.99CH37029). DOI: 10.1109/IECON.1999.819355.

[42] Gian Paolo Incremona, Antonella Ferrara, Lalo Magni. *"MPC for Robot Manipulators With Integral Sliding Modes Generation"*. In: IEEE/ASME Transactions on Mechatronics (Volume: 22, Issue: 3 , June 2017). DOI: 10.1109/TMECH.2017.2674701.

[43] Antonella Ferrara, Gian Paolo Incremona. *"Robust motion control of a robot manipulator via Integral Suboptimal Second Order Sliding Modes"*. In: 52nd IEEE Conference on Decision and Control. DOI: 10.1109/CDC.2013.6760030.

[44] Gianni Ferretti, Antonio Magnani, Paolo Rocco, Luca Vigani. *"The operational space control applied to a space robotic manipulator"*. In: Pmdlngs d the 2004 IEEE International Conference on Robotics and Automation New Orleans, LA - April 2004.

[45] Davide Nicolis, Marco Palumbo, Andrea Maria Zanchettin, Paolo Rocco. *"Occlusion-Free Visual Servoing for the Shared Autonomy Teleoperation of Dual-Arm Robots"*. In: IEEE Robotics and Automation Letters (Volume: 3, Issue: 2, April 2018). DOI: 10.1109/LRA.2018.2792143.

[46] L. Biagiotti, H. Liuz, G. Hirzinger, C. Melchiorri. *"Cartesian Impedance Control for Dexterous Manipulation"*. In: Proceedings of the 2003 IEEE/RSJ Intl. Conference on Intelligent Robots and Systems, Las Vegas, Nevada, October 2003. DOE: 0-7803-786 1/0.